Biospectroscopic investigation on bacterial response to antimicrobials

An alternative format thesis submitted for the degree of Doctor of Philosophy in the Faculty of Science and Technology
Lancaster University

December 2017

Naifu Jin MSc BSc

Lancaster Environment Centre

Declaration

I declare that this thesis is my work and has not been submitted for the award of a higher degree or qualification at this university or elsewhere.

ACKNOWLEDGEMENTS

First of all, I am grateful to Lancaster Environment Centre (LEC) and Chinese Scholarship Council (CSC) for funding and providing me the opportunity of studying in Lancaster University.

During the past three years, I am really fortunate that, I had the kind association as well as supervision of Prof Frank Martin, Dr Dayi Zhang and Prof Kirk Semple. Their exemplary guidance, constant encouragements, and careful monitoring throughout my study are so great that, even my most profound gratitude is not enough. They not only give me academic guides, but also offer me many advises for my life and future development.

At the end, I would also like to express a deep sense of gratitude to my parents, who provided me additional financial assistance and always stand as a strong support.

Abstract

Overuse and abuse of antimicrobial-associated materials in human activities may lead to microbes acquire resistance to antimicrobials since antimicrobials not only act as an eliminator for microbes but also a selective agent for the microorganisms with resistant abilities. Moreover, over 95% of bacteria living on earth are unculturable, and most of their living style is functioning as the microbiome, e.g., bacterial biofilms, which therefore substantially increase the difficulty regarding the investigation on microbial response to antimicrobials, or in other words, functional microbes under exposure of antimicrobials. Biospectroscopy, as an interdisciplinary tool including Raman and infrared spectroscopies, can generate conclusive information regarding the biological constituents, including lipids, proteins, carbohydrates and DNA/RNA, *etc*. Such biochemical information can be used to fingerprint microbiome and then assess the microbial functions which remain a challenge due to more conventional approaches are too expensive and/or time-consuming and often predicated on prior knowledge of the microorganisms one wishes to study. Additionally, computational analysis is subsequently applied to process and analyze the raw spectra generated by Raman and IR spectroscopies to obtain meaningful information and get a deeper insight into the wavenumbers-related biochemical alterations. This extra step may provide a solution of assessing a significant amount of complicated biochemical information derived from heterogeneous biological samples. The current project summarized the drawbacks within the conventional approaches and proposes a new perspective that using spectroscopic tools coupled with various of computational analysis such as multivariant analysis and a newly developed dispersion model to investigate microbial functions (primarily on antibiotic resistance) as well as set up a baseline to determine the factors may influence the microbiome; and ultimately develop a non-invasive sensor-based tool that could be applied to monitor the emergence of antibiotic-

resistant microorganisms in real-time. This would be hugely cost-efficient and allow for monitoring of antibiotic usage, a major problem currently.

Contents

List of abbreviations

AgNP: Nanoparticulate Silver

ARG: Antibiotic Resistance Gene

CFU: Colony-forming Unit

FTIR: Fourier-transform Infrared Spectroscopy

GIT: Gastrointestinal Tract

HGT: Horizontal Gene Transfer

IR: Infrared

LDA: Linear Discriminant Analysis

Low-E: Low-emissivity

MIR: Mid-Infrared

NIR: Near-Infrared

NP: Nanoparticle

PC: Principal Component

PCA: Principal Component Analysis

PCR: Polymerase Chain Reaction

ROS: Reactive Oxygen Species

S-G: Savizky-Golay

SIP: Stable Isotope Probing

SNT: Signal-to-Noise Ratio

General Introduction

1. Research rationale

1.1 Microbial functions in natural environment and their impacts on human health

Microbes, as a group of organisms have existed since the ancient time, played a vital role in the history of earth. Their ecological niche is significantly important in many ecological processes such as carbon, phosphate and nitrogen cycles (Breitbart and Rohwer, 2005, Fuhrman, 2009). Human health is also highly dependent on microbes as billions of bacteria symbiotically live in the human body. The total ratio of bacterial cells to human cells is nearly ten folds (Schmieder and Edwards, 2012). Most of these microbial cells settle in the gastrointestinal tract (GIT) and constitute the human intestinal microbiota. With a concentration of 10^{12} CFU/g of intestinal content, the human intestinal microbiota probably represents one of the most biodiverse, densest, and rapidly evolving bacterial ecosystems on earth (Candela et al., 2012, Hill et al., 2010, Bailey et al., 2011, Jernberg et al., 2010, Lu et al., 2014, Mutlu et al., 2012). Dynamics of human host microbial communities may count for numbers of diverse phenomena associated public health issues (Gonzalez et al., 2011, Takahashi, 2005). It is worth mentioning the microbial communities in humans are characteristic and complex mixtures of microorganism that have co-evolved with their human hosts. The species that form these communities vary between hosts due to restricted migration of microorganisms between hosts and strong ecological interactions within hosts. The shared evolutionary fate of humans and their symbiotic bacteria has selected for mutualistic interactions that are essential for human health, and ecological or genetic changes that uncouple this shared fate can result in disease (Dethlefsen et al., 2007).

1.2 Microbial response to antimicrobials

It has been recognized that antimicrobials have impacts on microbes, acting not only as an

efficient eliminator to microbes but also a selective agent helping in propagating organisms with the antimicrobial resistance ability. Particularly, the antibiotic resistance genes (ARGs), which have a notorious reputation in human pathogens because they are able to inactive a medicine efficiency to treat microbe-induced disease (Allen et al., 2010). Strikingly, with the help of horizontal gene transfer, ARGs initially found on transposons, integrons or plasmids become transferable. Evidence of the ARGs transfer to human commensal bacteria and pathogens as well as the phenomenon of gene transfer in the human intestinal microbiome have been extensively addressed in previous studies (Allen et al., 2010). The selection pressure from the residuals of antibiotics that are used in clinical and agricultural settings has accelerated the evolution and distribution of ARGs regardless of their origins (Allen et al., 2010, Smillie et al., 2011). Moreover, physical forces, e.g., wind blowing and watershed, provide important routes of routes for antibiotic resistance genes environmentally. Human activities may also increase the prevalence of ARGs in air and water. Furthermore, the contribution of wild animals to the movement of ARGs is unneglectable as well. Wild birds for instance, which travel a broad range of geographical distance and have access to many water bodies and mountains (Allen et al., 2010).

2. Technical challenges and development

2.1 Conventional approaches investigating microbial response to antimicrobials

In the past years, many methods have been developed to determine and quantify the ARGs. By far, investigations on microbial antibiotic resistance follow different techniques and methodologies, generally categorized as function- and molecular-based methods according to varied interest, i.e., function-based methods are designed for the investigation of particular phenomenon or mechanisms of individual microbes, while the molecular-based, herein principally referring to omics-based, are for the study of microbiota. Cultivation is the most applied function-based approach to the determination of microbial response to antibiotics

(Fuhrman, 2009, Schwartz et al., 2003, Martin et al., 1990). However, over 90% bacteria are yet-uncultivable but functional in-situ (Bartscht et al., 1999, Clardy and Walsh, 2004, Streit and Schmitz, 2004). Therefore, the capability of cultivation-independent methods on reflecting real scenario is always questioned (Nichols, 2007). Instead of targeting individual functional microbes, molecular-based approaches deal with microbiota as an integrated system by direct extraction of biological components (Nichols, 2007, Riesenfeld et al., 2004, Tyers and Mann, 2003, Sommer et al., 2009, Forsberg, 2015, Handelsman, 2004, Diaz-Torres et al., 2003). However, omics-based approaches have an inherent insufficiency that tracing back to specific functional microbes responding to the antibiotic resistance is tough; and also because of the application of cloning and sequencing techniques, molecular-based approaches may not meet the need for in-situ diagnosis of antibiotic resistance in real-time. Furthermore, the reality of functions of antibiotics in microbial community is never revealed clearly due to the in situ concentrations of the compounds with antibiotic activity have never been measured, and there are few ecological examples of probable antibiotic functions for microbial products in nature (Allen et al., 2010). Therefore, finding a new approach that could fast screen a microbiota to determine the in-situ bacterial antibiotic resistance in real-time is a matter of urgency.

2.2 *Bio-spectroscopic approaches*

Biospectroscopy refers to a range of techniques that allow the spectroscopic examination of biological samples. Such spectroscopic measurements are usually based on electronic transitions and vibrational changes of chemical bonds with spatial resolutions from the microscopic to the macroscopic, which not only examines the morphological contrast in biological samples but also reveals elemental or molecular information via further determination (Heraud and Tobin, 2009). Infrared (IR) and Raman spectroscopy are the two major applied bio-spectroscopy techniques since the 1950s (Heber et al., 1952, Norris, 1959).

Owing to the IR absorption of the vibration movements (*e.g.*, bending, stretching, wagging or

scissoring) in their chemical bonds, the characterization of biomolecules can be achieved via infrared spectroscopy. When biomolecules contain chemical bonds with an electric dipole moment, these vibrations are detectable and measurable by IR spectroscopy (Martin et al., 2010). Within the categories of infrared spectroscopy regarding the wavelengths (i.e. Near-IR, Mid-IR and Far-IR), mid-infrared (MIR) spectroscopy (4000-400 cm^{-1} in wavenumbers) is the most applied bio-spectroscopy because its attribute not only includes overtones but also contains fundamental vibrational transition providing inherently stronger signal intensities in terms of the increased absorption cross-section (Kelly et al., 2011a). However, there is a significant limitation within FTIR that water from instrumentation or samples may induce reduction of IR light transmission (Martin et al., 2010, Baker et al., 2014). Hence, it has to be considered crucially to purge the instrumentation with dry air or nitrogen, as well as desiccants to remove any water vapour before spectral acquisition (Baker et al., 2014).

Raman spectroscopy, a complementary bio-spectroscopic technique to IR spectroscopy, can generate information of chemical bond and sample composition even under a hydrated environment (Ahmadzai et al., 2012, Creton et al., 2012, Gajjar et al., 2013, Trevisan et al., 2010, Walsh et al., 2009). The principle of Raman spectroscopy is to determine the moment of change when the photon from the monochromatic light sources (commonly is a laser source) hit the chemical bond of molecules, which can exploit the inelastic scattering or Raman effect. In this process, the excitation of photons to virtual energy states and the resultant loss (Stokes) or gain (anti-Stokes) of energy occurs because of the interaction of light with vibrational modes associated with chemical bonds within the sample (Butler et al., 2016). This shift in energy is indicative of discrete vibrational modes of polarizable molecules, and thus a qualitative measurement of the biochemical composition can be obtained (Butler et al., 2016). However, this phenomenon does not occur efficiently, which only accounts for less than 1%. Thus, the backward light is then applied filtering off other interference, but the Raman scattering can

reach the detector.

In 1991, the innovative Fourier transform mid-infrared (FTIR) spectroscopy was introduced by Naumann as a sensitive and rapid screening tool for characterization, classification, and identification of micrograms (Naumann et al., 1991). Since then, biospectroscopy has been exclusively used in microbial research (Baker et al., 2014, Schmitt and Flemming, 1998, Bosch et al., 2006, Ojeda et al., 2008). Metabolomics is a critical field that bio-spectroscopy could fill in to investigate microbial metabolomes. FTIR, for instance, is a valuable metabolic fingerprinting tool owing to its abilities to characterize cellular compositions (Wood et al., 1998, Dunn and Ellis, 2005, Baker et al., 2014, Schmitt and Flemming, 1998, Bosch et al., 2006, Ojeda et al., 2008, Mariey et al., 2001). In the mid-IR spectroscopy, the biochemical fingerprint region is from 1800 – 900 cm^{-1}, and representative peaks including: Lipid (~1750 cm^{-1}), Amide I (~1650 cm^{-1}), Amide II (~1550 cm^{-1}), Amide III (~1260 cm^{-1}), Carbohydrate (~1155 cm^{-1}), Asymmetric phosphate stretching vibrations; v_{as} PO_2^-(~1225 cm^{-1}), Symmetric phosphate stretching vibrations; v_s PO_2^- (~1080 cm^{-1}), Glycogen (~1030 cm^{-1}), Protein phosphorylation (~970 cm^{-1}) (Lipiec et al., 2013, Dunn and Ellis, 2005, Baker et al., 2014, Butler et al., 2016, Martin et al., 2010). These peaks can be derived as biomarkers for characterization of microbial cell types (even at subspecies level) and diagnosis of microbe-induced diseases (Wood et al., 1998, Dunn and Ellis, 2005, Baker et al., 2014, Schmitt and Flemming, 1998, Bosch et al., 2006, Ojeda et al., 2008, Mariey et al., 2001).

2.3 Data analysis

It needs to be highlighted the most vital component associated with biospectroscopic determination for bacterial response to antimicrobials is to find discriminating biomarkers, i.e., the most absolute and representative peaks derived from acquired spectra, allowing subsequently high throughput screening for determination of bacterial resistant behaviour. Although some alterations of biomarkers can be visualized by eyes, the questions always

emerge regarding the existence of noticed difference and the reliability of subjective assessing by eyes. Hence, computational analysis is applied to exam the data due to the acquired spectrums holding an enormous number of features.

The pre-processing is the first step of computational analysis which aims to control the quality of data by reducing effects resulting from spectral acquisition (i.e., instrument saturation/malfunction, atmospheric changes, gas contamination, excessive scattering or dispersion phenomena, and excessive noise) (Trevisan et al., 2012); and subsequently enhancing the robustness and accuracy as well as making all the raw data comparable (Baker et al., 2014). Moreover, the multivariate statistical analysis is also an ideal tool for spectral analysis. Although after pre-processing, the obtained spectra still contain an enormous number of features. Therefore, PCA-LDA (Principle component analysis-Linear discriminate analysis) was applied to generate a small group of variable but still maintaining the core information representing the whole dataset of the wavenumber variables. Specifically, principle component analysis (PCA), is an unsupervised analysis method aiming to reduce dimensionality and make the data visible (Kelly et al., 2011b). However, it is incapable of recognizing inter- and intra-class variance due to the nature of the unsupervised attribute. Therefore, further data analysis is typically required, e.g., Linear discriminate analysis (LDA), which is a supervised technique to define the data into a new dimensional space where a few variables can be found in each observation and meanwhile observations from the same origin form clusters and their individuals can be clearly separated from each other. Consequently, PCA and LDA are combined as an ideal classification tool to investigate intra-class or interclass variation. As compared to PCA alone, the additional linear discriminant analysis of PCA-LDA derives vectors from the principal components (PCs) and minimises the within-category differences (mostly be associated with typical heterogeneity in any biological sample) while maximising between-category discriminating characteristics (i.e., those most likely to be induced by

treatments or other exogenous contributions) (Baker et al., 2014, Butler et al., 2016, Martin et al., 2010).

3. Prospects of bio-spectroscopy in environmental microbiology

3.1 Microbial fingerprints by bio-spectroscopy

As compared to the conventional microbial identification and characterization tools, bio-spectroscopy requires a very minimal amount of sample, simple sample preparation and very fast responding speed regarding analysis (Butler et al., 2016, Martin et al., 2010, Baker et al., 2014). In the history of the bio-spectroscopic application on microbiology, biofilm research, in particular, is a hotspot of microbial ecological study. Since microbiome is a very complicated bio-matrix, signals which are from many compositions such as extracellular polymeric substances, cell membrane, and the cytoplasm, can contribute to the overall spectra. The characteristic peaks from the spectra for biological macromolecules and a comparison between the biofilm samples and their planktonic could reveal relevant biochemical information of interacted targets (Karunakaran et al., 2011). Other applications of bio-spectroscopy on microbial issues including characterization of hospital isolates and rapid quantitative detection of the microbial spoilage of food products etc. (Lipiec et al., 2013, Naumann et al., 1991, Goodacre et al., 1996, Ellis et al., 2002, Dunn and Ellis, 2005). There is no doubt that bio-spectroscopy is a robust tool for the investigation of bacterial response to environmental exposures due to its particular attributes of being non-destructive, non-intrusive, high throughput and label-free (Baker et al., 2014, Martin et al., 2010). When coupled with conventional microscopy, bio-spectroscopy can produce cell construction from both the eye and biochemical perspective by the passing of spectral data through a variety of computational algorithms and obtain pictures at the same time (Baker et al., 2014, Martin et al., 2010). It allows visualized monitoring, and spectral interrogation undertakes in-situ at real-time, which is very helpful to understand the actual interactions between microbes and physical

environment (Baker et al., 2014, Butler et al., 2016, Heraud and Tobin, 2009, Huang et al., 2004, Martin et al., 2010, Dunn and Ellis, 2005).

3.2 *Single-cell Raman spectroscopy*

In microbiology, isolates followed by cultivation is a conventional approach to purify microbes of interest. However, the limitations of the culture-based approach, regarding uncultivable bacteria and their complicated community constructions, means microbial functioning in natural environments cannot be studied solely by culturing (Whitman et al., 1998, Huang et al., 2004). Cell sorting techniques as one of the most powerful tools to separate cell matrix, to some extent, solve the issues resulting from uncultivable microbes and growth circle circumstances in the environment. For example, Raman spectroscopy along with optical tweezers has been validated as a feasible approach for identification and separation of single cells (Huang et al., 2009). Within the procedure of sorting cells via optical tweezers, a highly focused laser beam is applied to provide an attractive or repulsive force to physically hold and move microscopic, neutral objects. This entire progression can be visualized via Raman microscopy (Song et al., 2016). As compared to conventional Raman spectroscopy, single cell analysis provides an opportunity to determine the cellular interactions with environmental exposures on individuals allowing the study of homogeneity or heterogeneity more accurately and convincingly.

3.3 *Investigation into microbial functions using biomarkers derived from bio-spectroscopy*

Bio-spectroscopy can reveal many biochemical features regarding chemical bonds from the interrogated sample. In the mid-IR spectroscopy, for instance, the biochemical fingerprint region is from 1800 - 900 cm^{-1}, and representative peaks include: lipids (~1750 cm^{-1}), Amide I (~1650 cm^{-1}), Amide II (~1550 cm^{-1}), Amide III (~1260 cm^{-1}), carbohydrates (~1155 cm^{-1}), asymmetric phosphate stretching vibrations (ν_{as} PO_2^-, ~1225 cm^{-1}), symmetric phosphate stretching vibrations ($\nu_s PO_2^-$, ~1080 cm^{-1}), glycogen (~1030 cm^{-1}), protein phosphorylation

(~970 cm^{-1}) (Lipiec et al., 2013, Dunn and Ellis, 2005, Baker et al., 2014, Butler et al., 2016, Martin et al., 2010). In Raman spectroscopy, the informative region of wavenumbers for biological samples is located within 400-2000 cm^{-1} and 2700-3500 cm^{-1}, including proteins (1500-1700 cm^{-1}), carbohydrates (470-1200 cm^{-1}), phosphate groups of DNA (980, 1080 and 1240 cm^{-1}) and higher-frequency bond vibrations of CH, NH and OH stretching in lipids and proteins(Butler et al., 2016, Movasaghi et al., 2007). These peaks can be derived as biomarkers for characterization of microbial cell types (even at subspecies level) and diagnosis of microbe-induced diseases (Wood et al., 1998, Dunn and Ellis, 2005, Baker et al., 2014, Schmitt and Flemming, 1998, Bosch et al., 2006, Ojeda et al., 2008, Mariey et al., 2001).

In general, applications of Bio-spectroscopy in microbiology include bacterial discrimination, isolation, and identification (Jarvis and Goodacre, 2004, Maquelin et al., 2002, Pahlow et al., 2015). Biospectroscopy can also diagnose microbe-induced diseases in clinical settings contributing to the advantages of early detection and stratification of at-risk patients to initiate timely and appropriate treatment (Bunaciu et al., 2015, Neugebauer et al., 2014, Premasiri et al., 2005, Zarnowiec et al., 2015). Raman spectroscopy has successfully identified sepsis in blood plasma from 70 patients with a satisfactory sensitivity of 1.0 and specificity of 0.82 (Neugebauer et al., 2014). The feasibility of biospectroscopic investigation into microbial alterations induced by exposures has been evaluated too. Riding et al. applied IR spectroscopy to fingerprint microbes followed by exposing to carbon nanoparticles, and revealed concentration- and size-dependent changes in cellular components (Riding et al., 2012). Another study (Heys et al., 2014) confirmed the ability of IR spectroscopy to characterize changes induced by carbon nanoparticles *via* investigating their effects in both Gram-positive and negative bacteria. Some discriminant biochemical markers, *i.e.*, Amide II and carbohydrate, were picked out to verify the distinct alterations in bacteria with respective cell wall structures. These studies prove that biospectroscopy is not only able to distinguish microbial response to

different kinds of exposures, but also specify variances resulting from bacterial structures, demonstrating its potential to diagnose antibiotic resistance with reliable biomarkers.

4. Research aims and objectives

Bio-spectroscopy has demonstrated great potential to biological studies in past years. By the end of the entire project, it is intended to have developed a non-invasive sensor-based tool that could be applied to monitor the emergence of antibiotic-resistant microorganisms in real-time. This would be hugely cost-efficient and allow for monitoring of antibiotic usage, a major problem currently. The primary objectives of the present project are to:

- Propose prospects and discuss the technical details of fingerprinting microbiomes towards screening for microbial antibiotic resistance.
- Develop a new tool coupling bio-spectroscopy and multivariate analysis to investigate the bacterial response to antimicrobial reagents.
- Bio-spectroscopically investigate intrinsic (bacterial type) and external factors (exposure time and type) on bacterial responsive uniqueness to antimicrobials.
- Quantify the occurrence and real-time dynamics of antibiotic resistance genes (ARGs) in complex microbiota via bio-spectroscopy.
- Evaluate the performance of fungal response to heavy metal exposure and discuss the mechanisms of metal adsorption via bio-spectroscopy.

5. Thesis structure

This thesis consists of five chapter, which is developed under the core purpose of investigation of microbial functions (mainly antibiotic resistance) via biospectroscopy. The first half of the thesis reviewed the background of biospectroscopy and proposed new insights into microbial functions (i.e., bacterial response to antimicrobials) from the spectroscopic perspective, emphasizing the challenges in such field and provided some relevant solutions. The latter half

demonstrated a new tool in order to solve the microbe associated issues (ARG and heavy metal biosorption) which not only characterized such problems at a mechanism level but also provided the quantitative explication.

To be more specific, the first chapter briefly reviewed the situation of microbial antibiotic resistance and proposed a new concept that spectral fingerprint microbiomes towards screening for microbial antibiotic resistance. In general, as compared to conventional approaches, which are too expensive and/or time-consuming and often predicated on prior knowledge of the microorganisms one wishes to study, this method can generate fingerprint spectra of biological material and such spectra are able to be classed according to biochemical changes in the microbiota with a non-destructive, non-intrusive manner. This work demonstrated the potential feasibility of applying biospectroscopy to readily fingerprint microbiomes that could lend itself to new approaches in determining microbial behaviours and emergence of antibiotic resistance.

In order to answer the challenge raised in Chapter one regarding the growth phase and environmental variants, Chapter two aims to prove the state-of-the-art biospectroscopy in diagnosing physiological features of bacteria and lend profound insights into the relationship between physiological characteristics of bacteria and their response to environmental insults. The study applied bio-spectroscopy coupled with multivariate analysis to investigate the growth- and species-dependent response of two bacterial cells, Gram-negative *Pseudomonas fluorescens* and Gram-positive *Mycobacterium vanbaalenii*, to low concentrations of tetracycline, nanoparticulate silver (AgNP) and their mixtures. Regarding the real world scenario, the work distinguished the distinct biospectral alterations in different bacterial types and growth phases, helping to understand the bacterial behaviour postexposure to low-level antimicrobials. The results indicated that the tendency of tetracycline-induced biospectral alterations widely exists in many outer-cellular components. The primarily interacted targets

are correlated with the bacterial membrane or outer-cellular components. Furthermore, significant lipid changes were only present in *P. fluorescens* cells comparing to *M. vanbaalenii*, owing to the differences of cell wall structure between Gram-positive and negative bacteria. This study also found distinct biospectral alterations in non-log phase comparing to log phase, confirming the bacterial growth-dependent response to environmental exposure. It implies that past studies on log phase only may underestimate the impacts from exposures of interest *in situ*, where bacteria stay in different growth stages.

As compared to Chapter Two which mainly focused on short-term exposure, Chapter Three was a comprehensive study primarily concentrated on long-term exposure as well as including a comparison between the impacts induced by short- and long-term exposure. This work applied attenuated total reflectance Fourier transform infrared (ATR-FTIR) microscopy coupled with multivariate analysis, as a high-throughput and nondestructive approach to investigate the bacterial response to prolonged low-level exposures of AgNP and tetracycline under nutrient depletion condition. Post-exposure to nanoparticulate silver (AgNP), tetracycline and their mixtures for 12 days, Gram-positive (*Mycobacterium vanbaalenii* PYR-1) and Gram-negative (*Pseudomonas fluorescens*) bacteria showed distinct IR spectral alterations. Multivariate analysis coupled with multivariate regression tree (MRT) indicates nutrient depletion and exposure time as the primary factors in bacterial behavior, followed by exposure category and bacterial type. Nutrient depletion and starvation during long-term exposure drives the bacterial cells into a dormant state or to exhibit additional cellular components (e.g., fatty acids) against the antimicrobials, consequently causing a broader range of spectral alteration comparing to short-term exposure. Our work is the first report highlighting the more important roles of exposure duration and nutrient depletion, instead of antimicrobial reagents, on microbial response to low-level and prolonged environmental exposure.

The Fourth Chapter demonstrated the potential feasibility of application of biospectroscopy to monitoring and quantify the ARGs in microbiota. The hypothesis was validated via application of infrared spectroscopy coupled with a dispersion model for quantifying the real-time dynamics of kanamycin resistance in artificial microbiota. This work employed attenuated total reflection Fourier-transform infrared (ATR-FTIR) spectroscopy and developed a spectrochemical tool to quantify the static and dynamic composition of kanamycin resistance in artificial microbiota to evaluate microbial antibiotic resistance. Second order differentiation was introduced in identifying the spectral biomarkers, and principal component analysis followed by linear discriminant analysis (PCA-LDA) was used for the multivariate analysis of the spectral data. The calculated results of the mathematical model based on spectral features showed high similarity to the designed microbiota structure, with no significant difference (P >0.05) in the static treatments. Moreover, our model successfully predicted the dynamics of kanamycin resistance within artificial microbiota under kanamycin pressures. This work lends new insights into the potential role of spectrochemical analyses in investigating the existence and trends of antibiotic resistance in microbiota.

Chapter five extended this work to test whether biospectrsocopy was a suitable tool to investigated other bacterial behaviours. This study applied ATR-FTIR coupled with Phenotype MicroArrays (PM) to characterize fungal absorption to Cd and Pb in the mediums with 48 solo carbon sources. This is the first study used spectroscopic tools to analysis fungal adsorption and the carbon source impact, which not only enrich database in such field but also provide an opportunity to better understand biosorption mechanism from a novel perspective. It was found spectral biomarkers associated with phosphor-lipids and proteins were significantly correlated with Cd adsorption indicating the cell wall components of *S. chinense* are the primary interactive targets. However, we did not find any biomarkers associated with Pb adsorption. The analysis of biosorption equilibrium models showed a clue that Cd adsorption was relatively

suited in Langmuir, but the Pb was well fitted with Freundlich isotherm model, which implies the absorptions of Pb and Cd by *S. chinense* follow two discriminating mechanisms that Cd adsorption is mainly driven by the cell surface sorption, but for Pb, the extracellular precipitation is possibly the main contribution.

REFERENCES

AHMADZAI, A. A., TREVISAN, J., FULLWOOD, N. J., CARMICHAEL, P. L., SCOTT, A. D. & MARTIN, F. L. 2012. The Syrian hamster embryo (SHE) assay (pH 6.7): mechanisms of cell transformation and application of vibrational spectroscopy to objectively score endpoint alterations. *Mutagenesis,* 27**,** 257-266.

ALLEN, H. K., DONATO, J., WANG, H. H., CLOUD-HANSEN, K. A., DAVIES, J. & HANDELSMAN, J. 2010. Call of the wild: antibiotic resistance genes in natural environments. *Nature Reviews Microbiology,* 8**,** 251-259.

BAILEY, M. T., DOWD, S. E., GALLEY, J. D., HUFNAGLE, A. R., ALLEN, R. G. & LYTE, M. 2011. Exposure to a social stressor alters the structure of the intestinal microbiota: implications for stressor-induced immunomodulation. *Brain Behav Immun,* 25**,** 397-407.

BAKER, M. J., TREVISAN, J., BASSAN, P., BHARGAVA, R., BUTLER, H. J., DORLING, K. M., FIELDEN, P. R., FOGARTY, S. W., FULLWOOD, N. J., HEYS, K. A., HUGHES, C., LASCH, P., MARTIN-HIRSCH, P. L., OBINAJU, B., SOCKALINGUM, G. D., SULE-SUSO, J., STRONG, R. J., WALSH, M. J., WOOD, B. R., GARDNER, P. & MARTIN, F. L. 2014. Using Fourier transform IR spectroscopy to analyze biological materials. *Nat Protoc,* 9**,** 1771-91.

BARTSCHT, K., CYPIONKA, H. & OVERMANN, J. 1999. Evaluation of cell activity and of methods for the cultivation of bacteria from a natural lake community. *FEMS Microbiology Ecology,* 28**,** 249-259.

BOSCH, A., SERRA, D., PRIETO, C., SCHMITT, J., NAUMANN, D. & YANTORNO, O. 2006. Characterization of Bordetella pertussis growing as biofilm by chemical analysis and FT-IR spectroscopy. *Applied microbiology and biotechnology,* 71**,** 736-747.

BREITBART, M. & ROHWER, F. 2005. Here a virus, there a virus, everywhere the same virus? *Trends Microbiol,* 13**,** 278-84.

BUNACIU, A. A., ABOUL-ENEIN, H. Y. & FLESCHIN, Ş. 2015. Vibrational spectroscopy in clinical analysis. *Applied Spectroscopy Reviews,* 50**,** 176-191.

BUTLER, H. J., ASHTON, L., BIRD, B., CINQUE, G., CURTIS, K., DORNEY, J., ESMONDE-WHITE, K., FULLWOOD, N. J., GARDNER, B., MARTIN-HIRSCH, P. L., WALSH, M. J., MCAINSH, M. R., STONE, N. & MARTIN, F. L. 2016. Using Raman spectroscopy to characterize biological materials. *Nat Protoc,* 11**,** 664-87.

CANDELA, M., BIAGI, E., MACCAFERRI, S., TURRONI, S. & BRIGIDI, P. 2012. Intestinal microbiota is a plastic factor responding to environmental changes. *Trends Microbiol,* 20**,** 385-91.

CLARDY, J. & WALSH, C. 2004. Lessons from natural molecules. *Nature,* 432**,** 829-837.

CRETON, S., AARDEMA, M. J., CARMICHAEL, P. L., HARVEY, J. S., MARTIN, F. L., NEWBOLD, R. F., O'DONOVAN, M. R., PANT, K., POTH, A. & SAKAI, A. 2012. Cell transformation assays for prediction of carcinogenic potential: state of the science and future research needs. *Mutagenesis,* 27**,** 93-101.

DETHLEFSEN, L., MCFALL-NGAI, M. & RELMAN, D. A. 2007. An ecological and evolutionary perspective on human–microbe mutualism and disease. *Nature,* 449**,** 811-818.

DIAZ-TORRES, M., MCNAB, R., SPRATT, D., VILLEDIEU, A., HUNT, N., WILSON, M. & MULLANY, P. 2003. Novel tetracycline resistance determinant from the oral metagenome. *Antimicrobial agents and chemotherapy,* 47**,** 1430-1432.

DUNN, W. B. & ELLIS, D. I. 2005. Metabolomics: current analytical platforms and methodologies. *TrAC Trends in Analytical Chemistry,* 24**,** 285-294.

ELLIS, D. I., BROADHURST, D., KELL, D. B., ROWLAND, J. J. & GOODACRE, R. 2002. Rapid and quantitative detection of the microbial spoilage of meat by Fourier transform infrared spectroscopy and machine learning. *Applied and environmental microbiology,* 68**,** 2822-2828.

FORSBERG, K. J. 2015. The Diversity, Ecology, and Clinical Implications of Antibiotic Resistance Genes in Uncultured Soil Microbial Communities.

FUHRMAN, J. A. 2009. Microbial community structure and its functional implications. *Nature,* 459**,** 193-9.

GAJJAR, K., TREVISAN, J., OWENS, G., KEATING, P. J., WOOD, N. J., STRINGFELLOW, H. F., MARTIN-HIRSCH, P. L. & MARTIN, F. L. 2013. Fourier-transform infrared spectroscopy coupled with a classification machine for the analysis of blood plasma or serum: a novel diagnostic approach for ovarian cancer. *Analyst,* 138**,** 3917-3926.

GONZALEZ, A., CLEMENTE, J. C., SHADE, A., METCALF, J. L., SONG, S., PRITHIVIRAJ, B., PALMER, B. E. & KNIGHT, R. 2011. Our microbial selves: what ecology can teach us. *EMBO Rep,* 12**,** 775-84.

GOODACRE, R., TIMMINS, E. M., ROONEY, P. J., ROWLAND, J. J. & KELL, D. B. 1996. Rapid identification of Streptococcus and Enterococcus species using diffuse reflectance-absorbance Fourier transform infrared spectroscopy and artificial neural networks. *FEMS Microbiology Letters,* 140**,** 233-239.

HANDELSMAN, J. 2004. Metagenomics: application of genomics to uncultured microorganisms. *Microbiology and molecular biology reviews,* 68**,** 669-685.

HEBER, J., SEVENSON, R. & BOLDMAN, O. 1952. Infrared spectroscopy as a means for identification of bacteria. *Science,* 116**,** ll.

HERAUD, P. & TOBIN, M. J. 2009. The emergence of biospectroscopy in stem cell research. *Stem Cell Res,* 3**,** 12-4.

HEYS, K. A., RIDING, M. J., STRONG, R. J., SHORE, R. F., PEREIRA, M. G., JONES, K. C., SEMPLE, K. T. & MARTIN, F. L. 2014. Mid-infrared spectroscopic assessment of nanotoxicity in gram-negative vs. gram-positive bacteria. *Analyst,* 139**,** 896-905.

HILL, D. A., HOFFMANN, C., ABT, M. C., DU, Y., KOBULEY, D., KIRN, T. J., BUSHMAN, F. D. & ARTIS, D. 2010. Metagenomic analyses reveal antibiotic-induced temporal and spatial changes in intestinal microbiota with associated alterations in immune cell homeostasis. *Mucosal Immunol,* 3**,** 148-58.

HUANG, W. E., GRIFFITHS, R. I., THOMPSON, I. P., BAILEY, M. J. & WHITELEY, A. S. 2004. Raman microscopic analysis of single microbial cells. *Analytical chemistry,* 76**,** 4452-4458.

HUANG, W. E., WARD, A. D. & WHITELEY, A. S. 2009. Raman tweezers sorting of single microbial cells. *Environmental Microbiology Reports,* 1**,** 44-49.

JARVIS, R. M. & GOODACRE, R. 2004. Discrimination of bacteria using surface-enhanced Raman spectroscopy. *Analytical Chemistry,* 76**,** 40-47.

JERNBERG, C., LOFMARK, S., EDLUND, C. & JANSSON, J. K. 2010. Long-term impacts of antibiotic exposure on the human intestinal microbiota. *Microbiology,* 156**,** 3216-23.

KARUNAKARAN, E., MUKHERJEE, J., RAMALINGAM, B. & BIGGS, C. A. 2011. "Biofilmology": a multidisciplinary review of the study of microbial biofilms. *Applied microbiology and biotechnology,* 90**,** 1869-1881.

KELLY, J. G., TREVISAN, J., SCOTT, A. D., CARMICHAEL, P. L., POLLOCK, H. M., MARTIN-HIRSCH, P. L. & MARTIN, F. L. 2011a. Biospectroscopy to metabolically

profile biomolecular structure: a multistage approach linking computational analysis with biomarkers. *J Proteome Res,* 10**,** 1437-48.

KELLY, J. G., TREVISAN, J., SCOTT, A. D., CARMICHAEL, P. L., POLLOCK, H. M., MARTIN-HIRSCH, P. L. & MARTIN, F. L. 2011b. Biospectroscopy to metabolically profile biomolecular structure: a multistage approach linking computational analysis with biomarkers. *Journal of proteome research,* 10**,** 1437-1448.

LIPIEC, E., BIRARDA, G., KOWALSKA, J., LEKKI, J., VACCARI, L., WIECHEĆ, A., WOOD, B. & KWIATEK, W. 2013. A new approach to studying the effects of ionising radiation on single cells using FTIR synchrotron microspectroscopy. *Radiation Physics and Chemistry,* 93**,** 135-141.

LU, K., ABO, R. P., SCHLIEPER, K. A., GRAFFAM, M. E., LEVINE, S., WISHNOK, J. S., SWENBERG, J. A., TANNENBAUM, S. R. & FOX, J. G. 2014. Arsenic exposure perturbs the gut microbiome and its metabolic profile in mice: an integrated metagenomics and metabolomics analysis. *Environ Health Perspect,* 122**,** 284-91.

MAQUELIN, K., KIRSCHNER, C., CHOO-SMITH, L.-P., VAN DEN BRAAK, N., ENDTZ, H. P., NAUMANN, D. & PUPPELS, G. 2002. Identification of medically relevant microorganisms by vibrational spectroscopy. *Journal of microbiological methods,* 51**,** 255-271.

MARIEY, L., SIGNOLLE, J., AMIEL, C. & TRAVERT, J. 2001. Discrimination, classification, identification of microorganisms using FTIR spectroscopy and chemometrics. *Vibrational Spectroscopy,* 26**,** 151-159.

MARTIN, C., TIMM, J., RAUZIER, J., GOMEZ-LUS, R., DAVIES, J. & GICQUEL, B. 1990. Transposition of an antibiotic resistance element in mycobacteria. *Nature,* 345**,** 739-743.

MARTIN, F. L., KELLY, J. G., LLABJANI, V., MARTIN-HIRSCH, P. L., PATEL, II, TREVISAN, J., FULLWOOD, N. J. & WALSH, M. J. 2010. Distinguishing cell types or populations based on the computational analysis of their infrared spectra. *Nat Protoc,* 5**,** 1748-60.

MOVASAGHI, Z., REHMAN, S. & REHMAN, I. U. 2007. Raman Spectroscopy of Biological Tissues. *Applied Spectroscopy Reviews,* 42**,** 493-541.

MUTLU, E. A., GILLEVET, P. M., RANGWALA, H., SIKAROODI, M., NAQVI, A., ENGEN, P. A., KWASNY, M., LAU, C. K. & KESHAVARZIAN, A. 2012. Colonic microbiome is altered in alcoholism. *Am J Physiol Gastrointest Liver Physiol,* 302**,** G966-78.

NAUMANN, D., HELM, D. & LABISCHINSKI, H. 1991. Microbiological characterizations by FT-IR spectroscopy. *Nature,* 351**,** 81-82.

NEUGEBAUER, U., TRENKMANN, S., BOCKLITZ, T., SCHMERLER, D., KIEHNTOPF, M. & POPP, J. 2014. Fast differentiation of SIRS and sepsis from blood plasma of ICU patients using Raman spectroscopy. *Journal of biophotonics,* 7**,** 232-240.

NICHOLS, D. 2007. Cultivation gives context to the microbial ecologist. *FEMS Microbiol Ecol,* 60**,** 351-7.

NORRIS, K. 1959. Infra-red spectroscopy and its application to microbiology. *Journal of Hygiene,* 57**,** 326-345.

OJEDA, J. J., ROMERO-GONZÁLEZ, M. E., BACHMANN, R. T., EDYVEAN, R. G. & BANWART, S. A. 2008. Characterization of the cell surface and cell wall chemistry of drinking water bacteria by combining XPS, FTIR spectroscopy, modeling, and potentiometric titrations. *Langmuir,* 24**,** 4032-4040.

PAHLOW, S., MEISEL, S., CIALLA-MAY, D., WEBER, K., RÖSCH, P. & POPP, J. 2015. Isolation and identification of bacteria by means of Raman spectroscopy. *Advanced drug delivery reviews,* 89**,** 105-120.

PREMASIRI, W., MOIR, D., KLEMPNER, M., KRIEGER, N., JONES, G. & ZIEGLER, L. 2005. Characterization of the surface enhanced Raman scattering (SERS) of bacteria. *The journal of physical chemistry B,* 109**,** 312-320.

RIDING, M. J., MARTIN, F. L., TREVISAN, J., LLABJANI, V., PATEL, II, JONES, K. C. & SEMPLE, K. T. 2012. Concentration-dependent effects of carbon nanoparticles in gram-negative bacteria determined by infrared spectroscopy with multivariate analysis. *Environ Pollut,* 163**,** 226-34.

RIESENFELD, C. S., GOODMAN, R. M. & HANDELSMAN, J. 2004. Uncultured soil bacteria are a reservoir of new antibiotic resistance genes. *Environmental microbiology,* 6**,** 981-989.

RIZZO, L., MANAIA, C., MERLIN, C., SCHWARTZ, T., DAGOT, C., PLOY, M., MICHAEL, I. & FATTA-KASSINOS, D. 2013. Urban wastewater treatment plants as hotspots for antibiotic resistant bacteria and genes spread into the environment: a review. *Science of the total environment,* 447**,** 345-360.

SCHMIEDER, R. & EDWARDS, R. 2012. Insights into antibiotic resistance through metagenomic approaches. *Future microbiology,* 7**,** 73-89.

SCHMITT, J. & FLEMMING, H.-C. 1998. FTIR-spectroscopy in microbial and material analysis. *International Biodeterioration & Biodegradation,* 41**,** 1-11.

SCHWARTZ, T., KOHNEN, W., JANSEN, B. & OBST, U. 2003. Detection of antibiotic-resistant bacteria and their resistance genes in wastewater, surface water, and drinking water biofilms. *FEMS microbiology ecology,* 43**,** 325-335.

SMILLIE, C. S., SMITH, M. B., FRIEDMAN, J., CORDERO, O. X., DAVID, L. A. & ALM, E. J. 2011. Ecology drives a global network of gene exchange connecting the human microbiome. *Nature,* 480**,** 241-4.

SOMMER, M. O. A., DANTAS, G. & CHURCH, G. M. 2009. Functional Characterization of the Antibiotic Resistance Reservoir in the Human Microflora. *Science,* 325**,** 1128-1131.

SONG, Y., YIN, H. & HUANG, W. E. 2016. Raman activated cell sorting. *Curr Opin Chem Biol,* 33**,** 1-8.

STREIT, W. R. & SCHMITZ, R. A. 2004. Metagenomics–the key to the uncultured microbes. *Current opinion in microbiology,* 7**,** 492-498.

TAKAHASHI, N. Microbial ecosystem in the oral cavity: metabolic diversity in an ecological niche and its relationship with oral diseases. International Congress Series, 2005. Elsevier, 103-112.

TREVISAN, J., ANGELOV, P. P., CARMICHAEL, P. L., SCOTT, A. D. & MARTIN, F. L. 2012. Extracting biological information with computational analysis of Fourier-transform infrared (FTIR) biospectroscopy datasets: current practices to future perspectives. *Analyst,* 137**,** 3202-15.

TREVISAN, J., ANGELOV, P. P., PATEL, I. I., NAJAND, G. M., CHEUNG, K. T., LLABJANI, V., POLLOCK, H. M., BRUCE, S. W., PANT, K. & CARMICHAEL, P. L. 2010. Syrian hamster embryo (SHE) assay (pH 6.7) coupled with infrared spectroscopy and chemometrics towards toxicological assessment. *Analyst,* 135**,** 3266-3272.

TYERS, M. & MANN, M. 2003. From genomics to proteomics. *Nature,* 422**,** 193-197.

WALSH, M. J., BRUCE, S. W., PANT, K., CARMICHAEL, P. L., SCOTT, A. D. & MARTIN, F. L. 2009. Discrimination of a transformation phenotype in Syrian golden hamster embryo (SHe) cells using AtR-FtIR spectroscopy. *Toxicology,* 258**,** 33-38.

WHITMAN, W. B., COLEMAN, D. C. & WIEBE, W. J. 1998. Prokaryotes: the unseen majority. *Proceedings of the National Academy of Sciences,* 95**,** 6578-6583.

WOOD, B. R., QUINN, M. A., TAIT, B., ASHDOWN, M., HISLOP, T., ROMEO, M. & MCNAUGHTON, D. 1998. FTIR microspectroscopic study of cell types and potential confounding variables in screening for cervical malignancies. *Biospectroscopy,* 4**,** 75-91.

ZARNOWIEC, P., LECHOWICZ, L., CZERWONKA, G. & KACA, W. 2015. Fourier Transform Infrared Spectroscopy (FTIR) as a Tool for the Identification and Differentiation of Pathogenic Bacteria. *Current medicinal chemistry,* 22**,** 1710-1718.

Chapter 1 Fingerprinting microbiomes towards screening for microbial antibiotic resistance

Naifu Jin, Dayi Zhang, Francis L. Martin

Integrative Biology, 2017, 9, 406 – 417.

Fingerprinting microbiomes towards screening for microbial antibiotic resistance

Naifu Jin[1], Dayi Zhang[1,*], Francis L. Martin[2,*]

[1]*Lancaster Environment Centre, Lancaster University, Lancaster LA1 4YQ, UK;*

[2]*School of Pharmacy and Biomedical Sciences, University of Central Lancashire, Preston PR1 2HE, UK*

***Corresponding authors:** Dayi Zhang, Email: d.zhang@lancaster.ac.uk; Francis L Martin, Email: flmartin@uclan.ac.uk

Abstract

There is an increasing need to investigate microbiomes in their entirety in a variety of contexts ranging from environmental to human health scenarios. This requirement is becoming increasingly important with emergence of antibiotic resistance. In general, more conventional approaches are too expensive and/or time-consuming and often predicated on prior knowledge of the microorganisms one wishes to study. Herein, we propose the use of biospectroscopy tools as relatively high-throughput, non-destructive approaches to profile microbiomes under study. Fourier-transform infrared (FTIR) or Raman spectroscopy both generate fingerprint spectra of biological material and such spectra can readily be subsequently classed according to biochemical changes in the microbiota, such as emergence of antibiotic resistance. FTIR spectroscopy techniques generally can only be applied to desiccated material whereas Raman can be applied to more hydrated samples. The ability to readily fingerprint microbiomes could lend itself to new approaches in determining microbial behaviours and emergence of antibiotic resistance.

1. Microbiomes and their response to the natural environment

Microbial communities, including bacteria, archaea, viruses, protists or fungi, play a vital role in many ecosystems. Global carbon cycles in the ocean, for instance, at least 50% of carbon dioxide is fixed through photosynthesis providing the energy for microbial respiration and reproduction[1, 2]. Human health is also highly dependent on microbes since a very abundant mix of bacterial species symbiotically survives within humans and many principal organs are their habitats. The skin surface is the largest habitat with multiple regional variations in cellular architecture and environmental exposures for microbes, where the density of bacteria can reach 10^7 cells per square centimetre[3]. However, bacteria colonizing on external surfaces only count for some 10% (*i.e.*, 10^{14} bacterial cells to 10^{13} human cells) while the rest 90% comprise the commensal microbiome living in the body[4-9]. A majority of these microbial cells exist in the gastrointestinal tract (GIT) and constitute the human intestinal microbiota, which has a concentration of 10^{12} CFU/g and probably represents one of the densest, most biodiverse and rapidly evolving bacterial ecosystems on earth[4-9]. Another representative example is the microbial flora in the oral cavity as the entrance of the digestive tract; over 500 microorganism species have been identified and can attach to oral surfaces and colonize to form a microbial matrix, *e.g.*, dental plaque or oral biofilm[10]. The dynamics of human host microbial communities account for many diverse phenomena associated with public health issues, *e.g.*, changes in the gut microbial community may be linked to metabolic disorders, obesity and Crohn's disease[11].

Antibiotics are widely used to treat microbe-induced diseases and are also applied at sub-therapeutic levels *via* animal feed to maintain meat quality and quantity. Since Sir Alexander Fleming identified penicillin in 1928, the environment has become the primary receiver for most applied antibiotics and their residues *via* excretion of human and animals[12-18]. Currently, antibiotics are ranked as the third most commonly prescribed class of agents, and

frequently used in human medicine, agriculture, aquaculture and the agri-food industry, resulting in an enormous amounts of antimicrobial usage[19]. Accordingly, antibiotic misuse may result in a seriously antibiotic-abundant circumstance for microbes as well as humans. Consequently, in response to such environmental stimuli, bacteria acquire the capability of antibiotic resistance, and ultimately superbugs may emerge[20]. It is worth highlighting that microbiota from humans and natural environments are not separated but connected *via* various routes of exposure. For example, horizontal gene transfer (HGT) allows rapid development of genetic divergence and therefore leads to virulence, antibiotic resistance, and xenobiotic metabolism, spreading through microbe populations inhabiting in human bodies and natural environments[21]. HGT accelerates the spread of antibiotic resistance genes (ARGs) and emergence of superbugs, which is a lethal threat to humans and therefore a major focus of scientific interest[22, 23].

With such growing concerns, ARGs and their relevant mechanisms have been identified in clinical and environmental contexts[12-18, 24-27]. Many approaches have been applied to investigate their existence and spread as well as their dynamics within natural microbiota. Herein, we briefly discuss the conventional methods used to determine antibiotic resistance and ARGs within the microbial community, both phenotypically and genetically, as well as how biospectroscopy can be applied to fingerprint microbiomes and microbial antibiotic resistance.

2. Conventional biological approaches to determine microbial antibiotic resistance

Research into microbial antibiotic resistance primarily uses different techniques and methodologies, generally categorized as function- and molecular-based methods according to focus, *i.e.*, function-based approaches aim at particular behaviour or mechanisms of individual microbes based on their roles or characteristics, while molecular-based approaches target in

high-throughput fashion the molecular components within the complex microbiotas.

2.1 Function-based approaches

Culturing is the most applied function-based approach to determine microbial response to antibiotics[2, 28, 29] due to its inherent merit which is a focus on individual strains, instead of the interrogated complexity and diversity of the whole microbiota[30, 31]. Most known antibiotic-resistant microbes and genes are identified by direct culturing, isolate purification, and further investigation into their resistance profiles[25,32, 33]. For example, colonies grown with antibiotics are screened for the presence of antibiotic biomarkers, located on either plasmids or chromosomes[33]. However, >90% bacteria are currently unculturable but functional *in-situ*[34-36]. Culture-dependent methods are always questioned for their ability to represent the real scenario and for an underestimation of ARG abundance[31]. Some improved techniques, such as stable isotope probing (SIP) and magnetic nanoparticle-mediated isolation, further enumerate the functional fractions, not individual, from the total microbiota[37, 38].

2.2 Molecular-based approaches

Instead of targeting microbes with specific functions, molecular-based approaches deal with microbiota as an integrated system by directly extracting biological components. With the rapid development of molecular tools, molecular-based approaches have evolved from polymerase chain reaction (PCR) and denaturing gradient gel electrophoresis (DGGE) to high-throughput sequencing and *Omics*[31, 39, 40], uncovering ARGs from all the microorganisms within a microbiota, including those uncultured[39, 41-43]. Notably, the recent development of *Omics*, from genomics to proteomics, allows generation of large-scale datasets for cellular components (DNA, RNA, and proteins) compositions, interactions and profiles, yielding a comprehensive database of genetic functions of ARGs[40], *e.g.*, isolating novel ARGs from microbial communities of human oral and soil[39, 44]. However, molecular-based approaches have an inherent insufficiency in confirming behavioural functions and linking those functions to

identities of antibiotic-resistant strains. Meanwhile, as destructive methods of collecting cellular components, molecular-based approaches may not meet the need for *in-situ* diagnosis of antibiotic resistance in real-time.

2.3 *Which is more important?*

Individual vs. microbiome. It is hard to answer which, single cells or the whole communities, needs to be investigated to better understand antibiotic resistance in the microbiome. ARGs and antibiotic resistance mechanisms vary between individuals, implying insight into the single cell may provide more comprehensive information. On the other hand, although individual cells hold their respective ecological niche, they also contribute to the overall function of the microbiome as a whole. Since most microbes are somewhat dormant in the natural environment within developing communities such as mat, sludge or biofilm, it is worth paying more attention for clinical purposes to the response of the microbiome to antibiotics, rather than that of individual cells, *i.e.*, typically, an unnecessary single-cell-level test is required for the diagnosis of diseases. Biofilm, for instance, consists 2% to 15% of microorganisms with the remainder being their self-produced matrix of extracellular polymeric substances (~90%) secreted by microbes making individual cells stick together and colonize on a surface; this overall community performs functional tasks similar to multi-cellular organisms for adaptation to environmental changes[45-49]. Extracellular polymeric substances matrix facilitates communication between cells (*e.g.*, such as quorum sensing), maintains biofilm hydration and protects microorganisms against environmental stresses. The chemical composition and structure of extracellular polymeric substances depend on cell species, metabolic activity, nutrient availability, biofilm maturity level and physicochemical conditions. Biofilm formation offers microbes an entirely different lifestyle weighing against the planktonic state providing protection from external exposures (*e.g.*, antibiotics) for the community[45-49]. Recently, the field of single cell study has developed some breakthroughs allowing characterisation and

interrogation of particular microbes at reasonable levels[50-60]. However, these remain insufficient to fulfil the need to study microbial interactions within the microbiome and their surrounding environment. Thus, further research into the functionality of the entire microbiome is needed.

Phenotype vs. genotype. Stochasticity in gene expression may induce genetically-identical cells under the same environmental exposures to express significant variation in molecular content and discriminating differences in phenotypic characteristics; this implies cell functions may be altered by non-genetic regulation providing a mechanism for phenotypic and cell-type diversification regardless of genotype[61-63]. Such phenotypic heterogeneity helps microbes survive exposures to antibiotics owing to the fact that a small genetically-identical subset of persistent cells can survive an extended period and get over the exposure time[61]. This phenomenon may bring another challenge regarding *in-situ* diagnosis of antibiotic resistances of interrogated microbiomes since the phenotype of the microbiome may be unpredictable even under an acknowledged circumstance due to the influence of epigenetic factors[64, 65]. Therefore, finding a new approach that can quickly screen the phenotype of a microbiome to determine the *in-situ* bacterial antibiotic resistance in real-time is urgently required.

3. A new dawn for biospectroscopy in microbiological research

3.1 Principles of biospectroscopy

Biospectroscopy encompasses a range of techniques that allow the spectroscopic examination of biological samples. Such spectroscopic measurements are usually based on electronic transitions and vibrational changes of chemical bonds with spatial resolutions from the microscopic to the macroscopic. These both examine the morphological contrast in biological samples and uncovers elemental or molecular information *via* further determination[66]. Infrared (IR) or Raman spectroscopy are the two most applied biospectroscopy techniques since the 1960s[67, 68].

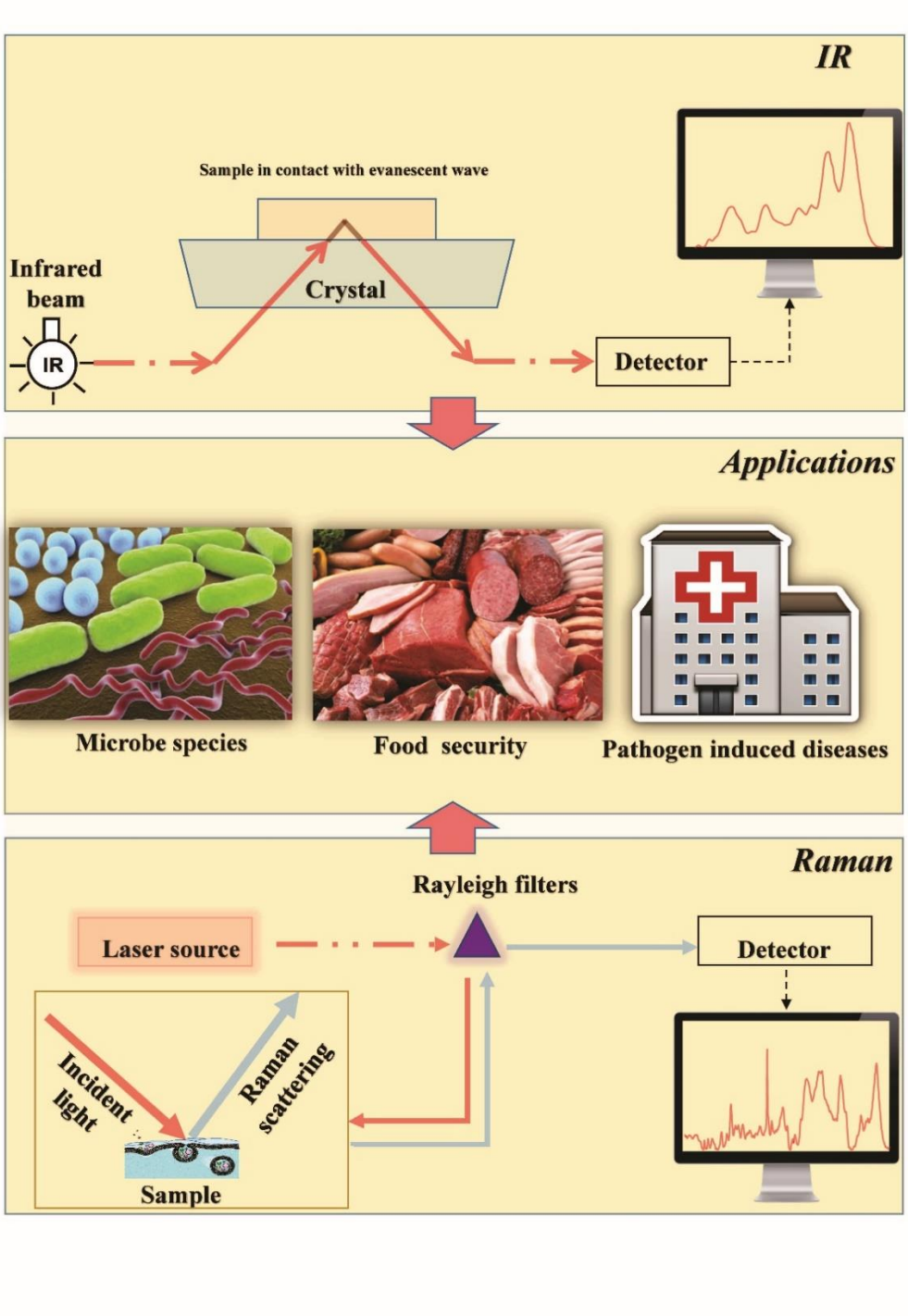

Figure 1. The principle of the biospectroscopic fingerprinting in identifying microbial species, examining food security and diagnosing pathogen-induced diseases. IR is capable of measuring the electric dipole state of chemical bonds in cellular molecules; Raman is a complementary tool exploiting the inelastic scattering of the targeted biological samples even under a hydrated environment.

When biomolecules contain chemical bonds with an electric dipole moment, these vibrations are detectable and measurable by IR spectroscopy[69]. Categorized according to wavelengths (*i.e.*, near-IR, mid-IR or far-IR), mid-IR (MIR) spectroscopy (4000-400 cm^{-1} in wavenumbers) is the most applied in biospectroscopy because it not only includes overtones but also contains fundamental vibrational transitions, providing inherently stronger signal intensities in terms of the increased absorption cross-section[70]. In 1991, FTIR spectroscopy was innovatively introduced as a sensitive and rapid screening tool for characterization, classification and identification of microorganisms[71]. Since then, FTIR has been extensively used in microbial research[72-75]. Among FTIR spectroscopic techniques, the most frequently applied IR spectroscopic techniques are transmission, transflection or attenuated total reflection (ATR)[72]. ATR-FTIR (***Figure 1***), for instance, which employs an internal reflection element with a high refractive index (*e.g.*, diamond, germanium or zinc selenide), directs the IR beam for the total internal reflection and produces an evanescent wave that penetrates beyond the element by 1 μm to 2 μm. It is used to interrogate biological samples allowing absorption of IR light and subsequently production of absorbance spectra[69, 72]. This process can reveal biochemical information regarding cellular changes or alterations of samples. However, there is a significant limitation within FTIR in that water from instrumentation or samples may induce reduction of IR light transmission[69, 72]. Hence, it is crucial to purge the instrumentation with dry air or nitrogen, as well as desiccants to remove any water vapour before spectral acquisition[72]. FTIR is a valuable metabolic fingerprinting tool owing to its abilities to characterize cellular composition[72-78]. In the mid-IR spectroscopy, the biochemical fingerprint region is from 1800 - 900 cm^{-1}, and representative peaks include: lipids (~1750 cm^{-1}), Amide I (~1650 cm^{-1}), Amide II (~1550 cm^{-1}), Amide III (~1260 cm^{-1}), carbohydrates (~1155 cm^{-1}), asymmetric phosphate stretching vibrations (ν_{as} PO_2^-, ~1225 cm^{-1}), symmetric phosphate stretching vibrations ($\nu_s PO_2^-$, ~1080 cm^{-1}), glycogen (~1030 cm^{-1}), protein phosphorylation

(~970 cm^{-1})[69, 72, 77, 79, 80]. These peaks can be derived as biomarkers for characterization of microbial cell types (even at subspecies level) and diagnosis of microbe-induced diseases[72-78]. Metabolomics is a critical field that biospectroscopy could complement in order to investigate microbial metabolism.

Raman spectroscopy, a complementary biospectroscopic technique to FTIR, can generate information regarding chemical bonds even under a hydrated environment[81-85]. The monochromatic light in the near-IR, visible or UV range is used in Raman spectroscopy (***Figure 1***) to exploit the inelastic scattering or Raman effect. In this process, the excitation of photons to virtual energy states and the resultant loss (Stokes) or gain (anti-Stokes) of energy occurs because of the interaction of light with vibrational modes associated with chemical bonds within the sample[80, 86]. This shift in energy is indicative of discrete vibrational modes of polarizable molecules, and thus a qualitative measurement of the biochemical composition can be obtained[80, 86]. However, the inelastic scattering does not occur efficiently, the incidence is <1% of the total photons absorbed by the molecules. Thus, backward light is then applied filtering off other interference, but the Raman scattering can reach the detector. Typically, the informative region of wavenumbers for biological samples is located within 400-2000 cm^{-1} and 2700-3500 cm^{-1}, including proteins (1500-1700 cm^{-1}), carbohydrates (470-1200 cm^{-1}), phosphate groups of DNA (980, 1080 and 1240 cm^{-1}) and higher-frequency bond vibrations of CH, NH and OH stretching in lipids and proteins[80, 87]. Applications of Raman spectroscopy in microbiology include bacterial discrimination, isolation, and identification[88-90].

3.2 *Applications of biospectroscopy in microbial research*

Compared to the conventional tools employed for identifying and characterizing the microbiome, biospectroscopy requires minimal sample amount and preparation, and is non-destructive and relatively high throughput[69, 72, 80]. Specifically, the minimal sample volume for ATR-FTIR and Raman spectroscopy is 3 μL and 1 μL respectively, much lower than those in

PCR, high-throughput sequencing, and *Omics* which require high quality and amount of DNA template extracted from several millilitres or grams of environmental samples. Additionally, biospectroscopy does not require extra labelling, primer design, and enzymatic reaction, significantly reducing the cost and time in diagnosing. More importantly, the non-destructive features of biospectroscopy allow its application *in vivo* and *in situ*. Some successful microbial applications of biospectroscopy (***Figure 1***) include characterization of hospital isolates and rapid quantitative detection of the microbial spoilage of food products[71, 77, 79, 91, 92]. There is no doubt that biospectroscopy is a robust tool for distinguishing bacterial responses to environmental exposures due to its particular attributes of being non-destructive, non-intrusive, high throughput and label-free[69, 72]. When coupled with conventional microscopy, biospectroscopy can be used to reproduce cell architecture from both the visual and biochemical perspective by the passing of spectral data through a variety of computational algorithms and capture of pictures simultaneously[69, 72]. It allows visualized monitoring and spectral interrogation undertaken *in-situ* in real-time, which is very helpful towards understanding the actual interactions between microbes and physical environment[66, 69, 72, 77, 80, 93, 94]. In the history of microbiological research, the microbiome is a particular hotspot in microbial ecology, challenging to all approaches to investigate it but bringing possibilities for biospectroscopy to be applied. As a very complicated bio-matrix, microbiomes contain various compositions contributing to the overall spectra, including extracellular polymeric substances (EPS), cell membrane, and the cytoplasm. The characteristic spectral peaks, *e.g.*, biological macromolecules, may assess the existence and composition of biofilms by summarising the wavenumbers of detected peaks. Most EPS induced biomarkers, for instance, fall in the range of 1700 - 100 cm^{-1} in Raman spectroscopy[95]. Also, the comparison between the microbial biofilms and planktonic communities could reveal relevant biochemical information[96]. Specifically, Bosch et al. found FTIR spectra of biofilms demonstrated higher intensity in the

absorption bands associated with polysaccharides (1200 - 900 cm^{-1} region) and vibrational modes of carboxylate groups (1627, 1405, and 1373 cm^{-1}) than those of the planktonic[74], showing evidence of dramatic difference of microbial living style within such communities.

4. Fingerprint microbiome *via* biospectroscopy

4.1 State of art

Owing to the non-destructive and high-throughput possibilities, biospectroscopy has many advantages in diagnosing antibiotic resistance within a microbiome over other approaches, either function- or molecular-based ones. It allows fast and low-cost screening for an enormous number of samples and also provides a chance for further analysis of relevant mechanisms. Additionally, biospectroscopy is capable of monitoring real-time population dynamics and subsequently providing information of genotypic changes. However, until now, few biospectroscopy-based studies have focused on microbial antibiotic resistance, and all of the published studies[97-99] investigate pure cultures. Lack of insight into microbiome structures *in situ* highlights the urgent need for novel approaches. The primary challenges currently include the lack of a reliable database, routine protocols, and reproducible computational analysis, which determine the feasibility of biospectroscopy distinguishing biomarkers representing antibiotic resistance from the numerous fingerprints in environmental backgrounds.

Herein, we propose a state-of-the-art biospectroscopic application in assessing microbial antibiotic resistance within a microbiome. Within a microbiota of interest, there is no doubt biospectroscopy has the ability to allow the quick identification of microbial species within a well-built dataset[97]. Furthermore, biospectroscopy can diagnose microbe-induced diseases in clinical settings contributing to the advantages of early detection and stratification of at-risk patients to initiate timely and appropriate treatment[100-103]. Raman spectroscopy has successfully identified sepsis in blood plasma from 70 patients with a satisfactory sensitivity of 1.0 and specificity of 0.82[101]. The feasibility of biospectroscopic investigation into microbial

alterations induced by exposures has also been evaluated. Riding et al. applied IR spectroscopy to fingerprint microbes following exposure to carbon nanoparticles, and revealed concentration- and size-dependent changes in cellular components[104]. Another study[105] confirmed the ability of IR spectroscopy to characterize changes induced by carbon nanoparticles *via* investigating their effects in both Gram positive and negative bacteria. Some discriminant biochemical markers, *i.e.*, Amide II and carbohydrate, were picked out to verify the distinct alterations in bacteria with respective cell wall structures. These studies prove that biospectroscopy is not only able to distinguish microbial response to different kinds of exposures, but also specify variances resulting from bacterial structures, demonstrating its potential to diagnose antibiotic resistance with reliable biomarkers.

To investigate *in-situ* the construction and composition of microbiota in real-time, a non-destructive and non-intrusive method is required to delineate differentiation. Biospectroscopy is such an optical sensor, an *in-situ* non-labelling complementary to other molecular-based techniques, by directly and remotely measuring molecular vibration spectra in living cells[106] and biofilms[107]. Given this, we propose a new system for characterizing antibiotic resistance within whole microbiomes *via* a rapid and high-throughput manner (***Figure 2***). Firstly, by well-trained databases, the abundance of ARGs or microbes with ARGs in microbiotas can be quantified by evaluating the alteration ratio of biomarkers from multivariate statistical analysis. Furthermore, the dynamics of ARGs in microbiotas might be assessed in real-time *via* the interrogation of changes in biomarker change. Achieved in-situ and real-time investigation of antibiotic resistance, the ultimate goal of this approach is to monitor and diagnose both the presence and change of ARGs in unknown environmental or human samples of interest, differentiating alterations of discriminating biomarkers *in-situ* and real-time without referencing trained datasets.

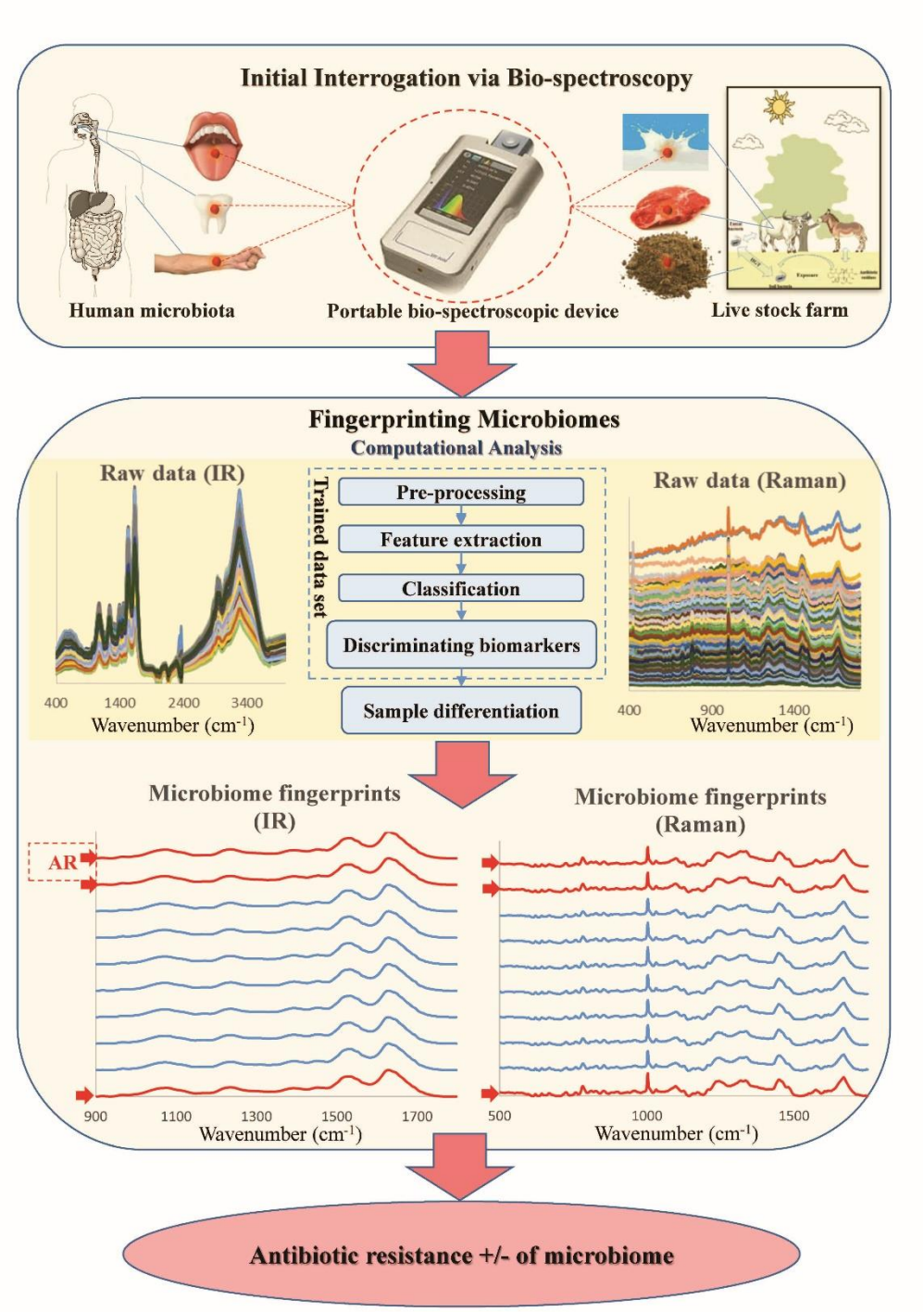

Figure 2. Schematic diagram of biospectroscopy fingerprinting microbiome for antibiotic resistance. Portal bio-spectroscopic devices achieve *in situ* and real-time interrogation of spectra from the samples of interest, e.g. human microbiome and livestock farm microbiome. The fingerprints are further processed via computational analysis (pre-processing, feature extraction, classification, discrimination, and differentiation) to distinguish the spectral

biomarkers of antibiotic resistance. Comparing to well-trained databases with both positive and negative controls, the biomarker alterations can examine the antibiotic resistance capability of the targeted microbiome or even quantify the abundance of antibiotic resistance genes.

4.2 *Proof of concept*

Our pre-validating results indicate biospectroscopy can determine the abundance of bacteria with ARG in microbiome (Figure 3A), despite disparate bacterial types and community composition (Gram-positive or Gram-negative; Figure 3B). From the well-trained dataset and discriminating biomarkers (Figure 3C), the fingerprints of unknown microbiomes are allocated and assigned with their ARGs abundance after encoding. Furthermore, both the static and dynamic microbial matrices can be quantified by biospectroscopy due to inherently non-destructive and non-intrusive attribute (Figure 3D). Here, biospectroscopy is validated as a high throughput screening method for characterization of microbial composition and ARGs abundance in complex matrices.

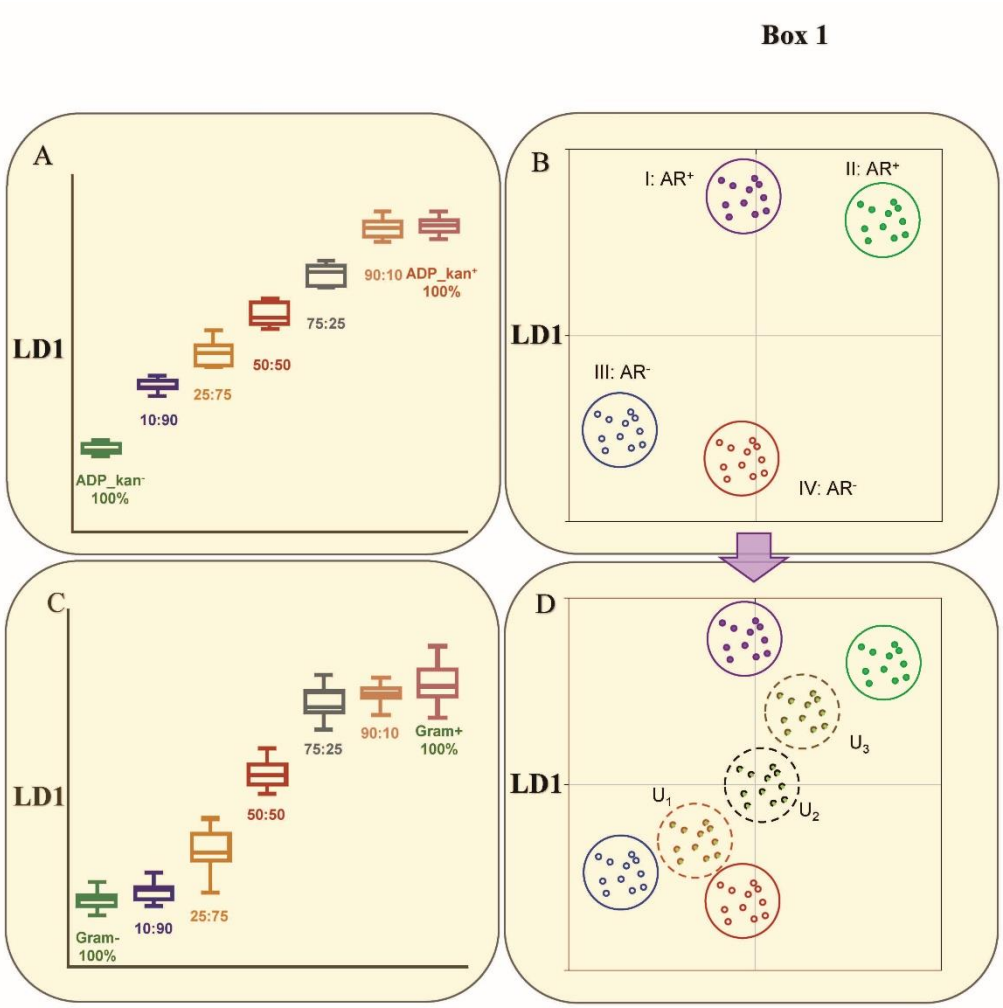

Figure 3. Pre-validation proves the feasibility of interrogating the abundance of ARGs and ratio of Gram-positive to Gram-negative bacteria in microbiomes. ARGs identification in microbiome by biospectroscopic fingerprints *via* a Bruker TENSOR 27 FTIR spectrometer (Bruker Optics Ltd., UK) equipped with a Helios ATR attachment containing a diamond internal reflection element (IRE). Instrument parameters were set at 32 scans, 16 cm^{-1}

resolution. A total of 30 spectra were acquired for each treatment (3 replicates) through the ATR magnification-limited viewfinder camera. (A) Prediction of ARGs abundance in artificial microbial communities containing different compositions of two *Acinetobacter baylyi* mutants, ADP_kan$^-$ and ADP_kan$^+$, which are genetically identical apart from the kanamycin resistance gene located on the chromosome of ADP_kan$^+$. Under kanamycin antibiotic pressure, *i.e.*, treated with final concentration of kanamycin, the discriminant biomarkers were (~980 cm^{-1}), Oligosaccharide C-OH stretching band (~1138 cm^{-1}), Deoxyribose (~1188 cm^{-1}), Amide III (~1242 cm^{-1}), In-plane CH bending vibration from the phenyl rings (~1500 cm^{-1}), C=O stretching, lipids (~1740 cm^{-1}). The LDA distance is positively correlated with the ratio of ADP_kan$^-$/ADP_kan$^+$ and the linear regression, therefore, can be used for ARG abundance calculation. (B) Prediction of microbial community composition artificial microbial communities containing Gram-positive (*Mycobacterium vanbaalenii*, Gram^{+ve}) and Gram-negative (*Acinetobacter baylyi* ADP_kan$^+$, Gram^{-ve}) bacteria. The positive correlation between LDA distance and the ratio of Gram^{+ve}/ Gram^{-ve} helps in determining the abundance of each strain. (C) Dataset from LDA differentiation of four reference bacterial strains (AGR$^+$: bacteria I and bacteria II with ARG; AGR$^-$: bacteria III and bacteria IV with no ARG). The dataset is well trained for separating ARG$^+$ and ARG$^-$ bacteria. (D) LDA differentiation of unknown microbiome (U_1, U_2, and U_3) compared to training dataset to determine the abundance of ARG. Based on the values generated from LDA analysis, their biochemical distances can be calculated. These results validate bio-spectroscopy is capable of characterizing and quantifying ARGs of microbes via their phenotypes in both genetically identical and differential microbial communities. Also, it can be used to determine antibiotic resistance of unknown samples by calculating their biochemical distances.

5. Challenges and solutions

5.1 *Dataset*

As mentioned above, a well-trained dataset is the key for biospectroscopic fingerprinting microbiome and also the first fundamental problem challenge concerned which can eliminate confounding factors, *i.e.*, criteria may contribute a disruption to the core purpose of the study. To achieve this goal, the database of relevant molecular fingerprint and their assignments (such as nucleic acids, proteins, polysaccharides, carbohydrate, and lipids) have to be well-characterised since the bio-spectroscopic classifications are based on calculating alterations of interaction involved cellular compositions. This work may significantly improve bio-spectroscopy from both quantity and quality criteria[108]. Detailed information of the most widely used peak frequencies and their assignments refers to the reviews of IR[108], Raman[52, 87], and ratios (X cm^{-1}/Y cm^{-1})[109]. These peaks with remarkable alterations are determined as discriminating biomarkers for diagnosis of changes resulted by specific exposures in many studies[69, 87, 104, 105, 108, 110]. However, no biospectroscopy-relevant study has yet been found associated with biomarkers for antibiotic resistance of microbiomes.

5.2 *Growth phase and environmental variants*

Another major concern for the overall study (*i.e.*, confounding factors) is bacterial communities are incredibly complicated in terms of their composition, species, dynamics of population, growth phase and nutrient depletion impacts[111-114]. Growth phase effect for instance, which may result in remarkable discrepancies within cell growth circle regarding physical features and biochemical compositions. Ede et al.[115] reported all the examined species showed significant spectral differences through their growth phases in a study of assessing cell population growth *via* ATR-FTIR. They found *B. stearothermophilus* had a major change associated with lipid content and reached peak position during the log phase; for the halophiles *H. salinarium and H.morrhuae*, the most significant alteration was the concentration of

sulphate ion. Mainly, at the mid-log phase, *A. aceti* cells showed increasing polysaccharide content along with and also a maximum change of lipid content was noticed during the log phase. These growth phase induced changes may lead to distinct responses of microbes to exposures[115-118].

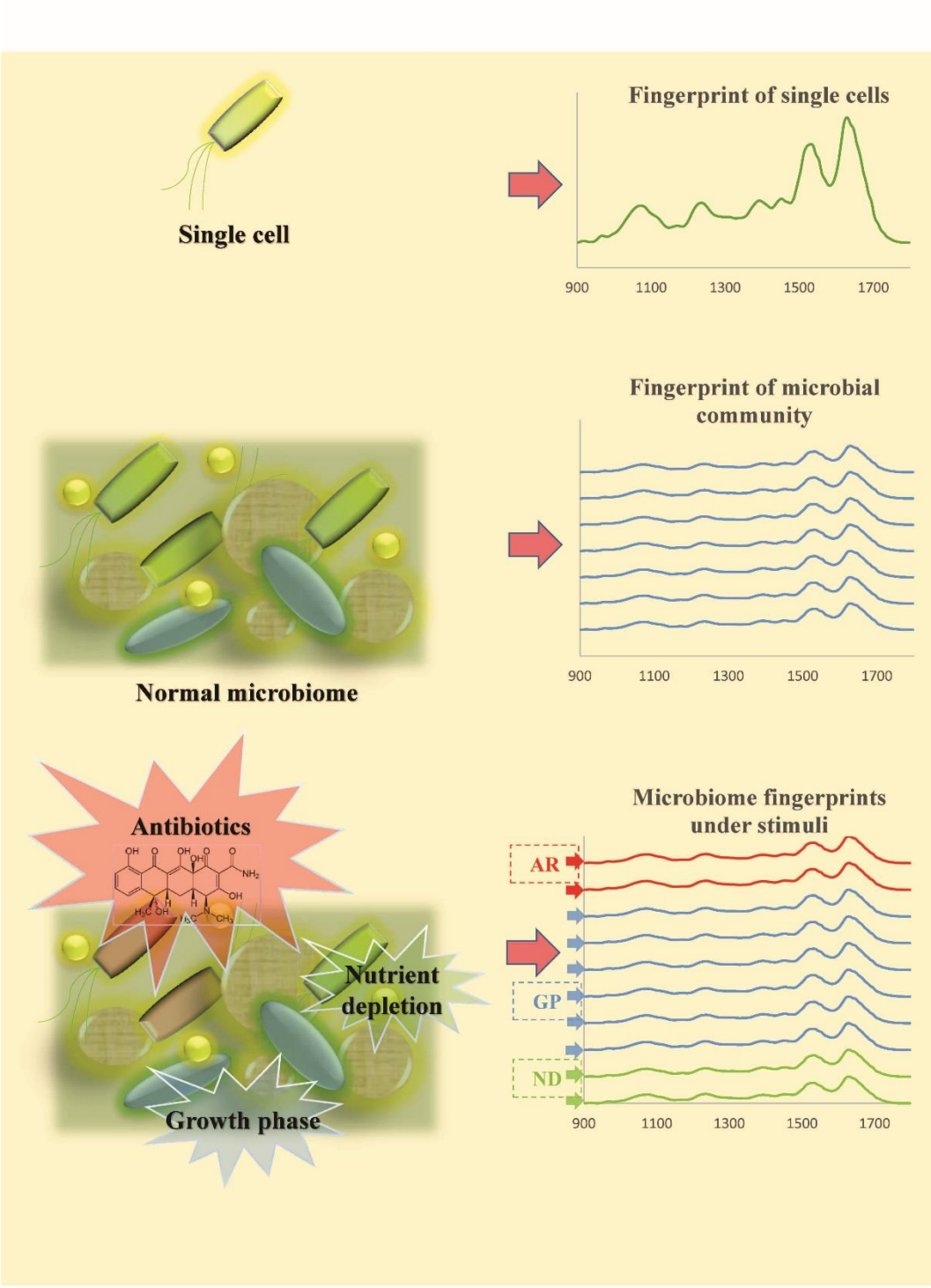

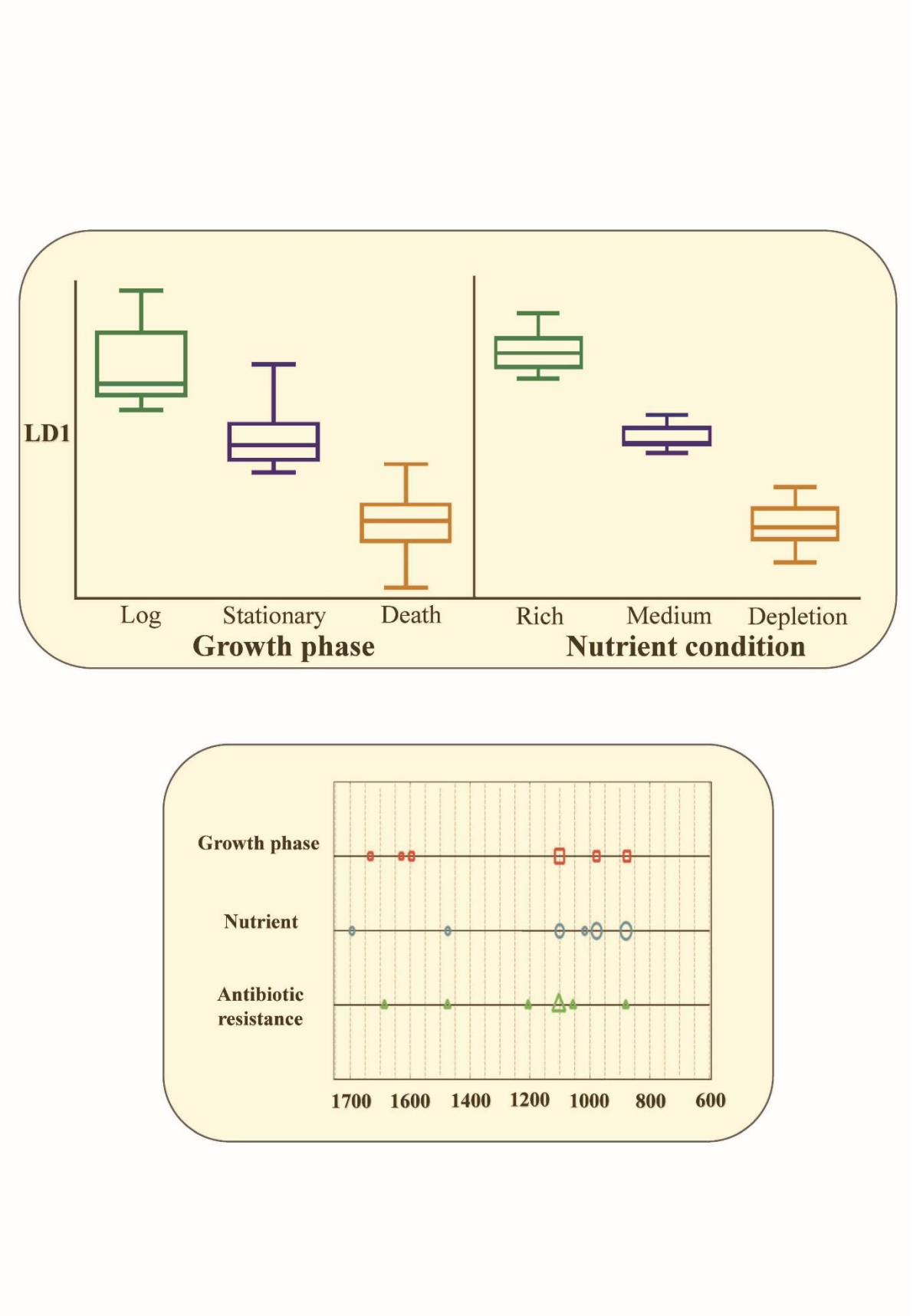

Figure 4. Pre-validation of solutions for proposed challenges of growth phase and nutrients.

The well-trained dataset eliminating other environmental interference is built-up in several steps: 1) Reference dataset acquisition from individual single cell of different species representing their biospectral attributes; 2) Biospectra acquisition from the targeted microbiome; 3) Biospectra acquisition from the targeted microbiome postexposure to antibiotics to recognize and separate the discriminating spectral alterations via multivariate analysis; 4) The identical and consistent spectral alterations representing antibiotic resistance markers are clustered for interrogating the targeted microbiome.

A substantial alteration gradient of bio-spectra is noticed along with growth phase and nutrient conditions, respectively. However, discrimination of antibiotic resistance biomarkers is independent of growth phase and nutrient conditions (Figure 4). The biomarkers of antibiotic resistance, *i.e.*, phenylalanine (protein assignment) (~1004 cm^{-1} and ~1376 cm^{-1}), hydroxyapatite, carotenoid, cholesterol (~957 cm^{-1}), uracil-based ring breathing mode (~780 cm^{-1}), carbohydrates (~1105 cm^{-1}), phenylalanine, hydroxyproline (~1586 cm^{-1}), are significantly discriminated from those of growth phases, phenylalanine or bound & free NADH (~1000 cm^{-1}), phosphatidylinositol (~776 cm^{-1}), C-C-N^+ symmetric stretching (lipids) or C-O-C ring (carbohydrate) (~877 cm^{-1} and ~1495 cm^{-1}), Amide I (~1634 cm^{-1} and ~1530 cm^{-1}); and nutrients, uracil-based ring breathing mode (~780 cm^{-1}), C-C-N^+ symmetric stretching (lipids) or C-O-C ring (carbohydrate) (~877 cm^{-1}), phenylalanine or bound & free NADH (~1000 cm^{-1}), proline, hydroxyproline or glycogen and lactic acid (~918 cm^{-1}, ~1695 cm^{-1} and ~1375 cm^{-1}) implying biospectroscopic is able to identify antibiotic resistance within a microbiome regardless of impacts from growth phase and nutrient condition. Therefore, these discriminating biomarkers associated with antibiotic resistance reveal the potential feasibility for *in-situ* diagnosis of real samples despite environmental variants. It is worth mentioning that discrimination of antibiotic resistance biomarkers might be also affected by the complicated effects of antibiotics on both targeted microbiome and their matrix environment, particularly

in case of interrogating biofilm on mammalian tissues. The production of tissue mucus and other components or the interference signals from mammalian tissues themselves can bring challenges in distinguishing the proper biospectral biomarkers. Although no previous report has answered this question yet, some potential solutions eliminating background noise include separating microbiome from via optical tweezers[119] or flow cytometry [120].

5.3 *Computational analysis*

It needs to be highlighted the most vital component associated with biospectroscopic determination for antibiotic resistance of microbiome is to find discriminating biomarkers, *i.e.*, the most absolute and representative peaks derived from acquired spectra, allowing subsequently high throughput screening for determination of antibiotic resistance. Although some alterations of biomarkers can be visualized by eyes, the questions always emerge regarding the existence of noticed difference and the reliability of subjective assessing by eye. Hence, computational analysis is applied to exam the data due to the acquired spectrums holding an enormous number of features.

The pre-processing is the first step of computational analysis which aims to reduce effects resulted from spectral acquisition and subsequently enhance the robustness and accuracy as well as making all the raw data comparable[72]. Categories of pre-processing include de-noising, spectral correction, normalization and combinations of these processes. For a raw dataset of Raman, a noise-reduction smoothing step is commonly applied to increase the SNR (signal-to-noise ratio) and highlight spectral features associated with biochemical information[69]. PCA is also used to achieve the purpose of de-nosing because the most valuable features of spectra can be represented by several significant PCs while the rest PCs containing a majority of noise can be ignored. Furthermore, there is a huge challenge in the procession of raw data, *i.e.*, sloped or oscillatory baselines associated with resonant Mie scattering in IR spectroscopy or fluorescence in Raman spectroscopy[72]. To solve this issue, rubber band baseline correction is applied for IR

which produced a convex polygonal line to correct the bottom edges of the spectra; and polynomial fit for Raman, which generates a polynomial baseline to adjust the spectral minima[121]. Also, the most vital part of pre-processing is the normalization, which eliminates the confounding factors, thickness or concentration, for instance, making acquired spectra comparable within intra-class and inter-class. For biological samples, Amide I (~1650 cm-1)/II (~1550 cm^{-1}) is usually applied after baseline correction for IR data; and vector normalization (Euclidean or L2-norm) is used for Raman data[72, 121].

Moreover, the multivariate statistical analysis is an ideal tool for spectral analysis. In 2010, Martin et al. proposed two objectives for spectral assessing biological materials using multivariate statistical analysis: (i) to determine similarities and differences between classes (categories within the dataset, *e.g.*, cell types); and (ii) to identify the spectral bands that mostly relate to these similarities and differences. So as to meet the objectives, classification is introduced as one of the core components in multivariate analysis, which typically relies on clustering techniques, such as hierarchical cluster analysis, k-means clustering, fuzzy C-means clustering and PCA. Furthermore, PCA-LDA is an ideal classification tool to investigate intra-class or interclass variation. As compared to PCA alone, the additional linear discriminant analysis derives vectors from the principal components (PCs) and minimizes the within-category differences (mostly be associated with typical heterogeneity in any biological sample) while maximizing between-category discriminating characteristics (i.e., those most likely to be induced by treatments or other exogenous contributions)[69, 72, 80].

6. Future prospects

The introduction of biospectroscopic screening allows rapid in-situ diagnosis of antibiotic resistance in microbiomes as well as real-time detection of population dynamics and determination of genotype flexibility (*e.g.*, HGT process and microbial response to antibiotic pressure) *via* monitoring phenotype differentiation, which can significantly improve the

understanding of antibiotic resistance in the clinical and physical environment. Furthermore, a combination of cultivation-based approaches coupled with fast screening may solve the inherent limitation of cultivation that microbial functioning in natural environments is difficult to study by cultivation solely due to uncultivable microbes and their complicated community constructions[93, 122]. Also, with the non-destructive character of bio-spectroscopic fast screening reducing the amount of interrogating targets, many other techniques can be attached for further investigation, *e.g.*, single cell sorting[54, 57], -omics[40], etc. One good example can be found in Huang's work describing novel marine strain identification via Raman spectroscopy coupled with single-cell genomics[123]. Raman spectra are also reported in morphology-specific genomic analysis of human tissues combined with microdissection sequencing[124] or characterizing metabolic alterations in mouse liver coupled with metabolomics and transcriptomics[125]. These combinations may significantly enhance the study of the relevant mechanisms providing an opportunity for direct determination of precisely functional genes and proteins. Ultimately, genotype and phenotype can be linked together from the population, single cell, and molecular perspectives to determine the antibiotic resistance in the microbiota of interest and consequently help us better understand the actual interactions among humans, microbes, and the physical environment.

REFERENCES

1. M. Breitbart and F. Rohwer, *Trends Microbiol.*, 2005, **13**, 278-284.
2. J. A. Fuhrman, *Nature*, 2009, **459**, 193-199.
3. N. Fierer, M. Hamady, C. L. Lauber and R. Knight, *Proc. Natl. Acad. Sci. U. S. A.*, 2008, **105**, 17994-17999.
4. M. Candela, E. Biagi, S. Maccaferri, S. Turroni and P. Brigidi, *Trends Microbiol.*, 2012, **20**, 385-391.
5. D. A. Hill, C. Hoffmann, M. C. Abt, Y. Du, D. Kobuley, T. J. Kirn, F. D. Bushman and D. Artis, *Mucosal Immunol.*, 2010, **3**, 148-158.
6. M. T. Bailey, S. E. Dowd, J. D. Galley, A. R. Hufnagle, R. G. Allen and M. Lyte, *Brain. Behav. Immun.*, 2011, **25**, 397-407.
7. C. Jernberg, S. Lofmark, C. Edlund and J. K. Jansson, *Microbiology*, 2010, **156**, 3216-3223.
8. K. Lu, R. P. Abo, K. A. Schlieper, M. E. Graffam, S. Levine, J. S. Wishnok, J. A. Swenberg, S. R. Tannenbaum and J. G. Fox, *Environ. Health Perspect.*, 2014, **122**, 284-291.
9. E. A. Mutlu, P. M. Gillevet, H. Rangwala, M. Sikaroodi, A. Naqvi, P. A. Engen, M. Kwasny, C. K. Lau and A. Keshavarzian, *Am J Physiol Gastrointest Liver Physiol*, 2012, **302**, G966-978.
10. N. Takahashi, *Int Congr. Ser.*, 2005, **1284**, 103-112
11. A. Gonzalez, J. C. Clemente, A. Shade, J. L. Metcalf, S. Song, B. Prithiviraj, B. E. Palmer and R. Knight, *EMBO Rep*, 2011, **12**, 775-784.
12. A. Koluman and A. Dikici, *Crit. Rev. Microbiol.*, 2013, **39**, 57-69.
13. J. W. Harrison and T. A. Svec, *Quintessence int.*, 1998, **29**, 223-229.
14. X. Ji, Q. Shen, F. Liu, J. Ma, G. Xu, Y. Wang and M. Wu, *J. Hazard. Mater.*, 2012, **235**, 178-185.
15. J. C. Chee-Sanford, R. I. Aminov, I. J. Krapac, N. Garrigues-Jeanjean and R. I. Mackie, *Appl. Environ. Microbiol.*, 2001, **67**, 1494-1502.
16. L. Cantas, S. Q. Shah, L. M. Cavaco, C. M. Manaia, F. Walsh, M. Popowska, H. Garelick, H. Burgmann and H. Sorum, *Front. Microbiol.*, 2013, **4**, 96.

17. M. Tandukar, S. Oh, U. Tezel, K. T. Konstantinidis and S. G. Pavlostathis, *Environ. Sci. Technol.*, 2013, **47**, 9730-9738.

18. J. L. Martinez and F. Baquero, *Ups. J. Med. Sci.*, 2014, **119**, 68-77.

19. J. Conly, *Can. Med. Assoc. J.*, 2002, **167**, 885-891.

20. M. Sundqvist, *Ups. J. Med. Sci.*, 2014, **119**, 142-148.

21. C. S. Smillie, M. B. Smith, J. Friedman, O. X. Cordero, L. A. David and E. J. Alm, *Nature*, 2011, **480**, 241-244.

22. G. D. Wright, *Chem. Biol.*, 2000, **7**, R127-R132.

23. T. Häusler, *Viruses vs. superbugs: a solution to the antibiotics crisis?*, Palgrave Macmillan, 2006.

24. P. Southern and P. Berg, *J. Mol. Appl. Genet.*, 1981, **1**, 327-341.

25. K. J. Forsberg, A. Reyes, B. Wang, E. M. Selleck, M. O. Sommer and G. Dantas, *Science*, 2012, **337**, 1107-1111.

26. J. L. Martínez, *Science*, 2008, **321**, 365-367.

27. A. A. Salyers, A. Gupta and Y. Wang, *Trends Microbiol.*, 2004, **12**, 412-416.

28. T. Schwartz, W. Kohnen, B. Jansen and U. Obst, *FEMS Microbiol. Ecol.*, 2003, **43**, 325-335.

29. C. Martin, J. Timm, J. Rauzier, R. Gomez-Lus, J. Davies and B. Gicquel, *Nature*, 1990, **345**, 739-743.

30. L. Rizzo, C. Manaia, C. Merlin, T. Schwartz, C. Dagot, M. Ploy, I. Michael and D. Fatta-Kassinos, *Sci. Total Environ.*, 2013, **447**, 345-360.

31. D. Nichols, *FEMS Microbiol. Ecol.*, 2007, **60**, 351-357.

32. M. R. Rondon, P. R. August, A. D. Bettermann, S. F. Brady, T. H. Grossman, M. R. Liles, K. A. Loiacono, B. A. Lynch, I. A. MacNeil and C. Minor, *Appl. Environ. Microbiol.*, 2000, **66**, 2541-2547.

33. N. A. Séveno, D. Kallifidas, K. Smalla, J. D. van Elsas, J.-M. Collard, A. D. Karagouni and E. M. Wellington, *Rev. Med. Microbiol.*, 2002, **13**, 15-27.

34. K. Bartscht, H. Cypionka and J. Overmann, *FEMS Microbiol. Ecol.*, 1999, **28**, 249-259.

35. J. Clardy and C. Walsh, *Nature*, 2004, **432**, 829-837.

36. W. R. Streit and R. A. Schmitz, *Curr. Opin. Microbiol.*, 2004, **7**, 492-498.

37. S. Radajewski, P. Ineson, N. R. Parekh and J. C. Murrell, *Nature*, 2000, **403**, 646-649.

38. D. Zhang, J. P. Berry, D. Zhu, Y. Wang, Y. Chen, B. Jiang, S. Huang, H. Langford, G. Li and P. A. Davison, *ISME J.*, 2015, **9**, 603-614.

39. C. S. Riesenfeld, R. M. Goodman and J. Handelsman, *Environ. Microbiol.*, 2004, **6**, 981-989.

40. M. Tyers and M. Mann, *Nature*, 2003, **422**, 193-197.

41. M. O. A. Sommer, G. Dantas and G. M. Church, *Science*, 2009, **325**, 1128-1131.

42. K. J. Forsberg, *The Diveristy, Ecology, and Clinical Implications of Antibiotic Resistance Genes in Uncultured Soil Microbial Communities*, PhD thesis, Univerisity in St. Louis, Washington, 2015.

43. J. Handelsman, *Microbiol. Mol. Biol. Rev.*, 2004, **68**, 669-685.

44. M. Diaz-Torres, R. McNab, D. Spratt, A. Villedieu, N. Hunt, M. Wilson and P. Mullany, *Antimicrob. Agents Chemother.*, 2003, **47**, 1430-1432.

45. H. C. Flemming and J. Wingender, *Nat. Rev. Microbiol.*, 2010, **8**, 623-633.

46. E. Karunakaran, J. Mukherjee, B. Ramalingam and C. Biggs, *Appl Microbiol Biotechnol*, 2011, **90**, 1869-1881.

47. X. N. Lu, D. R. Samuelson, B. A. Rasco and M. E. Konkel, *J. Antimicrob. Chemother.*, 2012, **67**, 1915-1926.

48. H. Y. N. Holman, R. Miles, Z. Hao, E. Wozei, L. M. Anderson and H. Yang, *Anal. Chem.*, 2009, **81**, 8564-8570.

49. P. S. Stewart, *Int. J. Med. Microbiol.*, 2002, **292**, 107-113.

50. D. Berry, E. Mader, T. K. Lee, D. Woebken, Y. Wang, D. Zhu, M. Palatinszky, A. Schintlmeister, M. C. Schmid and B. T. Hanson, *Proc. Natl. Acad. Sci. U.S.A.*, 2015, **112**, E194-E203.

51. W. E. Huang, M. J. Bailey, I. P. Thompson, A. S. Whiteley and A. J. Spiers, *Microb. Ecol.*, 2007, **53**, 414-425.

52. W. E. Huang, M. Q. Li, R. M. Jarvis, R. Goodacre and S. A. Banwart, A*dv. Appl. Microbiol., Vol 70*, 2010, **70**, 153-186.

53. W. E. Huang, Y. Song and J. Xu, *Microb. Biotechnol.*, 2015, **8**, 15-16.

54. W. E. Huang, A. D. Ward and A. S. Whiteley, *Environ. Microbiol. Rep.*, 2009, **1**, 44-49.

55. M. Li, D. G. Boardman, A. Ward and W. E. Huang, *Methods Mol. Biol.*, 2014, **1096**, 147-153.

56. M. Q. Li, J. Xu, M. Romero-Gonzalez, S. A. Banwart and W. E. Huang, *Curr. Opin. Biotechnol.*, 2012, **23**, 56-63.

57. Y. Song, H. Yin and W. E. Huang, *Curr. Opin. Chem. Biol.*, 2016, **33**, 1-8.

58. Y. Wang, Y. Chen, Q. Zhou, S. Huang, K. Ning, J. Xu, R. M. Kalin, S. Rolfe and W. E. Huang, *PLoS One*, 2012, **7**, e47530.

59. Y. Wang, W. E. Huang, L. Cui and M. Wagner, *Curr. Opin. Biotechnol.*, 2016, **41**, 34-42.

60. P. Zhang, L. Ren, X. Zhang, Y. Shan, Y. Wang, Y. Ji, H. Yin, W. E. Huang, J. Xu and B. Ma, *Anal. Chem.*, 2015, **87**, 2282-2289.

61. M. Kaern, T. C. Elston, W. J. Blake and J. J. Collins, *Nat Rev Genet*, 2005, **6**, 451-464.

62. M. B. Elowitz, A. J. Levine, E. D. Siggia and P. S. Swain, *Science*, 2002, **297**, 1183-1186.

63. J. M. Raser and E. K. O'Shea, *Science*, 2004, **304**, 1811-1814.

64. A. P. Feinberg and R. A. Irizarry, *Proc. Natl. Acad. Sci. U.S.A.*, 2010, **107**, 1757-1764.

65. J.-W. Veening, W. K. Smits and O. P. Kuipers, *Annu. Rev. Microbiol.*, 2008, **62**, 193-210.

66. P. Heraud and M. J. Tobin, *Stem Cell Research*, 2009, **3**, 12-14.

67. J. Heber, R. Sevenson and O. Boldman, *Science*, 1952, **116**, ll.

68. K. Norris, *J. Hyg. (Lond.)*, 1959, **57**, 326-345.

69. F. L. Martin, J. G. Kelly, V. Llabjani, P. L. Martin-Hirsch, Patel, II, J. Trevisan, N. J. Fullwood and M. J. Walsh, *Nat. Protoc.*, 2010, **5**, 1748-1760.

70. J. G. Kelly, J. Trevisan, A. D. Scott, P. L. Carmichael, H. M. Pollock, P. L. Martin-Hirsch and F. L. Martin, *J. Proteome Res.*, 2011, **10**, 1437-1448.

71. D. Naumann, D. Helm and H. Labischinski, *Nature*, 1991, **351**, 81-82.

72. M. J. Baker, J. Trevisan, P. Bassan, R. Bhargava, H. J. Butler, K. M. Dorling, P. R. Fielden, S. W. Fogarty, N. J. Fullwood, K. A. Heys, C. Hughes, P. Lasch, P. L. Martin-Hirsch, B. Obinaju, G. D. Sockalingum, J. Sule-Suso, R. J. Strong, M. J. Walsh, B. R. Wood, P. Gardner and F. L. Martin, *Nat. Protoc.*, 2014, **9**, 1771-1791.

73. J. Schmitt and H.-C. Flemming, *Int. Biodeterior. Biodegradation*, 1998, **41**, 1-11.

74. A. Bosch, D. Serra, C. Prieto, J. Schmitt, D. Naumann and O. Yantorno, *Appl. Microbiol. Biotechnol.*, 2006, **71**, 736-747.

75. J. J. Ojeda, M. E. Romero-González, R. T. Bachmann, R. G. Edyvean and S. A. Banwart, *Langmuir*, 2008, **24**, 4032-4040.

76. B. R. Wood, M. A. Quinn, B. Tait, M. Ashdown, T. Hislop, M. Romeo and D. McNaughton, *Biospectroscopy*, 1998, **4**, 75-91.

77. W. B. Dunn and D. I. Ellis, *TrAC, Trends Anal. Chem.*, 2005, **24**, 285-294.

78. L. Mariey, J. Signolle, C. Amiel and J. Travert, *Vib Spectrosc.*, 2001, **26**, 151-159.

79. E. Lipiec, G. Birarda, J. Kowalska, J. Lekki, L. Vaccari, A. Wiecheć, B. Wood and W. Kwiatek, *Radiat. Phys. Chem.*, 2013, **93**, 135-141.

80. H. J. Butler, L. Ashton, B. Bird, G. Cinque, K. Curtis, J. Dorney, K. Esmonde-White, N. J. Fullwood, B. Gardner, P. L. Martin-Hirsch, M. J. Walsh, M. R. McAinsh, N. Stone and F. L. Martin, *Nat. Protoc.*, 2016, **11**, 664-687.

81. A. A. Ahmadzai, J. Trevisan, N. J. Fullwood, P. L. Carmichael, A. D. Scott and F. L. Martin, *Mutagenesis*, 2012, **27**, 257-266.

82. S. Creton, M. J. Aardema, P. L. Carmichael, J. S. Harvey, F. L. Martin, R. F. Newbold, M. R. O'Donovan, K. Pant, A. Poth and A. Sakai, *Mutagenesis*, 2012, **27**, 93-101.

83. K. Gajjar, J. Trevisan, G. Owens, P. J. Keating, N. J. Wood, H. F. Stringfellow, P. L. Martin-Hirsch and F. L. Martin, *Analyst*, 2013, **138**, 3917-3926.

84. J. Trevisan, P. P. Angelov, I. I. Patel, G. M. Najand, K. T. Cheung, V. Llabjani, H. M. Pollock, S. W. Bruce, K. Pant and P. L. Carmichael, *Analyst*, 2010, **135**, 3266-3272.

85. M. J. Walsh, S. W. Bruce, K. Pant, P. L. Carmichael, A. D. Scott and F. L. Martin, *Toxicology*, 2009, **258**, 33-38.

86. K. Kneipp, H. Kneipp, I. Itzkan, R. R. Dasari and M. S. Feld, *Chem. Rev.*, 1999, **99**, 2957-2976.

87. Z. Movasaghi, S. Rehman and I. U. Rehman, *Appl. Surf. Sci.*, 2007, **42**, 493-541.

88. R. M. Jarvis and R. Goodacre, *Anal. Chem.*, 2004, **76**, 40-47.

89. K. Maquelin, C. Kirschner, L.-P. Choo-Smith, N. van den Braak, H. P. Endtz, D. Naumann and G. Puppels, *J. Microbiol. Methods*, 2002, **51**, 255-271.

90. S. Pahlow, S. Meisel, D. Cialla-May, K. Weber, P. Rösch and J. Popp, *Adv. Drug Deliv. Rev.*, 2015, **89**, 105-120.

91. R. Goodacre, E. M. Timmins, P. J. Rooney, J. J. Rowland and D. B. Kell, *FEMS Microbiol. Lett.*, 1996, **140**, 233-239.

92. D. I. Ellis, D. Broadhurst, D. B. Kell, J. J. Rowland and R. Goodacre, *Appl. Environ. Microbiol.*, 2002, **68**, 2822-2828.

93. W. E. Huang, R. I. Griffiths, I. P. Thompson, M. J. Bailey and A. S. Whiteley, *Anal. Chem.*, 2004, **76**, 4452-4458.

94. H. Li, F. L. Martin and D. Zhang, *Anal. Chem.*, 2017, **89**, 3909-3918.

95. T. Schwartz, C. Jungfer, S. Heißler, F. Friedrich, W. Faubel and U. Obst, *Chemosphere*, 2009, **77**, 249-257.

96. E. Karunakaran, J. Mukherjee, B. Ramalingam and C. A. Biggs, *Appl Microbiol Biotechnol*, 2011, **90**, 1869-1881.

97. R. Alvarez, A. J. Burdette, X. Wu, C. Kotanen, Y. Zhao and R. A. Tripp, *Rapid Identification of Bacterial Pathogens of Military Interest Using Surface-Enhanced Raman Spectroscopy*, DTIC Document, 2014.

98. P. N. Sampaio, B. Cunha, F. Rosa, K. Sales, M. Lopes and C. R. Calado, 2015.

99. H. Zhou, D. Yang, N. P. Ivleva, N. E. Mircescu, S. Schubert, R. Niessner, A. Wieser and C. Haisch, *Anal. Chem.*, 2015, **87**, 6553-6561.

100. A. A. Bunaciu, H. Y. Aboul-Enein and Ş. Fleschin, *Appl. Surf. Sci.*, 2015, **50**, 176-191.

101. U. Neugebauer, S. Trenkmann, T. Bocklitz, D. Schmerler, M. Kiehntopf and J. Popp, *J. Biophotonics*, 2014, **7**, 232-240.

102. W. Premasiri, D. Moir, M. Klempner, N. Krieger, G. Jones and L. Ziegler, *J. Phys. Chem. B*, 2005, **109**, 312-320.

103. P. Zarnowiec, L. Lechowicz, G. Czerwonka and W. Kaca, *Curr. Med. Chem.*, 2015, **22**, 1710-1718.

104. M. J. Riding, F. L. Martin, J. Trevisan, V. Llabjani, Patel, II, K. C. Jones and K. T. Semple, *Environ. Pollut.*, 2012, **163**, 226-234.

105. K. A. Heys, M. J. Riding, R. J. Strong, R. F. Shore, M. G. Pereira, K. C. Jones, K. T. Semple and F. L. Martin, *Analyst*, 2014, **139**, 896-905.

106. J.-X. Cheng and X. S. Xie, *Science*, 2015, **350**, aaa8870.

107. L. Cui, P. Y. Chen, B. F. Zhang, D. Y. Zhang, J. Y. Li, F. L. Martin and K. S. Zhang, *Water Res.*, 2015, **87**, 282-291.

108. Z. Movasaghi, S. Rehman and D. I. ur Rehman, *Appl. Surf. Sci.*, 2008, **43**, 134-179.

109. S. Kumar, T. Verma, R. Mukherjee, F. Ariese, K. Somasundaram and S. Umapathy, *Chem. Soc. Rev.*, 2016, **45**, 1879-1900.

110. J. Li, R. Strong, J. Trevisan, S. W. Fogarty, N. J. Fullwood, K. C. Jones and F. L. Martin, *Environ. Sci. Technol.*, 2013, **47**, 10005-10011.

111. E. K. Costello, C. L. Lauber, M. Hamady, N. Fierer, J. I. Gordon and R. Knight, *Science*, 2009, **326**, 1694-1697.

112. C. L. Lauber, M. Hamady, R. Knight and N. Fierer, *Appl. Environ. Microbiol.*, 2009, **75**, 5111-5120.

113. P. Marschner, C.-H. Yang, R. Lieberei and D. Crowley, *Soil Biol. Biochem.*, 2001, **33**, 1437-1445.

114. M. Wietz, B. Wemheuer, H. Simon, H. A. Giebel, M. A. Seibt, R. Daniel, T. Brinkhoff and M. Simon, *Environ. Microbiol.*, 2015, **17**, 3822-3831.

115. S. M. Ede, L. M. Hafner and P. M. Fredericks, *Appl Spectrosc*, 2004, **58**, 317-322.

116. M. R. Brown, D. G. Allison and P. GILBERT, *J. Antimicrob. Chemother.*, 1988, **22**, 777-780.

117. O. Fridman, A. Goldberg, I. Ronin, N. Shoresh and N. Q. Balaban, *Nature*, 2014, **513**, 418-421.

118. C. G. Mayhall and E. Apollo, *Antimicrob. Agents Chemother.*, 1980, **18**, 784-788.

119. C. G. Xie, D. Chen and Y. Q. Li, *Optics Letters*, 2005, **30**, 1800-1802.

120. K. Kogermann, M. Putrins and T. Tenson, *Eur. J. Pharm. Sci.*, 2016, **95**, 2-16.

121. J. Trevisan, P. P. Angelov, P. L. Carmichael, A. D. Scott and F. L. Martin, *Analyst*, 2012, **137**, 3202-3215.

122. W. B. Whitman, D. C. Coleman and W. J. Wiebe, *Proc. Natl. Acad. Sci. U.S.A.*, 1998, **95**, 6578-6583.

123. Y. Song, A.-K. Kaster, J. Vollmers, Y. Song, P. A. Davison, M. Frentrup, G. M. Preston, I. P. Thompson, J. C. Murrell and H. Yin, *Microb. biotechnol.*, 2017, **10**, 125-137.

124. T. Chen, C. Cao, J. Zhang, A. M. Streets, Y. Huang and T. Li, *bioRxiv*, 2017, 121616.

125. K. R. Jonscher, A. Alfonso-Garcia, J. L. Suhalim, D. J. Orlicky, E. O. Potma, V. L. Ferguson, M. L. Bouxsein, T. A. Bateman, L. S. Stodieck and M. Levi, *PLoS ONE*, 2016, **11**, e0152877.

Chapter 2 Spectrochemical analyses of growth phase-related bacterial responses to low (environmentally-relevant) concentrations of tetracycline and nanoparticulate silver

Naifu Jin, Kirk T. Semple, Longfei Jiang, Chunling Luo, Dayi Zhang, Francis L. Martin

Analyst, 2018, 143, 768 – 776.

Spectrochemical analyses of growth phase-related bacterial responses to low (environmentally-relevant) concentrations of tetracycline and nanoparticulate silver

Naifu Jin[1], Kirk T. Semple[1], Longfei Jiang[2], Chunling Luo[2], Dayi Zhang[1,*], Francis L. Martin[3,*]

[1]*Lancaster Environment Centre, Lancaster University, Lancaster LA1 4YQ, UK;*

[2]*Guangzhou Institute of Geochemistry, Chinese Academy of Sciences, Guangzhou 510640, China;*

[3]*School of Pharmacy and Biomedical Sciences, University of Central Lancashire, Preston PR1 2HE, UK*

***Corresponding authors:**

Francis L Martin, School of Pharmacy and Biomedical Sciences, University of Central Lancashire, Preston PR1 2HE, UK, Email: flmartin@uclan.ac.uk

Dayi Zhang, Lancaster Environment Centre, Lancaster University, Lancaster LA1 4YQ, UK, Email: d.zhang@lancaster.ac.uk

Abstract

Exposure to environmental insults generally occurs at low levels, making it challenging to measure bacterial responses to such interactions. Additionally, microbial behaviour and phenotype varies in differing bacterial types or growth phases, likely giving rise to growth- or species-specific responses to environmental stimuli. The present study applied a spectrochemical tool, infrared spectral interrogation coupled with multivariate analysis, to investigate the growth- and species-specific responses of two bacterial strains, Gram-negative *Pseudomonas fluorescens* and Gram-positive *Mycobacterium vanbaalenii*, to low concentrations of tetracycline, nanoparticulate silver (AgNP) or mixtures thereof. Results indicate the tendency for tetracycline-induced biospectral alterations to occur in outer-cellular components, *e.g.*, phospholipids or proteins, while AgNPs-induced changes are mainly associated with proteins (~ 964 cm^{-1}, ~ 1485 cm^{-1}, ~ 1550 cm^{-1}, ~ 1650 cm^{-1}). The primary altered targets are correlated with bacterial membranes or outer-cellular components. Furthermore, significant lipid changes at 1705-1750 cm^{-1} were only present in *P. fluorescens* cells compared to *M. vanbaalenii*, owing to differences in cell wall structure between Gram-positive and -negative bacteria. This study also found distinct biospectral alterations in non-log phase compared to log phase, confirming bacterial growth-dependent responses to environmental exposures. It implies that previous studies on log phase only may underestimate the impacts from exposures of interest *in situ*, where bacteria stay in different growth stages. Our work proves the feasibility of biospectroscopy in determining bacterial responses to low-level environmental exposures in a fast and efficient manner, revealing sufficient biochemical information continuously through growth phases. As a nondestructive approach, biospectroscopy may provide deeper insights into the actual and *in situ* interactions between microbes and environmental stimuli, regardless of the exposure level, growth phase, or bacterial types.

Introduction

The impacts of environmental insults on microorganisms have been widely studied. Antibiotics are a group of antimicrobial agents capable of causing environmental insults of major concern from both a scientific and public perspective. A significant number and quantity of antibiotics have been extensively applied in human and veterinary medicine[1]. Various means by which these drugs and their metabolites enter the environment post-excretion have been examined. The most common way by which antibiotics are discharged is *via* sewage treatment plants with ultimate release into surface or groundwater. Previous studies point to >40 different categories of antibiotics found in groundwater and even drinking water, ranging from nanogram per liter to microgram per liter[1-4]. Strikingly, residues of veterinary antibiotics enter the environment in a much more direct way through application of liquid manure as fertilizer[5, 6].

Additionally, nanoparticles (NPs) may also pose high risks to our living environment. Nanoparticulate silver (AgNP) is one of the most widely-used NPs, occurring in analytical pathogen-detecting devices, as antibacterial additives in commercial products (clothing, food containers, wound dressings, implant coatings, and refrigerators), and in ultrafiltration membranes for water purification[7-9]. The abuse and widespread usage of antibiotics and AgNPs may exacerbate risks of antimicrobial resistance[10]. Although many studies have addressed such consequences in living microorganisms, they usually employ very high-level exposures of antibiotics and AgNPs in the laboratory, generally 100- or even 1000-fold greater than exposures in real-world scenarios. Thus, the *in-vitro* outcome of high-level exposure in reflecting real-world impacts is always questioned[11, 12].

Bacteria play a critical role in geochemical processes and are ubiquitously present in the environment as a unique group of microorganisms. They can be used advantageously to study the impacts of environmental exposures, but their communities are incredibly complicated with

regards to composition, functions and dynamics[13-16]. Gram staining depending on cell membrane structure, for instance, is the general classification method for categorizing bacteria into Gram-positive or -negative groupings. The fundamental difference between these two categories is membrane structure, *i.e.*, there is only a thin peptidoglycan layer (~2-3 nm) between the cytoplasmic membrane and the outer membrane of Gram-negative bacteria while Gram-positive bacteria exhibit a thick peptidoglycan layer of 30 nm but lack an outer membrane[17]. Differing attributes of membrane structure may result in distinct responsive behaviors towards environmental exposures, for instance towards toxicity and anti-biocide actions[18]. Additionally, growth phase is another major concern in studying bacterial communities. Bacterial growth is typically divided *via* growth rate, *i.e.*, lag phase, acceleration phase, exponential phase (log-phase), retardation phase, stationary phase, and phase of decline. In previous studies, log-phase has been the most investigated, but this condition is seldom found in the natural environment due to rarity of optimal growth conditions [19]. Instead, stationary- to death-phase representing nutrient depletion circumstances may be more representative[20].

To date, a wide range of techniques have been used to assess bacterial responses to environmental exposures, such as Christensen test-tube method (CTT)[21, 22], Congo red agar method (CRA)[23], IcaADB gene detection using polymerase chain reaction (PCR)[24, 25], and pulsed-field gel electrophoresis (PFGE)[26, 27]. However, these approaches target specific endpoints and are not feasible for diagnosing bacterial responses to environmental exposures. CTT and CRA primarily require access to pure cultures. The others are molecular-based, defining the genotype of a whole community rather than the individual phenotype or behavior. For instance, distinguishing the functions or behaviours of individual bacterial cells within a bacterial biofilm is almost impossible *via* molecular-based methods, owing to the enormous diversity of bacterial strains and complexity in community structure. Additionally, these

approaches have to be performed under restrictive laboratory conditions[28-30], making it unachievable to discriminate bacterial phenotypes within complex bacterial communities in real environmental samples. Therefore, an increasing need for novel high-throughput approaches is raised, allowing one to analyze the real environmental microbiota *in situ via* a non-destructive means.

Biospectroscopy has a long history of application in microbiology since the 1960s[31, 32]. Attributes of biospectroscopy include non-destructive, non-invasive, high-throughput and label-free, which provide many advantages for the investigation of environmental and biochemical dynamic changes in low-level exposure circumstances. In recent studies, biospectroscopy has proved sensitive to physiological and morphological alterations resulted from low-level environmental exposures[33-35]. Specifically, infrared (IR) spectroscopy exploits the principle that biochemical bonds perform some degree of vibrations induced by stretching, bending, scissoring or twisting after energy absorption at particular wavelengths. The "biochemical-cell fingerprint" region is located within the mid-IR region, which is the most information-rich about biochemical structures[36]. Through assessing derived spectral peaks or alterations, *i.e.*, bio-fingerprints, the biochemical structure of interrogated targets can be revealed[37-39]. Additionally, Raman spectroscopy, as a complementary method to IR, can provide information on chemical bonds and composition even under a hydrated environment[40, 41]. Furthermore, another merit of biospectroscopy over other techniques is that it allows investigations to be undertaken *in situ* in real-time, which can generate continuous biochemical information through the entire biological processes rather than only obtaining static results from specific time points.

The present study discriminated and assessed the bacterial response to tetracycline and AgNP *via* biospectroscopy coupled with multivariate analysis. The tetracycline has a broad spectrum of antibiotic action i.e. it is effective to both Gram positive and negative bacteria with

only a few exceptions[42]. Also, tetracyclines have a history of several decades used in animal feed, which may present much more ubiquitously in the environment than other in-house antibiotics (e.g. kanamycin)[43]. Furthermore, in recent years, many studies were focus on synergistic antibacterial effects of antibiotic effects combined with metals and nanoparticules[44, 45]. The current study also provided a new way to characterize such effect via infrared spectroscopy. Regarding the real-world scenario, our work distinguished the distinct biospectral alterations in different bacterial types and growth phases, helping one to understand the bacterial behaviour post-exposure to low-level antimicrobials. We aim to demonstrate that biospectroscopy approaches can characterise physiological features of bacteria and lend profound insights into the relationship between these and bacterial responses to environmental insults.

Materials and methods

Sample preparation

Unless stated otherwise, all the chemicals used in this study were purchased from Sigma-Aldrich (UK). The AgNPs were also purchased from Sigma-Aldrich (UK) (the size is 10 nm) at a stock concentration of 0.02 mg/mL dissolved in aqueous buffer (sodium citrate as stabilizer). Two classic bacterial strains, *Mycobacterium vanbaalenii* PYR-1 representing Gram-positive bacteria and *Pseudomonas fluorescens* representing Gram-negative bacteria were selected. These two strains are common environmental strains, and their metabolic pathways have been extensively studied in the past studies[36, 46-48]. Bacteria were cultured in Luria–Bertani (LB) broth at 30±2ºC with 150 rpm shaking for 24 h. Bacterial growth was measured every 10 min by optical density at 600 nm (OD_{600}) with a microplate reader (FLUOstar Omega, BMG Labtech, UK). AgNPs, tetracycline or AgNPs-tetracycline mixture was added into cell suspensions in early log-phase (OD_{600}=0.6), respectively. Exposure

concentrations were 4 μg/L for AgNPs and 1 μg/L for tetracycline. The exposure concentrations were chosen based on natural level[49-52]. One millilitre of bacterial suspension was taken 2, 8 and 24 h post-exposure, representing log-phase, stationary-phase and death-phase, respectively. For each sample, bacterial cells were harvested by centrifugation at 4000 relative centrifugal force (rcf) for 5 min, and the cell pellets were subsequently washed three times with sterile deionized water and 70% ethanol to fix bacteria and remove residues of growth media. The fixed samples were then applied onto Low-E slides for subsequent spectrochemical analysis.

Spectrochemical analysis

IR spectra were acquired *via* a Bruker TENSOR 27 FTIR spectrometer (Bruker Optics Ltd., UK) equipped with a Helios ATR attachment containing a diamond internal reflection element (IRE). Instrument parameters were set at 32 scans and 16 cm^{-1} resolution. A total number of 30 spectra were acquired per sample through the ATR magnification-limited viewfinder camera. Before measuring each new specimen, the crystal was cleaned with deionized water, and background readings were retaken.

Raman spectra were acquired *via* an InVia Renishaw Raman spectrometer (Renishaw Inc. Gloucester, Gloucestershire, UK). After calibration, sample slides were placed on an operating stage (a Renishaw automated 100 nm encoded XYZ stage), and a 50× objective (numeral aperture 0.75) was applied to focus on the cell pellet. The parameters of measurement included: grating scan type (extended); spectrum range (400 to 1800 cm^{-1}); configuration (Laser, 785 nm edge); grating (1200 l/mm 633/790); exposure time (30 s); accumulations (1); and, laser power (100%). When all the parameters were set up, a map measurement was used for analyzing each colony. The spectrometer's entrance slit of 50 μm combined with a 1200 lines/mm (~1.0 cm^{-1} spectral resolution) diffraction grating dispersing Raman signals onto a master Renishaw Pelletier cooled charge coupled detector (CCD). A white light camera mounted on the

microscope was used to obtain the darkfield images and visualize locations for spectral acquisition. For each captured picture of a cell pellet, 25 spectra were randomly obtained.

Spectrochemical data processing

All the initial data generated from ATR-FTIR spectroscopy were analyzed using MATLAB R2011a (TheMathsWorks, Natick, MA, USA) coupled with the IRootLab toolbox (http://irootlab.googlecode.com)[53]. The acquired IR spectra were cut to the biochemical-cell fingerprint region (1800 - 900 cm^{-1}), undertaken rubberband baseline correction and normalized to Amide I (1650 cm^{-1}). Multivariate analysis of principal component analysis-linear discriminant analysis (PCA-LDA) was applied to the pre-processed data to derive ten uncorrelated principal components (PCs) from acquired spectra, which account for >99% of the total variance and also maximize inter-class variance whilst minimizing intra-class variance[54-56]. Cross-calculation was subsequently performed to mitigate risk resulting from LDA overfitting[57]. The PCA-LDA loadings using n – 1 samples (n = number of samples in dataset) was trained via leave-one-out cross-validation and then calculate the scores of the rest sample. This process was performed for all scores within the test. To investigate roles of reactive oxygen species (ROS) in antibiotic action and resistance, the CySS-to-protein ratio was calculated from derived Raman spectra by dividing the intensity of cysteine band (CySS, 668 cm^{-1}) by that of protein band (1447 cm^{-1})[58].

Statistical analysis

Statistical significance of differences and variance analysis (*P*-value <0.05) of biospectral alterations among different treatments of bacterial types and growth phases was performed using one-way analysis of variance (ANOVA) with Tukey's post-hoc test. All statistical analyses were carried out in GraphPad Prism 6. Multivariate regression trees (MRT) were used to analyze the influence of bacterial type, growth phase and exposure on biospectral alterations

using the R package "mvpart". Herein, Gram-positive (*M. vanbaalenii*) and Gram-negative (*P. fluorescens*) strains were assigned as 1 and 0. For growth phase, the log-phase, stationary-phase, and death-phase were assigned as 1, 2 and 3, respectively. The exposure of AgNPs, tetracycline and their mixtures were assigned as 1, 2 and 3, respectively.

Results and discussion

Growth curves post-exposure to AgNPs and tetracycline

Growth curves (Figure 1) for *M. vanbaalenii* (Figure 1A) and *P. fluorescens* (Figure 1B) show that both strains exhibit approximately a 3 h lag-phase and the log-phase starts some 3.5 h after initial culture. Both enter the stationary-phase at approximately 11 h (OD_{600}=1.2). After about 30 h culture, significant fluctuations indicate the death phase stage for both strains. There was no significant difference regarding the growth between control (non-exposure) and exposure groups (P >0.05). Although previous work reports a remarkable inhibition of bacterial growth post-exposure to AgNPs[59], the exposure levels herein (4 ng/mL) are much lower than the previous study (10-100 μg/mL) and it therefore appeared not to significantly impact either bacterial strain. Similarly, low concentrations of tetracycline did not induce any apparent changes on the respective growth curves either. A previous study reports that *Synechocystis* sp. exposure to 1 μg/L of tetracycline for five days exhibited no apparent effect, possibly because of natural variability in tetracycline resistance[60]. Additionally, *M. vanbaalenii* and *P. fluorescens* are both environmental bacteria widespread in natural habitats (water and soil), and they are reported to tolerate insults from low-level exposures of antimicrobials[36]. Thus, their growth curves are hardly affected by low-level exposures to AgNPs or tetracycline.

Growth-dependent spectrochemical alterations derived from IR spectra

Raw spectra reveal very limited information because low-level exposures may only induce miniscule alterations (Figure 1C and 1D). Multivariate analysis helps in highliting the spectraal

changes and distinguishing key biomarkers representing spectral differences. Previous studies indicate that most features align along linear discriminant one (LD1), which includes most of the spectral information (Figure 2)[34, 36]. The observed segregation in PCA-LDA scores plots (Figure 2A and 2E) is significant (P <0.05), indicating distinct biospectral alterations between the growth phases. The results of one-way ANOVA [see Electronic Supporting Information (ESI) Table S1 and S2] also demonstrate the statistically significant means of all segregation categories in each growth phase (P <0.05).

Biospectral discriminant peaks and their tentative assignments illustrate the interactions between cellular components in different growth stages (Figure 3). The spectra of *M. vanbaalenii* show a broad range of variations in stationary-phase compared to log-phase (Figure 3A), including glycogen (~1018 cm^{-1}), carbohydrate (~1165 cm^{-1}), symmetric phosphate stretching vibrations (~1088 cm^{-1}), COO- symmetric stretching vibrations of fatty acids and amino acid (~1377 cm^{-1}), lipid (~1701 cm^{-1}), and proteins (~1474 cm^{-1})[61]. The main discriminant peaks in death-phase include Amide I (~1650 cm^{-1}), Amide II (~1550 cm^{-1}), glycogen (~1018 cm^{-1}), and proteins (~1481 cm^{-1})[36, 61]. In contrast, the major spectral features of *P. fluorescens* are identical in stationary-phase and death-phase (Figure 3E), mainly comprising proteins and lipids, *i.e.*, Amide I (~1650 cm^{-1}), Amide II (~1550 cm^{-1}), and lipids (1705-1750 cm^{-1})[58, 62]. For both strains, the degrees of all the growth-related alterations illustrate an increasing tendency from stationary-phase to death-phase, possibly attributed to cellular differentiation under nutrient depleted conditions in stationary-phase and death-phase, which cause the changing cell wall structure to adapt to growth circumstances[20, 63, 64]. The spectral differences between the two strains is principally contributed by cell membrane structure in that Gram-negative bacteria contain two lipid-associated bilayers compared to Gram-positive cells[17]. The extra membrane in Gram-negative strains (*P. fluorescens*) might increase more detectable alterations related to proteins and lipids across growth phases.

Spectrochemical alterations with AgNPs/tetracycline exposure

Although the exposures herein are low-level, characterizable effects can be identified post-exposure to AgNPs, tetracycline or their mixtures *via* biospectrsocopy coupled with multivariate analysis. The key alterations in *M. vanbaalenii* post-exposure to AgNPs include glycogen (~1022 cm^{-1}), proteins (~1485 cm^{-1}), symmetric phosphate stretching vibrations (~1088 cm^{-1}, 1092 cm^{-1}), carbohydrate (~1165 cm^{-1}), lipids (~1705 cm^{-1}, 1709 cm^{-1}), Amide I (~1670 cm^{-1}), and protein phosphorylation (~964 cm^{-1}) (Figure 3B)[36, 65]. Tetracycline exposure led to discriminating alterations in *M. vanbaalenii* in Amide III (~1269 cm^{-1}), protein phosphorylation (~964 cm^{-1}), glycogen (~1022 cm^{-1}), Amide I (~1609 cm^{-1}, 1612 cm^{-1}, 1659 cm^{-1}), COO- symmetric stretching vibrations of fatty acids and amino acid (~1408 cm^{-1}), and lipids (~1701 cm^{-1}, 1713 cm^{-1}) (Figure 3C)[61]. However, for *P. fluorescens*, the biomarkers in both individual treatments are further concentrated on proteins (~1650 cm^{-1}, ~1550 cm^{-1}) and lipids (1705-1750 cm^{-1})[36, 58] (Figure 3F and 3G).

In binary exposure treatments, a more complex difference in profiles of spectral alterations in ATR-FTIR spectra are observed. The primary changes in *M. vanbaalenii* are consistent with proteins (~1650 cm^{-1}) and lipids (1705-1750 cm^{-1}) in all growth phases (Figure 3D)[36, 58]. In contrast, the exposure-associated spectral alterations in *P. fluorescens* vary significantly with growth phase (Figure 3H), *e.g.*, the biomarkers in stationary-phase with binary effects include glycogen (~1053 cm^{-1}), Amide I (~1609 cm^{-1}), COO- symmetric stretching vibrations of fatty acids and amino acid (~1389 cm^{-1}), asymmetric phosphate stretching vibrations (~ 1196 cm^{-1}), lipid (~ 1732 cm^{-1}), and Amide II (~1508 cm^{-1})[61, 62]. They change to lipid (~1709 cm^{-1} and 1751 cm^{-1}), Amide I (~1609 cm^{-1}), Amide II (~1543 cm^{-1}), asymmetric phosphate stretching vibrations (~1211 cm^{-1}) and glycogen (~1053 cm^{-1})[36, 61] in death-phase.

In general, most spectral alterations post-exposure are associated with lipids and proteins indicating bacterial cell membranes are primary targets, probably because tetracycline or

AgNPs penetrate bacterial cells *via* passive diffusion and inhibits bacterial growth by disturbing protein synthesis or altering membrane structure[66]. Through growth phases, Gram-negative bacteria inhibit a broad range of alterations associated with lipids, *e.g.*, (1705 − 1750 cm^{-1}), which is absent in Gram-positive bacteria, mainly attributed to their different cell wall composition. The rigidity and extended cross-linking may reduce target sites on cell wall for environmental exposure and increase difficulties in antimicrobial penetration[67 7].

Factors influencing spectrochemical alteration

From conducted spectral analysis, factors inducing IR spectral alterations can be classified as intrinsic and external categories. The inherent one includes bacterial type (Gram-positive or Gram-negative) and growth phase, and the external category refers to the types of exposure. These factors function and interact simultaneously, with distinct impacts on microbial responses to environmental exposures. To quantify the importance of each factor, multivariate regression tree (MRT) analysis was conducted through the isolated discriminating biomarkers (characteristic peaks). The MRT graph illustrates the relationship of spectral variations and impact factors with four splits according to bacterial types, growth phase and exposure groups, explaining 90.8% of spectral variance (Figure 5).

Spectral variation is first split by bacterial type which accounts for 65.6% of the total variation, owing to more changes associated with membrane components observed in *P. fluorescens* (Gram-negative) than *M. vanbaalenii* (Gram-positive), *e.g.*, proteins and phospholipid-derived fatty acids. Multivariate analysis also illustrates various spectrochemical alterations between *P. fluorescens* and *M. vanbaalenii*. For example, significant lipid changes (1705-1750 cm^{-1}) present in *P. fluorescens* treatments are absent in *M. vanbaalenii* treatments. The cell membrane of Gram-negative bacteria contains two lipid associated bilayers, which is likely to increase the influence of applied exposure on the cell wall structure, while there is only one lipid bilayer in the membrane and a thick ring of peptidoglycan and teichoic acid of

Gram-positive bacteria[17]. This difference may influence the structural integrity and eventually the microbial response to external stimuli. Furthermore, both Gram-positive and -negative bacteria from stationary phase show a comprehensive range of alterations in cellular components (*i.e.*, Amide I, II, III, asymmetric/symmetric phosphate stretching vibrations, glycogen, carbohydrates, lipids, etc.; Figure 6), indicating many underlying biological activities. This can be primarily attributed to a growing cell wall from log to stationary phase, which increases the amounts of membrane components[68] and induces changes on the surface of the bacterial envelope and protein synthesis[20]. Such changes may have considerable influence on the rigidity of the cells, resistance to environmental changes, as well as immunochemical properties. Results of both MRT and multivariate analyses therefore suggest bacterial type as the primary intrinsic factor determining IR alterations post-exposure to AgNP or tetracycline.

Growth phase also shows significant impacts on bacterial spectra after environmental exposure. The Gram-negative group is further split in the MRT graph by growth phase (*i.e.*, log-phase *vs.* stationary-phase and death-phase), owing to increasing alterations of membrane components along with the growth stage, which explains 13.2% of total variation (Figure 5). Similarly, multivariate analysis demonstrates the same growth-dependent results. Post-exposure to AgNP for instance, the spectra of both strains in log-phase are clearly separated from those in stationary-phase or death-phase (Figure 2B-D). The induced alterations from growth phases are associated with various cellular components. Specifically in log-phase, IR spectral biomarkers reflecting the major alterations of *M. vanbaalenii* post-exposure to AgNP are Amide I (~1612 cm^{-1}), COO- symmetric stretching vibrations of fatty acids and amino acid (~1381 cm^{-1}), lipid (~1717 cm^{-1}), glycogen (~1011 cm^{-1}), asymmetric phosphate stretching vibrations (~1215 cm^{-1}), and carbohydrate (~1165 cm^{-1}) (Figure 6A)[36, 61]. However, samples from stationary-phase exhibit a contrasting profile consisting only of alterations of proteins

(~1377 cm^{-1}) and Amide I, II, III (~1609 cm^{-1}, 1566 cm^{-1}, 1254 cm^{-1}) (Figure 6B)[65]. In tetracycline or tetracycline-AgNP mixture treatments, the most-induced biomarkers in log-phase shift to proteins, *i.e.*, Amide I (~1163 cm^{-1}, 1616 cm^{-1}), Amide II (~1520 cm^{-1}, 1558 cm^{-1}) and Amide III (~1327 cm^{-1}) (Figure 6A)[65], but they are associated more with cellular components in stationary-phase, including Amide I (~1589 cm^{-1}), Amide II (~1551 cm^{-1}), Amide III (~1269 cm^{-1}; 1273 cm^{-1}), proteins (~1485 cm^{-1}), lipid (~1717 cm^{-1}, 1721 cm^{-1}), COO- symmetric stretching vibrations of fatty acids and amino acid (~1342 cm^{-1}; 1381 cm^{-1}), symmetric phosphate stretching vibrations (~1069 cm^{-1}), asymmetric phosphate stretching vibrations (~1196 cm^{-1}) and glycogen (~1018 cm^{-1}) (Figure 6B)[61]. Samples from death-phase cultures exhibit distinct patterns as compared to log- or stationary-phase in that AgNP and tetracycline-AgNP mixture show more impacts on proteins (Figure 6C). These results indicate the changing physiological profiles of bacterial cells with growth stage, and the different modifications associated with cellular components with adaptation to the living environment. For instance, bacteria facing nutrient depletion are reported to produce more hydrophobic molecules to protect the starved cells, resulting in less fluid and permeable membranes attributed to the transformations within the fatty acid composition, which increase protection and insulation from a stressful environment[20, 63, 64]. Moreover, entering stationary phase, a wide range of protein synthesis is also altered by the global gene regulatory network, which tends to swap the core functions from metabolism or catabolism to the maintenance of cellular viability[20], possibly explaining more spectral alterations of proteins in stationary- and death-phase than log-phase.

Besides intrinsic factors, external environmental exposure explains 12.0% of total variation in MRT for Gram-positive (2.7%) and Gram-negative (9.3%) bacteria. For both strains, segregation mainly results from different spectrochemical alterations between AgNP exposure and tetracycline/binary groups. The key spectral alterations in the AgNP category are

located at COO- symmetric stretching vibrations of fatty acids and amino acid (~1373 cm^{-1}), (~1736 cm^{-1}), proteins (~984 cm^{-1}, 988 cm^{-1}), Amide I (1612 cm^{-1}, 1694), Amide II (1543 cm^{-1}, 1562 cm^{-1}), and symmetric phosphate stretching vibrations (1088 cm^{-1}) (Figure 3B and 3F)[36, 61]. In contrast, changes induced by tetracycline or tetracycline-AgNP mixture are associated with COO- symmetric stretching vibrations of fatty acids and amino acid (~1373 cm^{-1}), proteins (~984 cm^{-1}), lipids (~1697 cm^{-1}; 1732 cm^{-1}), and Amide I, II (~1562 cm^{-1}, 1616 cm^{-1}) (Figure 3C and 3G)[61].

It can be concluded that AgNP-induced spectral changes are mainly associated with proteins, whereas broader cellular components are affected post-exposure to tetracycline or tetracycline-AgNP mixture. It might be explained by tetracycline penetrating cells *via* passive diffusion, which alters bacterial growth by inhibiting protein synthesis or destroying the membrane. Phospho-lipids or proteins are therefore more significantly affected as the primary receptors of passively accumulated tetracycline[66]. Although mechanisms of AgNP interacting with cytoplasmic membranes and penetrating into cells remain unclear[59, 69], our data suggest that AgNP-induced alterations might be derived from some specific active sites interacting with AgNP, *e.g.*, sulfur-containing proteins following a similar mechanism as thiol groups of respiratory chain proteins and transport proteins[70-72].

To further assess the impact of exposure, the inter-category multivariate distances of each category were also evaluated. PCA-LDA scores plots that compare the spectrochemical alterations of the two bacterial strains within the same growth phase are shown in Figure 4. The results illustrate distinct clustering of tetracycline exposure away from the control category, but not for AgNP categories, whereas the binary group is located between AgNP and tetracycline categories. The spectral differences of *M. vanbaalenii* between categories of control and binary exposure are slightly reduced within 0.1 as compared to the tetracycline exposure category, indicating that AgNP may confer the exposure effect of tetracycline.

Similar alterations are observed for *P. fluorescens*. Additionally, for both *M. vanbaalenii* and *P. fluorescens*, the AgNP and tetracycline categories in the stationary- or death-phase shift in an opposite direction from the control, and the binary exposure category locates closer to the tetracycline exposure group than control or AgNP exposure. This finding is supported by a range of identical alterations identified in both AgNP and binary exposure groups from stationary-phase to death-phase (*i.e.*, lipids, Amide I, II, III, asymmetric/symmetric phosphate stretching vibrations).

Additionally, the analysis of reactive oxygen species (ROS) was also conducted to evaluate the exposure impacts by calculating the CySS-to-protein ratio, derived from Raman spectra (Figure 7), which points to cellular ROS levels[34]. Interestingly, comparing to control category, only tetracycline-binary exposure appears to increase ROS level (P <0.05), whereas the induction of AgNP and tetracycline exposure is not significant. Previous studies report the independent mechanisms of antimicrobials on the involvement of ROS[73, 74]. The results herein hint at no ROS generation from individual AgNP or tetracycline exposure, and the spectrochemical alterations more likely result from the direct inhibition of cell-wall assembly, protein synthesis and DNA replication. In binary exposure, AgNP penetration across the cell membrane might increase permeability and result in more tetracycline entering the bacterial cell, consequently triggering a ROS response[67, 75-78].

Conclusions

The present study demonstrates that spectrochemical techniques coupled with multivariate analysis are a robust tool for investigating the bacterial response to environmental exposures, revealing biochemical information longnitudinally at low-level exposures. This approach can be applied to characterize and assess bacterial alterations effectively post-exposure to a tetracycline and/or AgNP through growth phases and is potentially feasible for *in situ*

interrogation of antimicrobial effects in real-time. Deeper insights into biospectral alterations in non-log phases pertaining nutrient depletion conditions, which fits better with the real-world scenario of microcosms, uncovers the distinct changes of biochemical fingerprints across growth periods, hinting at an underestimation of antimicrobial effects in previous studies. Bacterial type is ranked as the primary factor affecting microbial response to environmental stimuli by MRT analysis, followed by growth phase and types of antimicrobials. These findings will help our better understanding of the real interactions between microbes and low-level antimicrobials under natural environmental conditions, *e.g.*, nutrient depletion.

Conflicts of interest

There are no conflicts of interest to declare.

ACKNOWLEDGEMENTS N.J. was funded by Chinese Academy of Sciences and China Scholarship Council.

REFERENCES

1. G. Hamscher, S. Sczesny, H. Höper and H. Nau, *Anal. Chem.*, 2002, **74**, 1509-1518.
2. J. W. Harrison and T. A. Svec, *Quintessence Int.*, 1998, **29**, 223-229.
3. J. C. Chee-Sanford, R. I. Aminov, I. J. Krapac, N. Garrigues-Jeanjean and R. I. Mackie, *Appl. Environ. Microbiol.*, 2001, **67**, 1494-1502.
4. L. Cantas, S. Q. Shah, L. M. Cavaco, C. M. Manaia, F. Walsh, M. Popowska, H. Garelick, H. Burgmann and H. Sorum, *Front. Microbiol.*, 2013, **4**, 96.
5. M. Tandukar, S. Oh, U. Tezel, K. T. Konstantinidis and S. G. Pavlostathis, *Environ. Sci. Technol.*, 2013, **47**, 9730-9738.
6. J. L. Martinez and F. Baquero, *Ups. J. Med. Sci.*, 2014, **119**, 68-77.
7. H. H. Lara, N. V. Ayala-Núñez, L. d. C. Ixtepan Turrent and C. Rodríguez Padilla, *World J. Microbiol. Biotechnol.*, 2009, **26**, 615-621.
8. R. J. Griffitt, N. J. Brown-Peterson, D. A. Savin, C. S. Manning, I. Boube, R. A. Ryan and M. Brouwer, *Environ. Toxicol. Chem.*, 2012, **31**, 160-167.
9. Y. Kampmann, E. De Clerck, S. Kohn, D. Patchala, R. Langerock and J. Kreyenschmidt, *J. Appl. Microbiol.*, 2008, **104**, 1808-1814.
10. A. Gupta and S. Silver, *Nat. Biotechnol.*, 1998, **16**, 888-888.
11. O. I. Kalantzi, R. Hewitt, K. J. Ford, L. Cooper, R. E. Alcock, G. O. Thomas, J. A. Morris, T. J. McMillan, K. C. Jones and F. L. Martin, *Carcinogenesis*, 2004, **25**, 613-622.
12. J. L. Barber, M. J. Walsh, R. Hewitt, K. C. Jones and F. L. Martin, *Mutagenesis*, 2006, **21**, 351-360.
13. E. K. Costello, C. L. Lauber, M. Hamady, N. Fierer, J. I. Gordon and R. Knight, *Science*, 2009, **326**, 1694-1697.
14. C. L. Lauber, M. Hamady, R. Knight and N. Fierer, *Appl. Environ. Microbiol.*, 2009, **75**, 5111-5120.
15. P. Marschner, C.-H. Yang, R. Lieberei and D. Crowley, *Soil Biol. Biochem.*, 2001, **33**, 1437-1445.
16. M. Wietz, B. Wemheuer, H. Simon, H. A. Giebel, M. A. Seibt, R. Daniel, T. Brinkhoff and M. Simon, *Environ. Microbiol.*, 2015, **17**, 3822-3831.
17. J. R. Morones, J. L. Elechiguerra, A. Camacho, K. Holt, J. B. Kouri, J. T. Ramirez and M. J. Yacaman, *Nanotechnology*, 2005, **16**, 2346-2353.
18. S. M. Ede, L. M. Hafner and P. M. Fredericks, *Appl Spectrosc*, 2004, **58**, 317-322.

19. J. Monod, *Annu. Rev. Microbiol.*, 1949, **3**, 371-394.
20. R. Kolter, D. A. Siegele and A. Tormo, *Annu. Rev. Microbiol.*, 1993, **47**, 855-874.
21. F. Růžička, V. Holá, M. Votava, R. Tejkalová, R. Horvát, M. Heroldová and V. Woznicová, *Folia Microbiol. (Praha)*, 2004, **49**, 596-600.
22. F. Ruzicka, M. Horka, V. Hola and M. Votava, *J. Microbiol. Methods*, 2007, **68**, 530-535.
23. T. Mathur, S. Singhal, S. Khan, D. Upadhyay, T. Fatma and A. Rattan, *Indian J. Med. Microbiol.*, 2006, **24**, 25.
24. D. Klug, F. Wallet, S. Kacet and R. J. Courcol, *J. Clin. Microbiol.*, 2003, **41**, 3348-3350.
25. P. Vasudevan, M. K. M. Nair, T. Annamalai and K. S. Venkitanarayanan, *Vet. Microbiol.*, 2003, **92**, 179-185.
26. E. Muñoz-Atienza, C. Araújo, R. del Campo, P. E. Hernández, C. Herranz and L. M. Cintas, *LWT-Food Sci. Technol.*, 2016, **65**, 357-362.
27. F. C. Tenover, R. D. Arbeit, R. V. Goering, P. A. Mickelsen, B. E. Murray, D. H. Persing and B. Swaminathan, *J. Clin. Microbiol.*, 1995, **33**, 2233.
28. E. E. Vaughan, F. Schut, H. Heilig, E. G. Zoetendal, W. M. de Vos and A. D. Akkermans, *Curr. Issues Intest. Microbiol.*, 2000, **1**, 1-12.
29. M. Espy, J. Uhl, L. Sloan, S. Buckwalter, M. Jones, E. Vetter, J. Yao, N. Wengenack, J. Rosenblatt and F. Cockerill, *Clin. Microbiol. Rev.*, 2006, **19**, 165-256.
30. D. Klein, *Trends Mol. Med.*, 2002, **8**, 257-260.
31. J. Heber, R. Sevenson and O. Boldman, *Science*, 1952, **116**, ll.
32. K. Norris, *J. Hyg. (Lond.)*, 1959, **57**, 326-345.
33. M. J. Baker, J. Trevisan, P. Bassan, R. Bhargava, H. J. Butler, K. M. Dorling, P. R. Fielden, S. W. Fogarty, N. J. Fullwood, K. A. Heys, C. Hughes, P. Lasch, P. L. Martin-Hirsch, B. Obinaju, G. D. Sockalingum, J. Sule-Suso, R. J. Strong, M. J. Walsh, B. R. Wood, P. Gardner and F. L. Martin, *Nat. Protoc.*, 2014, **9**, 1771-1791.
34. J. Li, R. Strong, J. Trevisan, S. W. Fogarty, N. J. Fullwood, K. C. Jones and F. L. Martin, *Environ. Sci. Technol.*, 2013, **47**, 10005-10011.
35. F. L. Martin, J. G. Kelly, V. Llabjani, P. L. Martin-Hirsch, Patel, II, J. Trevisan, N. J. Fullwood and M. J. Walsh, *Nat. Protoc.*, 2010, **5**, 1748-1760.
36. K. A. Heys, M. J. Riding, R. J. Strong, R. F. Shore, M. G. Pereira, K. C. Jones, K. T. Semple and F. L. Martin, *Analyst*, 2014, **139**, 896-905.
37. J. Schmitt and H.-C. Flemming, *Int. Biodeterior. Biodegrad.*, 1998, **41**, 1-11.

38. A. Bosch, D. Serra, C. Prieto, J. Schmitt, D. Naumann and O. Yantorno, *Appl. Microbiol. Biotechnol.*, 2006, **71**, 736-747.
39. J. J. Ojeda, M. E. Romero-González, R. T. Bachmann, R. G. Edyvean and S. A. Banwart, *Langmuir*, 2008, **24**, 4032-4040.
40. S. J. Clarke, R. E. Littleford, W. E. Smith and R. Goodacre, *Analyst*, 2005, **130**, 1019-1026.
41. N. Pradhan, S. K. Pradhan, B. B. Nayak, P. S. Mukherjee, L. B. Sukla and B. K. Mishra, *Res. Microbiol.*, 2008, **159**, 557-561.
42. I. Chopra and M. Roberts, *Microbiol. Mol. Biol. Rev.*, 2001, **65**, 232-260.
43. M. D. Barton, *Nutr. Res. Rev.*, 2000, **13**, 279-299.
44. A. M. Fayaz, K. Balaji, M. Girilal, R. Yadav, P. T. Kalaichelvan and R. Venketesan, *Nanomedicine*, 2010, **6**, 103-109.
45. P. Li, J. Li, C. Wu, Q. Wu and J. Li, *Nanotechnology*, 2005, **16**, 1912.
46. S.-J. Kim, O. Kweon, R. C. Jones, J. P. Freeman, R. D. Edmondson and C. E. Cerniglia, *J. Bacteriol.*, 2007, **189**, 464-472.
47. J.-S. Seo, Y.-S. Keum and Q. X. Li, *Int. J. Environ. Res. Public Health*, 2009, **6**, 278-309.
48. L. S. Thomashow and D. M. Weller, *J. Bacteriol.*, 1988, **170**, 3499-3508.
49. R. Hirsch, T. Ternes, K. Haberer and K.-L. Kratz, *Sci. Total Environ.*, 1999, **225**, 109-118.
50. R. Hirsch, T. A. Ternes, K. Haberer, A. Mehlich, F. Ballwanz and K.-L. Kratz, *J. Chromatogr. A*, 1998, **815**, 213-223.
51. G. Artiaga, K. Ramos, L. Ramos, C. Cámara and M. Gómez-Gómez, *Food Chem.*, 2015, **166**, 76-85.
52. T. Silva, L. R. Pokhrel, B. Dubey, T. M. Tolaymat, K. J. Maier and X. Liu, *Sci. Total Environ.*, 2014, **468**, 968-976.
53. J. Trevisan, P. P. Angelov, A. D. Scott, P. L. Carmichael and F. L. Martin, *Bioinformatics*, 2013, btt084.
54. F. L. Martin, M. J. German, E. Wit, T. Fearn, N. Ragavan and H. M. Pollock, *J. Comput. Biol.*, 2007, **14**, 1176-1184.
55. F. L. Martin, J. G. Kelly, V. Llabjani, P. L. Martin-Hirsch, I. I. Patel, J. Trevisan, N. J. Fullwood and M. J. Walsh, *Nat. Protoc.*, 2010, **5**, 1748-1760.
56. M. J. Riding, F. L. Martin, J. Trevisan, V. Llabjani, Patel, II, K. C. Jones and K. T. Semple, *Environ. Pollut.*, 2012, **163**, 226-234.

57. J. Li, G. G. Ying, K. C. Jones and F. L. Martin, *Analyst*, 2015, **140**, 2687-2695.
58. J. Li, R. Strong, J. Trevisan, S. W. Fogarty, N. J. Fullwood, K. C. Jones and F. L. Martin, *Environ. Sci. Technol.*, 2013, **47**, 10005-10011.
59. I. Sondi and B. Salopek-Sondi, *J. Colloid Interface Sci.*, 2004, **275**, 177-182.
60. F. Pomati, A. G. Netting, D. Calamari and B. A. Neilan, *Aquat. Toxicol.*, 2004, **67**, 387-396.
61. Z. Movasaghi, S. Rehman and D. I. ur Rehman, *Appl. Surf. Sci.*, 2008, **43**, 134-179.
62. F. L. Martin, J. G. Kelly, V. Llabjani, P. L. Martin-Hirsch, Patel, II, J. Trevisan, N. J. Fullwood and M. J. Walsh, *Nat. Protoc.*, 2010, **5**, 1748-1760.
63. J. C. Betts, P. T. Lukey, L. C. Robb, R. A. McAdam and K. Duncan, *Mol. Microbiol.*, 2002, **43**, 717-731.
64. T. Hampshire, S. Soneji, J. Bacon, B. W. James, J. Hinds, K. Laing, R. A. Stabler, P. D. Marsh and P. D. Butcher, *Tuberculosis*, 2004, **84**, 228-238.
65. M. J. Baker, J. Trevisan, P. Bassan, R. Bhargava, H. J. Butler, K. M. Dorling, P. R. Fielden, S. W. Fogarty, N. J. Fullwood, K. A. Heys, C. Hughes, P. Lasch, P. L. Martin-Hirsch, B. Obinaju, G. D. Sockalingum, J. Sule-Suso, R. J. Strong, M. J. Walsh, B. R. Wood, P. Gardner and F. L. Martin, *Nat. Protoc.*, 2014, **9**, 1771-1791.
66. D. Schnappinger and W. Hillen, *Arch. Microbiol.*, 1996, **165**, 359-369.
67. A. M. Fayaz, K. Balaji, M. Girilal, R. Yadav, P. T. Kalaichelvan and R. Venketesan, *Nanomedicine*, 2010, **6**, 103-109.
68. G. D. Shockman, J. J. Kolb and G. Toennies, *J. Biol. Chem.*, 1958, **230**, 961-977.
69. C. Marambio-Jones and E. M. Hoek, *J. Nanopart. Res.*, 2010, **12**, 1531-1551.
70. O. Gordon, T. V. Slenters, P. S. Brunetto, A. E. Villaruz, D. E. Sturdevant, M. Otto, R. Landmann and K. M. Fromm, *Antimicrob. Agents Chemother.*, 2010, **54**, 4208-4218.
71. A. J. Kowaltowski and A. E. Vercesi, *Free Radical Biol. Med.*, 1999, **26**, 463-471.
72. J. F. Turrens, *Biosci. Rep.*, 1997, **17**, 3-8.
73. Y. Liu and J. A. Imlay, *Science*, 2013, **339**, 1210-1213.
74. I. Keren, Y. Wu, J. Inocencio, L. R. Mulcahy and K. Lewis, *Science*, 2013, **339**, 1213-1216.
75. H. H. Lara, N. V. Ayala-Núñez, L. d. C. Ixtepan Turrent and C. Rodríguez Padilla, *World Journal of Microbiology and Biotechnology*, 2010, **26**, 615-621.
76. Z.-M. Xiu, J. Ma and P. J. Alvarez, *Environ. Sci. Technol.*, 2011, **45**, 9003-9008.

77. J. R. Morones, J. L. Elechiguerra, A. Camacho, K. Holt, J. B. Kouri, J. T. Ramírez and M. J. Yacaman, *Nanotechnology*, 2005, **16**, 2346.

78. D. Trachootham, Y. Zhou, H. Zhang, Y. Demizu, Z. Chen, H. Pelicano, P. J. Chiao, G. Achanta, R. B. Arlinghaus and J. Liu, *Cancer cell*, 2006, **10**, 241-252.

Figure Cations

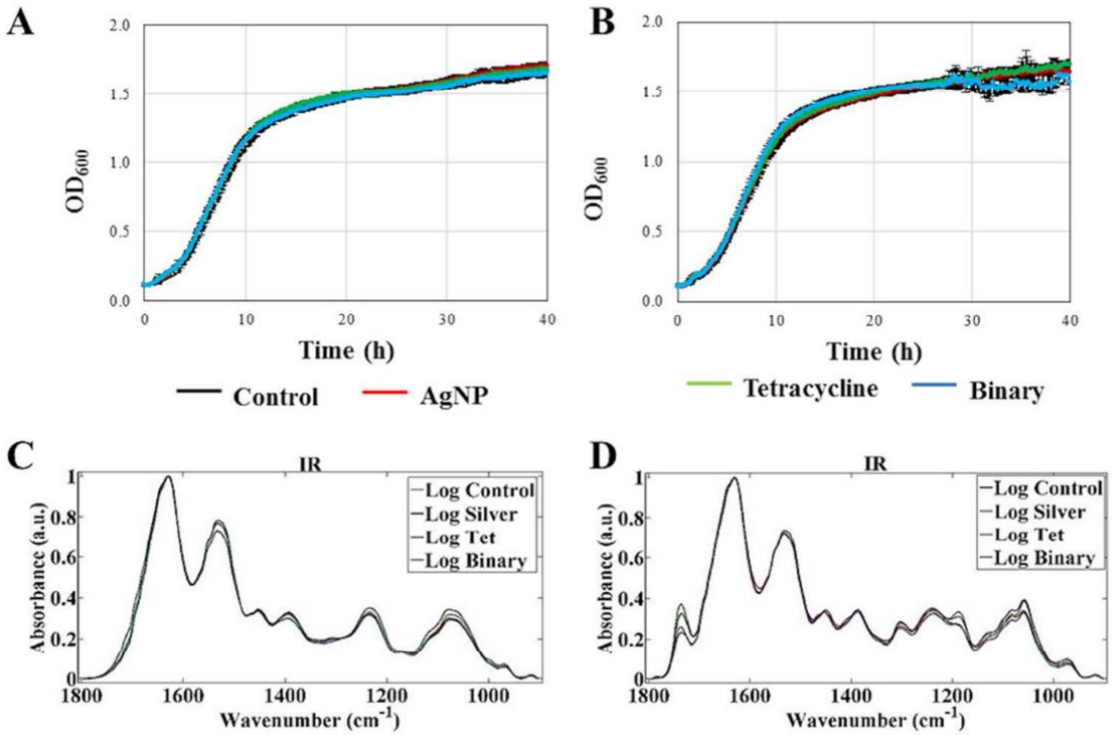

Figure 1. Growth curves of *M. vanbaalenii* (A) and *P. fluorescens* (B) under AgNP, tetracycline and AgNP-tetracycline binary exposures. The exposure concentrations were 4 μg/L for AgNP and 1 μg/L for tetracycline. IR spectral average of *M. vanbaalenii* (C) and *P. fluorescens* (D) in different exposure treatments. The groups of "Log control", "Log silver", "Log tet" and "Log binary" refer to sample collected at log-phase from the treatments of control, silver, tetracycline and binary-exposure.

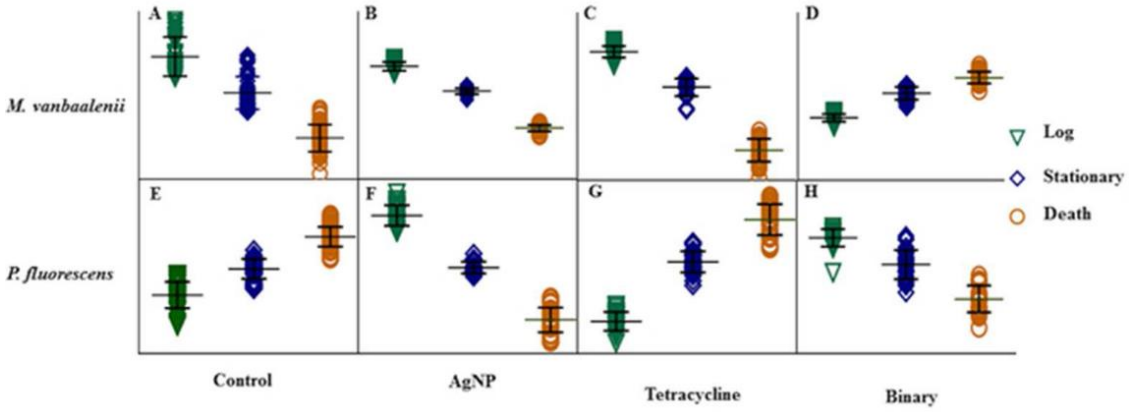

Figure 2. Exposure effects within different growth phases (scale range of Y axis: -0.2 ~ 0.2). The Y axis refers to the values of LD1. *M. vanbaalenii*: control (A), post-exposure to AgNP (B), post-exposure to tetracycline (C), and post-exposure to AgNP-tetracycline mixture (D). *P.*

fluorescens: control (E), post-exposure to AgNP (F), post-exposure to tetracycline (G), and post-exposure to AgNP-tetracycline mixture (H).

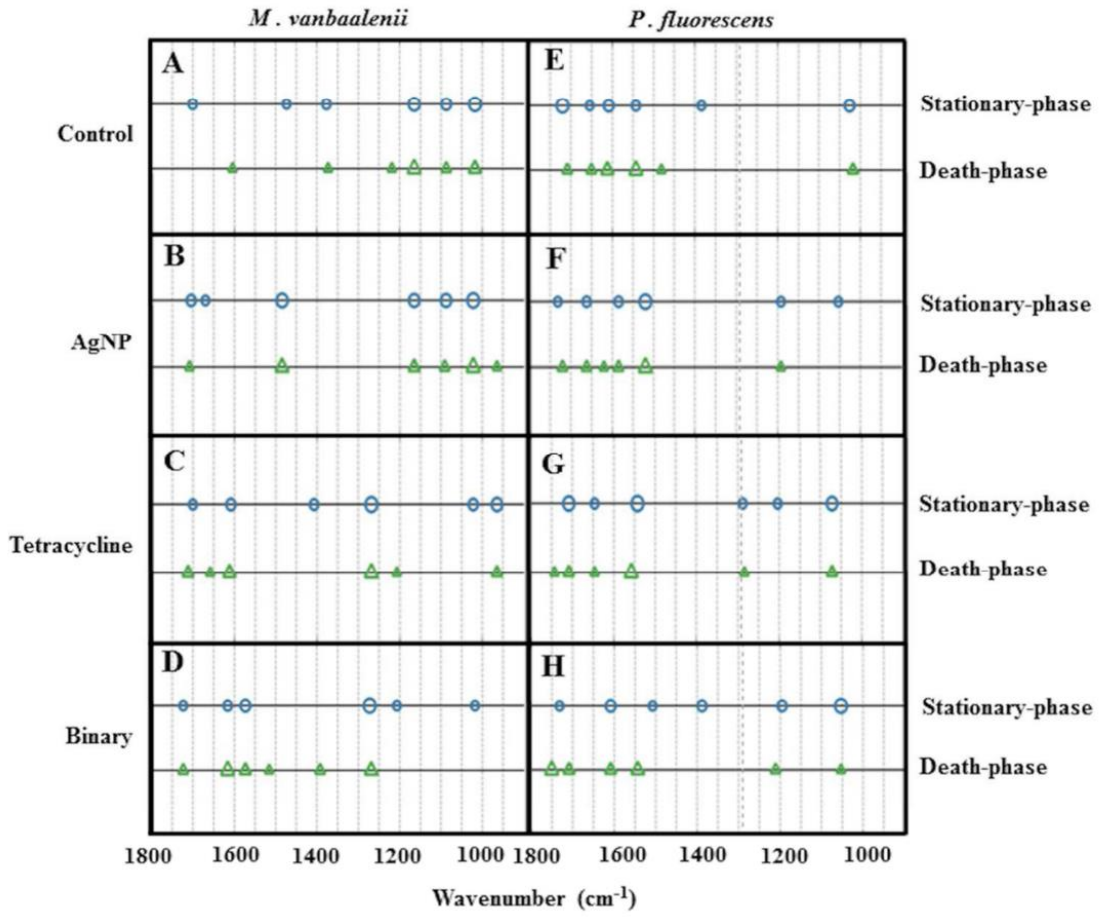

Figure 3. Vector-cluster analysis of exposure effects within different growth phases. *M. vanbaalenii*: control (A), post-exposure to AgNP (B), post-exposure to tetracycline (C), and post-exposure to AgNP-tetracycline mixture (D). *P. fluorescens*: control (E), post-exposure to AgNP (F), post-exposure to tetracycline (G), and post-exposure to AgNP-tetracycline mixture (H).

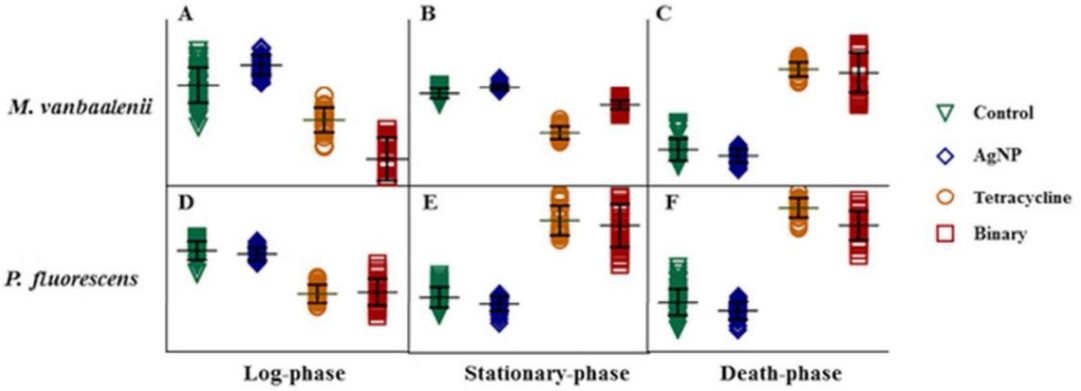

Figure 4. Exposure effects within the same growth phase. The Y axis refers to the values of LD1 in range of -0.2 to 0.2. *M. vanbaalenii*: log-phase (A), stationary-phase (B), and death-phase (C). *P. fluorescens*: log-phase (D), stationary-phase (E), and death-phase (F).

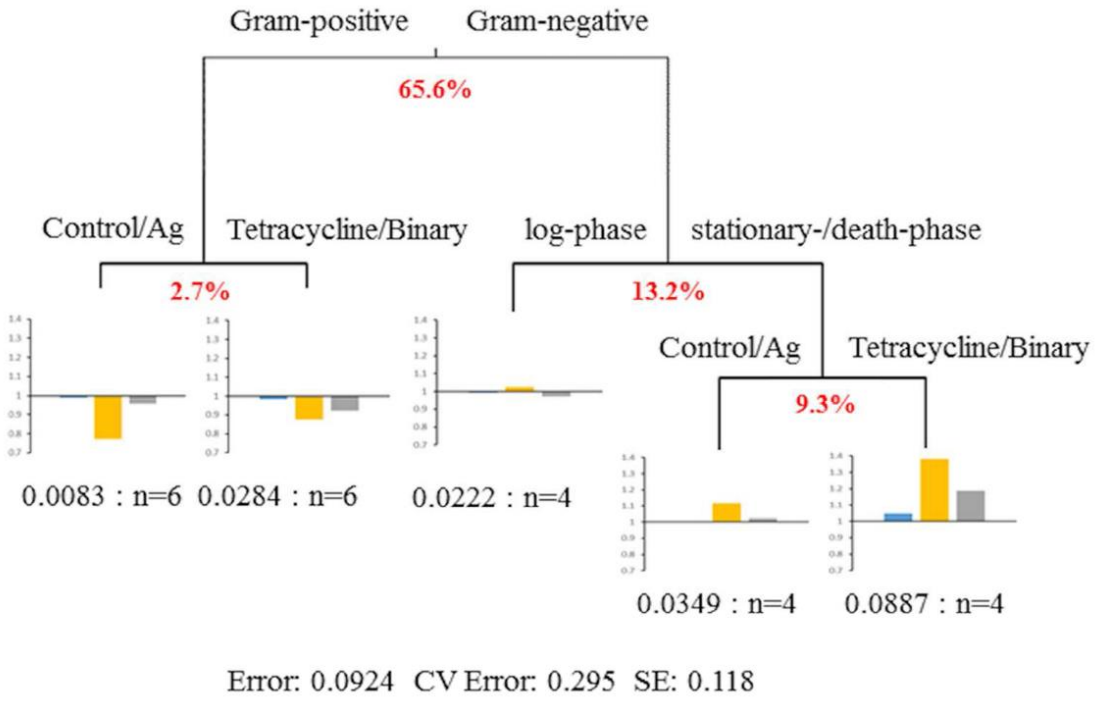

Figure 5. Multivariate regression tree (MRT) analysis of environmental variables explaining the discriminating biomarkers. The scale of the sub-figures represents the alteration degree (1.0 refers to the average level). Blue bars for wavelengths representing proteins, yellow bars for phospholipid-derived fatty acids, and grey bars for other cellular components.

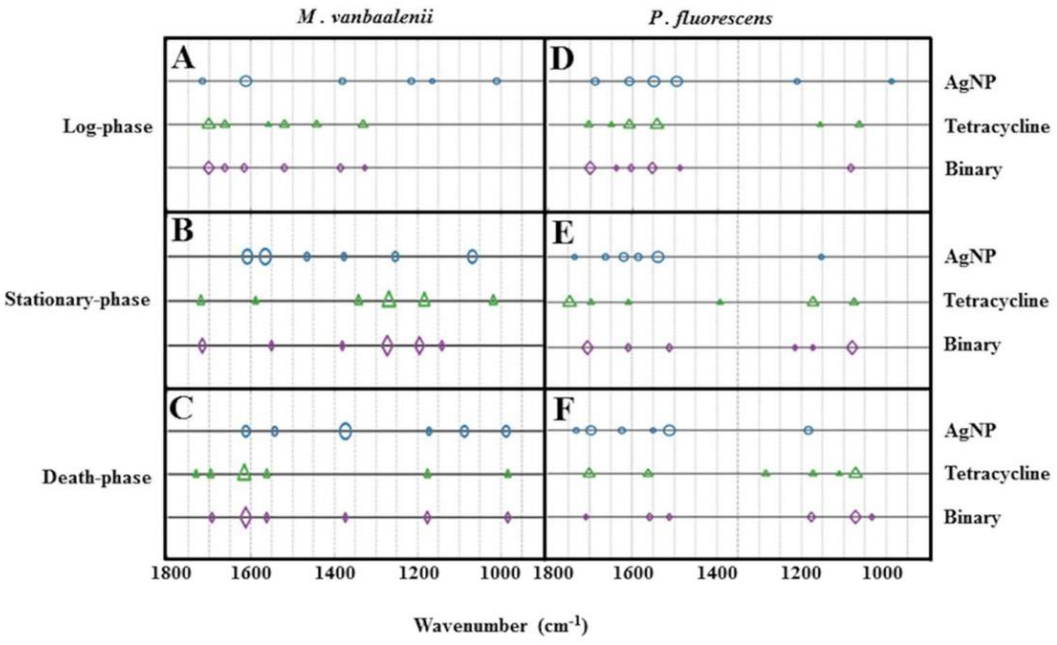

Figure 6. Vector-cluster analysis of exposure effects within the same growth phase. *M. vanbaalenii*: log-phase (A), stationary-phase (B), and death-phase (C). *P. fluorescens*: log-phase (D), stationary-phase (E), and death-phase (F).

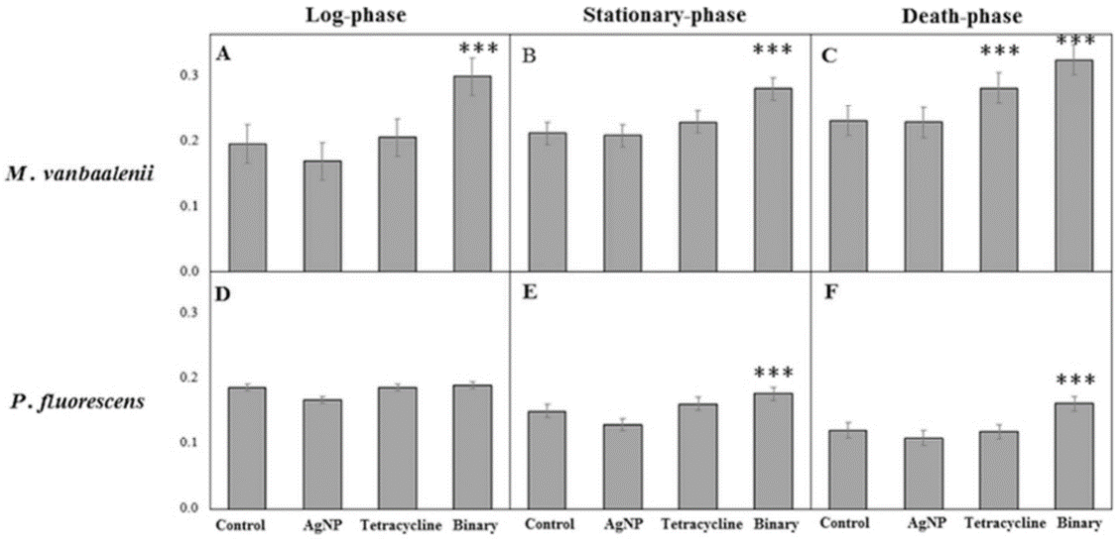

Figure 7. Ratio of cysteine (CySS, 668 cm^{-1}) to protein (1447 cm^{-1}) derived from Raman spectra. Data are presented in mean ± standard error.

Spectrochemical analyses of growth phase-related bacterial responses to low (environmentally-relevant) concentrations of tetracycline and nanoparticulate silver

Naifu Jin[1], Kirk T. Semple[1], Longfei Jiang[2], Chunling Luo[2], Dayi Zhang[1,4,*], Francis L. Martin[3,*]

[1]*Lancaster Environment Centre, Lancaster University, Lancaster LA1 4YQ, UK;*

[2]*Guangzhou Institute of Geochemistry, Chinese Academy of Sciences, Guangzhou 510640, China;*

[3]*School of Pharmacy and Biomedical Sciences, University of Central Lancashire, Preston PR1 2HE, UK;*

[4]*School of Environment, Tsinghua University, Beijin 100084, China*

***Corresponding authors:**

Francis L Martin, School of Pharmacy and Biomedical Sciences, University of Central Lancashire, Preston PR1 2HE, UK, Email: flmartin@uclan.ac.uk

Dayi Zhang, Lancaster Environment Centre, Lancaster University, Lancaster LA1 4YQ, UK; School of Environment, Tsinghua University, Beijin 100084, China. Email: d.zhang@lancaster.ac.uk

Table S1. Growth impact under each treatment (M. vanbaalenii PYR-1).

Treatment	Control	AgNP	Tetracycline	Binary
P-value	P < 0.0001	P < 0.0001	P < 0.0001	P < 0.0001
Are means significantly different? (P<0.05)	Yes	Yes	Yes	Yes
Paired-group comparison	Significant?	Significant?	Significant?	Significant?
Log vs. Stationary	Yes (****)	Yes (****)	Yes (****)	Yes (****)
Log vs. Death	Yes (****)	Yes (****)	Yes (****)	Yes (****)
Stationary vs. Death	Yes (****)	Yes (****)	Yes (****)	Yes (****)

One-way analysis of variance (ANOVA) with Tukey's post hoc test.

Table S2. Growth impact under each treatment (P. fluorescens).

Treatment	Control	AgNP	Tetracycline	Binary
P-value	P < 0.0001	P < 0.0001	P < 0.0001	P < 0.0001
Are means significantly different? (P<0.05)	Yes	Yes	Yes	Yes
Paired-group comparison	Significant?	Significant?	Significant?	Significant?
Log vs. Stationary	Yes (****)	Yes (****)	Yes (****)	Yes (****)
Log vs. Death	Yes (****)	Yes (****)	Yes (****)	Yes (****)
Stationary vs. Death	Yes (****)	Yes (****)	Yes (****)	Yes (****)

One-way analysis of variance (ANOVA) with Tukey's post hoc test.

Table S3. Treatment impact in each growth phase (M. vanbaalenii PYR-1)

Growth phase	Exponential	Stationary	Death
P-value	P < 0.0001	P < 0.0001	P < 0.0001
Are means significantly different? (P<0.05)	Yes	Yes	Yes
One- or two-tailed P-value?	Two-tailed	Two-tailed	Two-tailed
Paired-group comparison	Significant?	Significant?	Significant?
Control vs. Silver	Yes (****)	Yes (****)	Yes (****)
Control vs. Tet	Yes (****)	Yes (****)	Yes (****)
Sliver vs. Tet	Yes (****)	Yes (****)	Yes (****)
Control vs. Binary	Yes (****)	Yes (****)	Yes (****)

One-way analysis of variance (ANOVA) with Tukey's post hoc test.

Table S4. Treatment impact in each growth phase (P. fluorescens).

Growth phase	Exponential	Stationary	Death
P-value	P < 0.0001	P < 0.0001	P < 0.0001
Are means significantly different? (P<0.05)	Yes	Yes	Yes
One- or two-tailed P-value?	Two-tailed	Two-tailed	Two-tailed
Paired-group comparison	Significant?	Significant?	Significant?
Control vs. Silver	Yes (****)	Yes (****)	Yes (****)
Control vs. Tet	Yes (****)	Yes (****)	Yes (****)
Sliver vs. Tet	Yes (****)	Yes (****)	Yes (****)
Control vs. Binary	Yes (****)	Yes (****)	Yes (****)

One-way analysis of variance (ANOVA) with Tukey's post hoc test.

Chapter 3 Spectrochemical determination of unique bacterial responses following long-term low-level exposure to antimicrobials

Naifu Jin, Kirk T Semple, Longfei Jiang, Chunling Luo, Francis L Martin, Dayi Zhang

Analytical Methods, 2018, 10, 1602 – 1611.

Spectrochemical determination of unique bacterial responses following long-term low-level exposure to antimicrobials

Naifu Jin[a,b], Kirk T Semple[a], Longfei Jiang[c], Chunling Luo[c], Francis L Martin[d,*], Dayi Zhang[a,,b*]

[a]*Lancaster Environment Centre, Lancaster University, Lancaster, LA1 4YQ, UK*

[b]*School of Environment, Tsinghua University, Beijin 100084, China*

[c]*Guangzhou Institute of Geochemistry, Chinese Academy of Sciences, Guangzhou 510640, China*

[d]*School of Pharmacy and Biomedical Sciences, University of Central Lancashire, Preston PR1 2HE, UK*

***Corresponding authors:**

Francis L Martin, School of Pharmacy and Biomedical Sciences, University of Central Lancashire, Preston PR1 2HE, UK; Email: flmartin@uclan.ac.uk

Dayi Zhang, School of Environment, Tsinghua University, Beijing 100084, China; Email: zhangdayi@tsinghua.org.cn

Abstract

Agents arising from engineering or pharmaceutical industries may induce significant environmental impacts. Particularly, antimicrobials not only act as efficient eliminators of certain microbes but also facilitate the propagation of organisms with antimicrobial resistance, raising critical health issues, *e.g.*, the bloom of multidrug-resistant bacteria. Although many investigations have examined microbial responses to antimicrobials and characterized relevant mechanisms, they have focused mainly on high-level and short-term exposures, instead of simulating real-world scenarios in which the antimicrobial exposure is at a low-level for long periods. Herein, we developed a spectrochemical tool, attenuated total reflection Fourier-transform infrared (ATR-FTIR) spectroscopy, as a high-throughput and nondestructive approach to interrogate the long-term effects of low-level antimicrobial exposure in bacterial cells. Post-exposure to nanoparticulate silver (AgNP), tetracycline or their mixtures for 12 days, Gram-positive (*Mycobacterium vanbaalenii* PYR-1) and Gram-negative (*Pseudomonas fluorescens*) bacteria exhibited distinct IR spectral alterations. Multivariate analysis coupled with multivariate regression tree (MRT) indicates nutrient depletion and exposure time as the primary factors in bacterial behavior, followed by exposure category and bacterial type. Nutrient depletion and starvation during long-term exposure drives bacterial cells into a dormant state or to exhibit additional cellular components (*e.g.*, fatty acids) in response to antimicrobials, consequently causing a broader range of spectral alterations compared to short-term exposure. This work is the first report highlighting the more important roles of exposure duration and nutrient depletion, instead of treatment regimen of antimicrobial, on microbial responses to low-level and prolonged environmental exposures.

1. Introduction

Environmental exposure to antimicrobials is a critical issue for both human and microbial communities. Antibiotics are currently ranked as the third most commonly prescribed drugs[1]. In human and veterinary medicine there is abuse of antibiotics, especially for keeping animals healthy at a sub-therapeutic level[2-9]. The primary sink for such antibiotic usage is the environment, *e.g.*, waters and soils, *via* various pathways post-excretion[2, 3 4, 6]. Another group of frequently-used antimicrobial agents is silver-associated entities. Notably, unlike silver ion or salts whose antimicrobial effects are well-studied, the mechanisms of nanoparticulate silver (AgNP) activity remain unclear. However, AgNP is widely exploited for its antibacterial activity, in clothing, food containers, wound dressings, ointments, implant coatings, and ultrafiltration membranes for water purification[10-14]. Developing a reliable approach to interrogate microbial responses to antimicrobials is therefore a matter of urgency, contributing to better understanding of the mechanisms and impacts of antimicrobial agents on environmental microbes[15].

A major issue is the translation from laboratory culture to the real-world scenario of bacteria living in their natural habitats. In contrast to most laboratory culture conditions, *e.g.*, nutrient rich broth, free-living bacteria commonly face nutrient depletion or even more prohibitive circumstances[16]. For instance, cells inhabiting biofilm may be exposed to different concentrations of nutrients, metabolites or environmental stimuli (*e.g.*, temperature, pH, oxygen, etc.)[17-21] across the biofilm matrix and local microenvironment, leading to heterogeneous growth rates and behaviours amongst the cell populations[22, 23]. Amongst these, a small proportion might differentiate into a highly protected phenotypic state and coexist with neighbouring populations that are antibiotic sensitive, resulting from inherent strain differences and adaptation to relatively low concentrations of exposure[16, 22, 23]. Moreover, although regulatory agencies and pharmaceutical administration generally employs high

doses of antimicrobials in *in-vivo* and *in-vitro* trials to ensure the safety of test chemicals, residual exposure is typically associated with extremely low-levels in the physical environment; this raises question as to whether high-concentrations of exposure represent the real-world outcomes[24-29]. Thus, research on prolonged low-level exposures of antimicrobials is required in order to shed deeper insights into microbial responses to antimicrobials in the real-world environment[15].

Despite recently developed molecular techniques towards targeting microbial phenotypes, such approaches to identify minor or pre-stage phenotypic alterations induced by low-level exposure remain limited[30-33]. Meanwhile, other confounding factors (*e.g.*, microbial species, growth phase, exposure time, etc.) may also influence test results[16, 31, 34]. In 1991, FTIR spectroscopy was innovatively introduced as a sensitive and rapid screening tool for characterization, classification and identification of microorganism[16]. Since then, the emerging application of spectrochemical techniques with computational analysis as an inter-discipline approach is proving feasible in microbiology and cytology[30-36]. In the recent decade, ATR-FTIR and chemometrics were exploited broadly for microbial characterization, determination and related functions and activities[16, 30, 31, 33, 34, 37, 38]. This technical combination provides a major advantage in terms of the high-throughput and label-free nature of a relatively inexpensive application[30], allowing sample interrogation *via* a nondestructive and nonintrusive manner, which has great potential in monitoring real-world scenarios in real time[30-32, 34].

The current study applied attenuated total reflection Fourier-transform infrared (ATR-FTIR) microscopy coupled with multivariate analysis to investigate bacterial responses to prolonged low-level exposures of AgNP and tetracycline under nutrient depletion conditions. Compared to short-term exposure, we found that length of exposure plays a more important role than treatment with antimicrobial reagents or bacterial type, further uncovering key

influential factors of bacterial responses to antimicrobials during *cell growth associated with nutrient depletion.*

2. Methodology

2.1 Cell strains and sample preparation

The two bacterial strains used in this study were *Mycobacterium vanbaalenii* PYR-1 (Gram-positive) and *Pseudomonas fluorescens* (Gram-negative). They were both grown in minimal medium with 20 mM sodium succinate, undertaken in a dark rotary shaker at 150 rpm and the culture temperature was 30±2°C. The four treatments included non-exposure negative control (CK), 4 μg/L of AgNP, 1 μg/L of tetracycline, and a mixture of 4 μg/L AgNP plus 1 μg/L tetracycline (Binary) were applied to mimic the low-level exposure in nature environment as well as keep consistency with our previous work for the convenience of comparison[38]. The exposure was added in early log-phase (OD_{600}=0.6). The samples of short-term exposure were taken after 2 h (late log-phase, T_0) and 48 h (T_1), respectively. To create a nutrient-depletion condition for long-term exposure, the cells were cultivated in 10-times diluted minimal medium and the culture medium was refreshed every 72 h. The samples were collected at 3 (T_2), 6 (T_3), 9 (T_4) and 12 (T_5) days. The collected cells were then harvested by centrifugation at 4000 rcf for 5 min, washed three times with sterile deionized water, and finally fixed with 70% ethanol to prevent further exposure. The prepared samples were then applied onto Low-E slides and dried for analysis by ATR-FTIR spectroscopy.

2.2 Spectrochemical analysis

The prepared samples (minimal amount > 5 μL) were then applied onto Low-E slides and dried for analysis by ATR-FTIR spectroscopy. A Bruker TENSOR 27 FTIR spectrometer (Bruker Optics Ltd., UK) with a Helios ATR attachment containing a diamond internal reflection element (IRE) was applied to acquire IR spectra. The data were attained at a resolution of 3.84

cm^{-1}, 2.2 kHz mirror velocity and 32 co-additions. The instrument parameters were set at 32 scans and 16 cm^{-1} resolution. To collect the data, a total of 30 individual spectral measurements were taken randomly from each sample using the aid of the ATR magnification-limited viewfinder camera. Prior to analysing each new specimen, the crystal was cleaned using deionized water and a background reading was taken.

2.3 Multivariate analysis and statistics

All the initial data generated from ATR-FTIR spectroscopy were analysed using MATLAB R2011a (*TheMathsWorks, Natick, MA, USA*) coupled with the IRootLab toolbox (http://irootlab.googlecode.com)[39]. The acquired IR spectra were merged and cut to the biochemical-cell fingerprint region (1800-900 cm^{-1}). Then a rubber-band baseline correction was applied to remove any slopes in this area. The data were then normalized to Amide I (1650 cm^{-1}) and the means were centered allowing alignment of the different spectra for comparison.

Principal component analysis-linear discriminant analysis (PCA-LDA) was applied after data pre-processing to reduce the number of spectra to 10 uncorrelated principal components (PCs), which accounts for >99% of the total variance; LDA is a suprevised technique coupled with PCA in order to maximize interclass and minimize intraclass varance[30, 31, 40]. Cross-calculation was subsequently performed mitigate risk resulting from LDA overfitting[41]. The PCA-LDA loadings using (n – 1) samples (n = number of samples in dataset) was trained via leave-one-out cross-validation and then calculated the scores of the rest sample. This process was performed for all scores within the test.

PCA-LDA cluster vectors are pseudo-spectra highlighting the key biochemical alterations of each group in the dataset[35], which allows one to simplify the identification of discriminating differences amongst groups. The centre of the control cluster itself is moved to the origin of the PCA-LDA factor space. The extent of peak deviation away from the origin of

the factor space then occurs according to the centre of each corresponding agent-induced cluster, proportional to the discriminating extent of biochemical differences[31, 41]. Cluster vectors plots were also applied to indicate the most prominent six significant peaks.

Multivariate regression trees (MRT) were used to analyse the influence of bacterial type, exposure time and exposure category on biospectral alterations using the R package "mvpart". Herein, Gram-positive (*M. vanbaalenii*) and Gram-negative (*P. fluorescens*) strains were assigned as 1 and 0. The exposure of AgNP, tetracycline and their mixtures were assigned as 1, 2 and 3, respectively. The samples collected at different time points (T_0, T_1, T_2, T_3, T_4 and T_5) were assigned to 1, 2, 3, 4, 5 and 6, respectively.

One-way analysis of variance (ANOVA) with Tukey's post-hoc test/or *t*-test was employed to test the differences between treatments. All statistical analyses were carried out in GraphPad Prism 6.

3. Results and discussion

3.1 Growth-dependent spectrochemical alterations

Throughout the study, a spectral class mean for the bacterial control group has been derived, which generates an average spectrum based on all raw data from the same group. However, minor variability is visualised from the class mean data directly between groups at different time points (Figure 1A and 1B). Although previous studies suggest that bacteria with limited nutrients are more likely to enter a dormant state waiting suitable growth conditions[42, 43], the spectral alterations induced by nutrient depletion are limited. Therefore, a further cluster vectors analysis is applied to highlight the minor alterations derived from nutrient depletion (Figure 1C and 1D). The identical spectral biomarkers in both Gram-positive (*M. Vanbaalenii*) and Gram-negative (*P. fluorescens*) bacteria are associated with Amide I, Amide III (~1204 cm^{-1}, ~1647 cm^{-1})[30, 33] (Table 1). The main changes appearing in *M.*

Vanbaalenii are Amide III, (~1204 cm^{-1}, ~1400 cm^{-1}), C=N adenine (~1574 cm^{-1}), Amide I (~1652 cm^{-1}), and C=O band (~1725 cm^{-1})[33, 44]. Of these, the amino acid-associated alterations possibly contributing to nucleotide metabolism, which is important for cellular catabolism are significant. Along with long-term starvation and oxygen depletion, decreasing amounts of nucleotides are associated with reduced cell activities and replication compared to log-phase. Furthermore, alterations in other cellular components (*e.g.*, proteins) might be mainly responsible for cell wall maintenance, based on previous study[45].

The specific spectrochemical alterations of *P. fluorescens* include Amide III (~1278 cm^{-1}), CH_2 bending of the methylene chains in lipids (~1470 cm^{-1}), protein Amide II absorption (~1540 cm^{-1}), C=N cytosine (~1601 cm^{-1}), ν(C=C) lipids, and fatty acids (~1750 cm^{-1})[34, 44]. Accordingly, more lipid alterations under nutrient depletion conditions are found in Gram-negative *P. fluorescens versus* Gram-positive *M. vanbaalenii* owing to their differing cell wall structures. There is only a thin peptidoglycan layer (~2-3 nm) between the cytoplasmic and outer membrane in Gram-negative bacteria, whereas the outer membrane in Gram-positive bacteria is a thick peptidoglycan layer of 30 nm with no other additional structure[46]. The attributes of membrane structure may explain the distinct spectrochemical alterations between *P. fluorescens* and *M. vanbaalenii* under nutrient depletion, which might lead to different responses towards long-term exposure of antimicrobials.

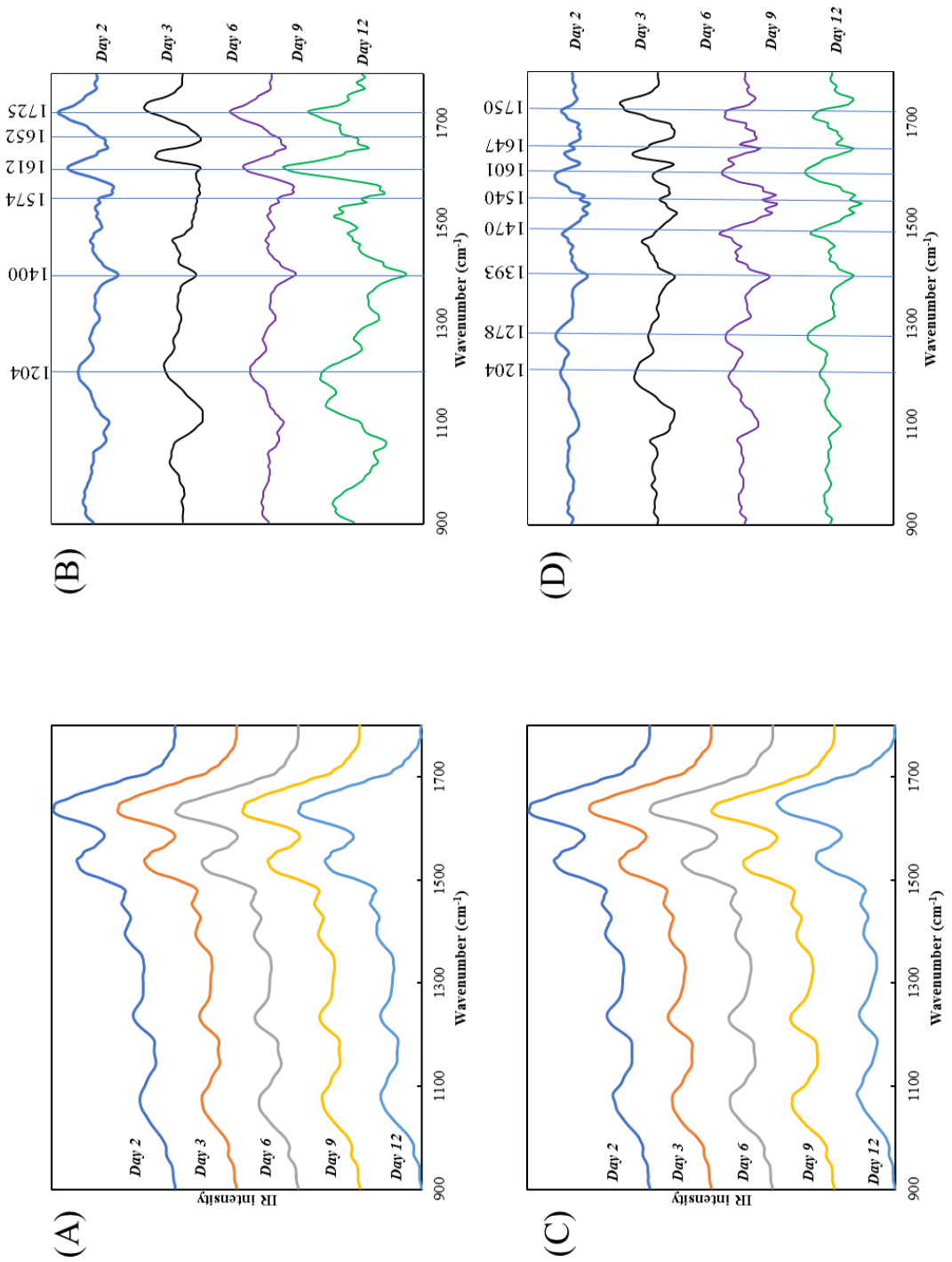

Figure 1. Spectrochemical alterations with length of culture. Infrared spectra of *M. vanbaalenii* (A) and *P. fluorescens* (C) from control group. Cluster vectors plots of *M. vanbaalenii* (B) and *P. fluorescens* (D) from control group, indicating significant wavenumbers contributing to segregating spectral alterations that develop with increasing culture time.

Table 1. Significant spectral biomarkers peaks derived from cluster vectors of *M. vanbaalenii* (Gram-positive) and *P. fluorescens* (Gram-negative) post-exposure to AgNP, tetracycline and their mixtures. Red dots represent identical biomarkers for both Gram-positive and Gram-negative bacteria, and green and blue dots indicate biomarkers appear only in Gram-positive or Gram-negative bacteria, respectively.

Wavenumber (cm^{-1})	**Annotation**	**Gram-positive**				**Gram-negative**			
		Growth	AgNP	Tetracycline	Binary	Growth	AgNP	Tetracycline	Binary
~ 964	*C-C, C-O deoxyribose*	-	●	-	-	-	-	-	-
~ 1084	DNA	-	-	●	●	-	-	-	-
~ 1204	Amide III	●	-	-	-	●	-	-	-
~ 1212	Phosphate	-	●	-	-	-	-	-	-
~ 1220	PO_2^- stretching in RNA and DNA	-	-	●	●	-	-	●	●
~ 1278	Amide III	-	-	-	-	●	-	-	-
~ 1307	Amide III	-	●	-	●	-	-	-	-
~ 1327	Stretching C-N thymine, adenine	-	-	-	-	-	●	-	●
~ 1393		-	-	-	-	●	-	-	-
~ 1400	Proteins	●	-	-	-	-	-	-	-
~ 1404	CH_3 asymmetric deformation	-	-	-	●	-	-	-	-
~ 1423		-	-	-	-	-	●	●	●
~ 1458	Lipids and proteins	-	-	-	-	-	-	●	-
~ 1462		-	-	-	●	-	-	-	●
~ 1468		-	-	-	-	-	●	-	-
~ 1470	CH_2 bending of the methylene chains in lipids	-	-	-	-	●	-	-	-
~ 1477		-	-	●	-	-	-	-	-
~ 1520	Amide II	-	-	-	-	-	-	-	●
~ 1540	Protein amide II absorption	-	-	-	-	●	-	-	-
~ 1555	Ring base	-	●	●	●	-	-	-	-
~ 1574	C=N adenine	●	-	-	-	-	-	-	-
~ 1577	C-C stretch	-	-	-	-	-	●	-	-

~ 1601	C=N cytosine	-	-	-	-	●	-	-	-
~ 1612		●	-	-	-	-	-	-	-
~ 1624		-	-	-	-	-	●	-	-
~ 1632	C-C stretch	-	-	-	●	-	-	-	-
~ 1639	Amide	-	-	-	-	-	-	●	-
~ 1647	Amide I	●	-	●	-	●	-	●	-
~ 1652	Amide I	●	-	-	-	-	-	-	-
~ 1666	C=O stretching vibration of pyrimidine base	-	-	-	-	-	●	-	●
~ 1670	Amide I	-	●	-	-	-	-	-	-
~ 1694	Proteins	-	-	-	-	-	-	●	-
~ 1706	C=O thymine	-	●	-	-	-	-	-	-
~ 1725	C=O band	●	-	-	-	-	-	-	-
~ 1740	C=O, lipids	-	-	-	-	-	-	●	●
~ 1750	ν(C=C) lipids, fatty acids	●	-	●	-	●	-	●	-

3.2 Spectrochemical alterations with long-term AgNP/tetracycline exposure

To identify exposure-induced alterations, the spectral data of each treatment group are compared with the control group at the same time point, eliminating the impacts of cell growth and nutrient depletion (Figure 2). In Gram-positive M. Vanbaalenii, the AgNP-induced alterations are C-C, C-O deoxyribose (~964 cm^{-1}), phosphate (~1212 cm^{-1}), Amide III (~1307 cm^{-1}), ring base (~1555 cm^{-1}), Amide I (~1670 cm^{-1}), and C=O thymine (~1706 cm^{-1})[30, 33, 38]. Post-exposure to tetracycline, the representative peaks are DNA (~1084 cm^{-1}), PO_2^- stretching in RNA and DNA (~1220 cm^{-1}), ring base (~1555 cm^{-1}), Amide I (~1647 cm^{-1}), lipids, and fatty acids (~1750 cm^{-1})[33, 38, 44]. With the binary exposure, the alterations are different from individual exposures, and the specific spectral biomarkers are DNA (~1084 cm^{-1}), PO_2^- stretching in RNA and DNA (~1220 cm^{-1}), Amide III (~1307 cm^{-1}), CH_3 asymmetric deformation (~1404 cm^{-1}, ~1462 cm^{-1}), ring base (~1555 cm^{-1}), and C-C stretch (~1632 cm^{-1})[38, 44]. It is worth mentioning that the binary effects of AgNP and tetracycline on *M. vanbaalenii* spectra are mainly driven by tetracycline as more identical discriminating peaks are observed between these two groups (Table 1). To evaluate the impacts of each exposure, PCA-LDA score plots were generated and illustrate the increasing segregation between groups with increasing exposure time (from day 3 to day 12, Figure 3). Particularly, the biochemical distances of tetracycline and binary groups are co-located, apparently separated from the control

group and markedly on day 12. However, the AgNP-treated groups only show slight shifting of biochemical differences compared to the control group. This result is consistent with cluster vectors analysis that the binary-exposure effects in M. vanbaalenii are closer to tetracycline alone than AgNP.

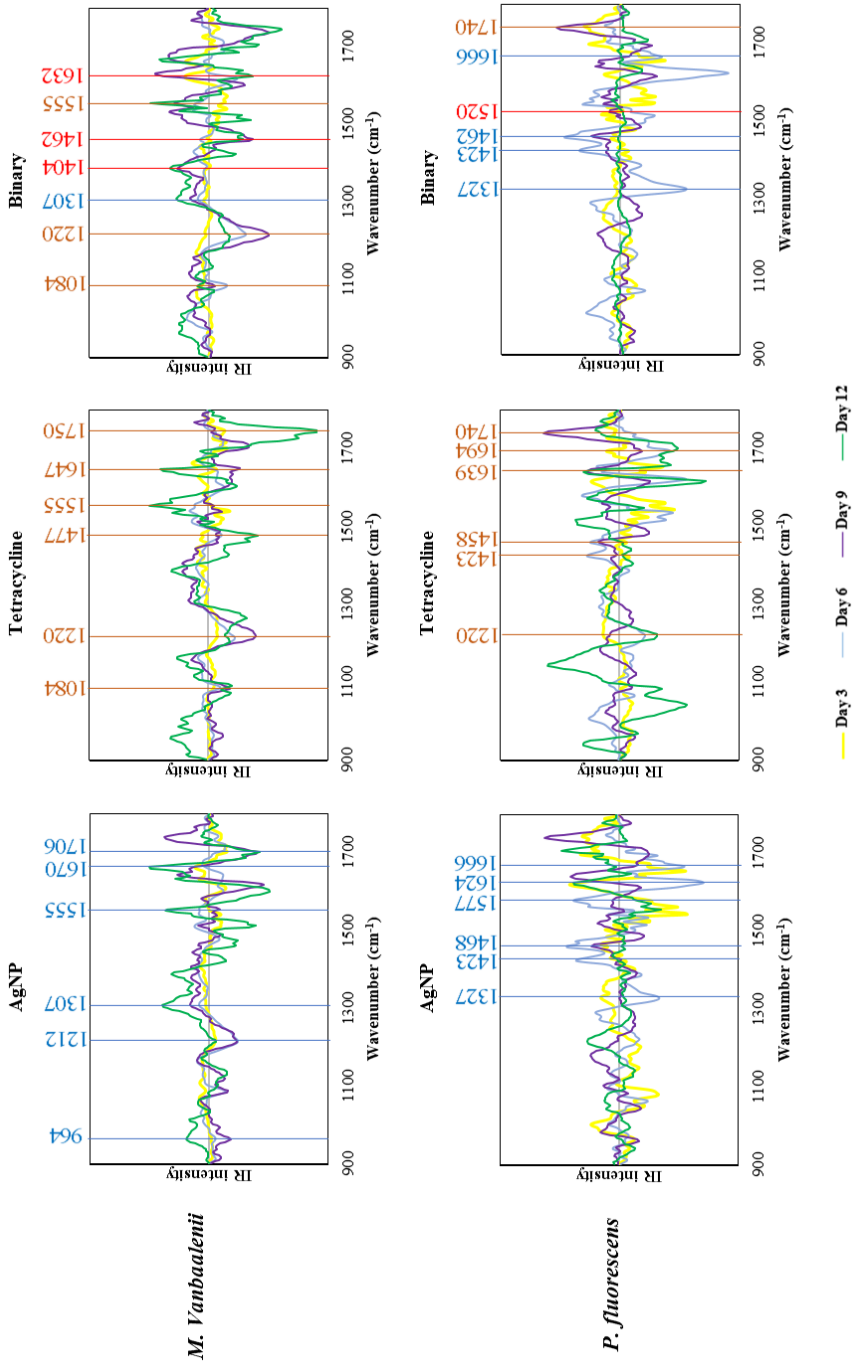

Figure 2. Cluster vectors plots after PCA-LDA, indicating significant wavenumbers for the segregation of *M. vanbaalenii* and *P. fluorescens* following long-term exposure (day 3 to day 12) to AgNP, tetracycline or their mixtures.

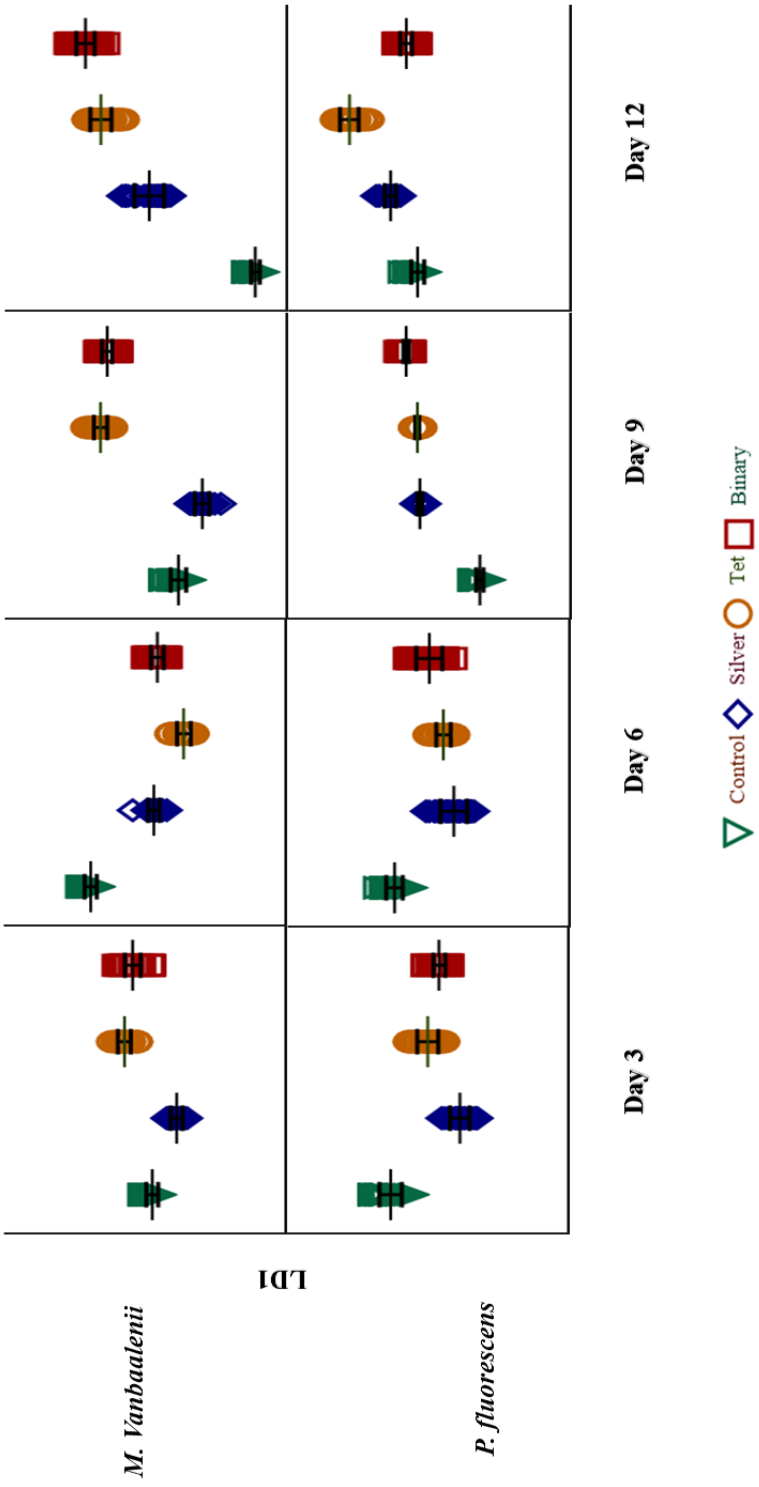
M. Vanbaalenii
P. fluorescens
LD1
Day 3
Day 6
Day 9
Day 12
Control
Silver
Tet
Binary

Figure 3. PCA-LDA score plots for the biospectral alteration of *M. vanbaalenii* and *P. fluorescens* following long-term exposure (day 3 to day 12) to AgNP, tetracycline or their mixtures.

In Gram-negative *P. fluorescens,* all the exposure groups are clearly separated from the control group in the PCA-LDA score plots (Figure 3), and there is no significant difference between each treatment. *T*he AgNP-induced alterations include stretching C-N thymine, adenine (~1327 cm^{-1}), lipids and proteins (~1458 cm^{-1}), C-C stretch (~1577 cm^{-1}), (~1624 cm^{-1}), and C=O stretching vibration of pyrimidine base (~1666 cm^{-1})[44]. The tetracycline-induced peaks are DNA (~1220 cm^{-1}); (~1423 cm^{-1}), collagen (~1458 cm^{-1}), Amide I (~1639 cm^{-1}, ~1694 cm^{-1}), and C=O lipids (~1740 cm^{-1}). Generally, outer cellular components are widely affected by both AgNP and tetracycline, including Amides I/II and proteins (~1307 cm^{-1}, ~1647 cm^{-1}, 1639 -1694 cm^{-1}), and lipids and/or fatty acids (1750 cm^{-1}, 1458 cm^{-1}, 1740 cm^{-1}), indicating that the cell membrane is the primary reactive target associated with both antimicrobials which penetrate bacterial cells *via* passive diffusion and inhibit bacterial growth by perturbing protein synthesis or altering membrane structure[47]. Additionally, more inner cellular components are identified to be associated with tetracycline exposure than AgNP, *e.g.*, inherent DNA and RNA, possibly due to the antibiotic mechanism of tetracycline which blocks the elongation cycle by preventing incoming aminoacyl-tRNA (aa-tRNA) from binding to the ribosomal A-site and

inhibiting protein synthesis[48]. Different from Gram-positive strains, AgNP-induced alterations contribute predominantly to the binary effects in *P. fluorescens*, *i.e.*, stretching C-N thymine, adenine (~1327 cm^{-1}, ~1423 cm^{-1}, ~1462 cm^{-1}), Amide II (~1520 cm^{-1}), C=O stretching vibration of pyrimidine base (~1666 cm^{-1}), and C=O lipids (~1740 cm^{-1})[31, 34]. These findings imply the antimicrobial synergism of AgNP and tetracycline. A previous study suggests that antibiotics' efficacy against microbes may increase in the presence of AgNP because of the bonding reaction between antibiotics and nanofillers, owing to the chelating reaction of hydroxyl and amide groups in antibiotic molecules with AgNP[49].

3.3 Impacts of exposure time on spectrochemical alterations

Although short-term impacts by antimicrobials on bacteria is obvious and well-studied, their consequences may last for extended periods and remain unknown[50]. To unravel such long-term exposure effects, we measured the biospectral alterations at different time points, and found distinguishing biomarkers post-exposure to antimicrobials between short-term *versus* long-term treatments (Figure 4). Generally, in short-term exposure (≤3 days), spectral changes are associated with components from cell membranes wherein most antimicrobial-induced alterations occur in both strains, including glycogen (~1022 cm^{-1}), symmetric phosphate stretching vibrations (~1088 cm^{-1}, 1092 cm^{-1}), carbohydrates (~1165 cm^{-1}), protein phosphorylation (~964 cm^{-1}), Amide I (~1609 cm^{-1}, 1612 cm^{-1}, 1659 cm^{-1}, ~1670 cm^{-1}), Amide III

(~1269 cm^{-1}), COO- symmetric stretching vibrations of fatty acids and amino acid (~1408 cm^{-1}), proteins (~1485 cm^{-1}, ~1550 cm^{-1}, ~1650 cm^{-1}), and lipids (~1701 cm^{-1}, 1705-1750 cm^{-1})[30, 32, 38, 44]. Besides external cellular components, some inherent elements are significantly influenced in long-term exposure (>3 days). For instance, long-term tetracycline-induced alterations in *P. fluorescens* include RNA and DNA (*e.g.*, ~1220 cm^{-1}, ~1423 cm^{-1}). Compared to prolonged exposure, short exposure induces minimal alterations, possibly owing to bacteria undergoing pre-stage reactions against antimicrobials. During extended exposure periods, the more obvious biospectral alterations might be explained by increasing tetracycline accumulation *via* penetration and stronger antibiotic effects, which prevent RNA binding to the ribosomal A-site and protein synthesis[48], and further inhibit RNA/DNA synthesis and duplication[51]. Another explanation is the post-antibiotic effect (PAE) or lag of bacterial regrowth induced by long-term antimicrobial exposure, driving bacterial entry into a growth suppression state[52, 53].

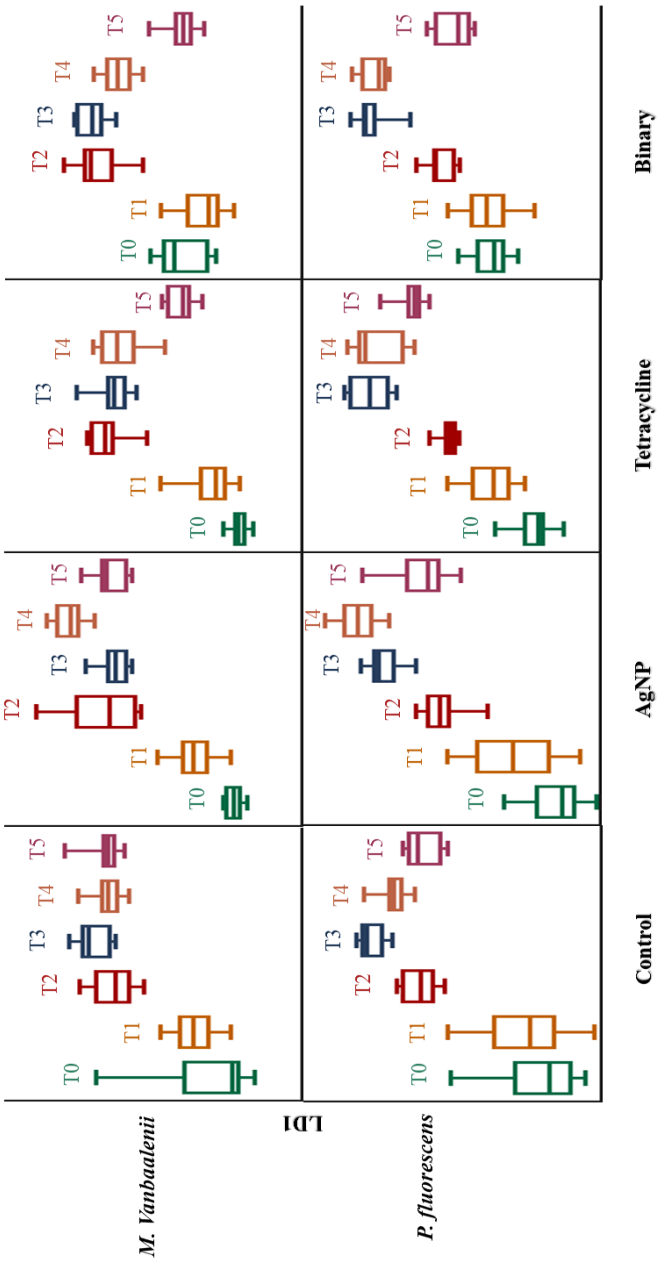

Figure 4. PCA-LDA score plots of the biospectral alteration of *M. vanbaalenii* and *P. fluorescens* in both short-term and long-term exposure to AgNP, tetracycline and their mixtures. T_0, T_1, T_2, T_3, T_4 and T_5 represent exposure time of 2 h, 2 days, 3 days, 6 days, 9 days and 12 days, respectively.

3.4 Influential factors determining bacterial long-term responses to antimicrobials

Although distinct impacts of different antimicrobials on bacteria have been well-documented, many variables including intrinsic and external factors may alter such influences in real-world scenarios. In the present study, we evaluated bacterial type, exposure category, exposure time and nutrient depletion, but which factor is the most dominating remains unlcear. To answer this question, a multivariate regression trees (MRT) analysis based on isolated discriminating biomarkers is conducted to quantify the impacts of these four factors on spectral alterations. MRT visualizes these influencing factors on spectral variations in a tree with four splits based on exposure time, exposure category, bacterial type and nutrient depletion, explaining 63.7% of the total spectral variance (Figure 5). Level of influence is ranked as exposure time > exposure type > bacterial type = nutrient depletion. Exposure time accounts for 17.8% of the total variance, with the first split separating the group of 12-day exposure owing to the relatively lower intensities of DNA. In the 12-day exposure group, exposure category explains 16.1% of the variance and splits spectra into two groups of control/tetracycline and AgNP/binary, mainly based on DNA spectral biomarkers. The group of exposure <12 days is further split by bacterial type, accounting for 14.9% of the total variance and attributed to differences in DNA, phospholipid-derived fatty acids and proteins. The final split representing nutrient depletion separates the groups of 6-9 day and 0-3 day for Gram-positive bacteria (*M.*

vanbaalenii, 14.9%), owing to higher cellular activities reflected by significant variations in DNA, phospholipid-derived fatty acids and proteins.

The MRT results are consistent with PCA-LDA score plots (Figure 4). The spectral distances of *P. fluorescens*, for instance, are similar regardless of exposure categories from day 9 due to cell regeneration against the exposure and exhibiting resistance to antimicrobials[42]. A prior study reported that long-term exposure (5 days) to 1 μg/L of tetracycline shows no apparent effect on cyanobacterial cells due to their natural variability in tetracycline resistance[54]. It might explain the closer distance between groups of control and tetracycline. Moreover, the distinct behaviours of *M. vanbaalenii* and *P. fluorescens* upon starvation can explain the fourth split in MRT, *i.e.*, *M. vanbaalenii* enters a replicative state after 6-day exposure to adapt to conditions of insufficient nutrients, whereas *P. fluorescens* appears more susceptible to nutrient depletion and starts regrowth. Evidence can be found from the additional collular components produced in Gram-negative *P. fluorescens*, *e.g.*, fatty acids (~1750 cm^{-1}), as their predominant energy to survive[42].

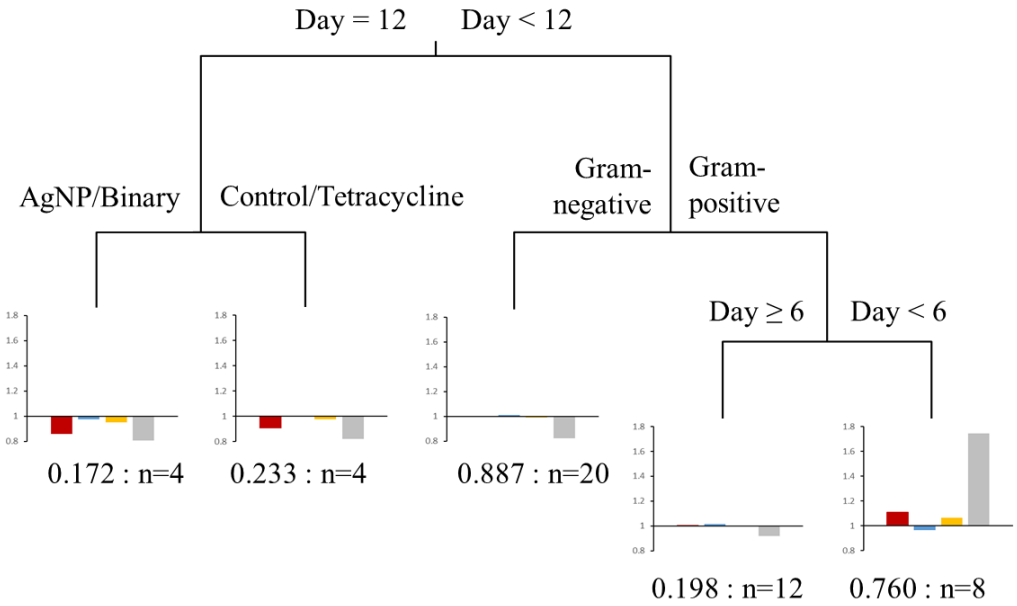

Figure 5. Multivariate regression tree (MRT) analysis of environmental variables explaining discriminating biomarkers. The scale of the sub-figures reflects the alteration degree (number one represents the average level). Red bars represent biomarkers assigned to DNA; blue bars represent biomarkers associated with proteins; yellow bars represent biomarkers assigned to phospholipid-derived fatty acids; and, grey bars represent other cellular components.

Moreover, bacterial type may also have impacts on the consequences posed by antimicrobials since bacteria differ in their cellular structures. Antimicrobials acting as both efficient eliminators to microbes and selective agents help to propagate

organisms with resistance ability[55]. Herein, we found discriminating alterations between Gram-positive and Gram-negative strains within the same exposure treatment. All the treatments exhibit distinct alterations in Gram-positive *M. vanbaalenii* under nutrient depletion conditions (Day 3 to Day 12), although AgNP generates very limited impact as compared to tetracycline or binary exposure groups; these are not observed in *P. fluorescens*. The results from PCA-LDA scores plots (Figure 3) and MRT (Figure 5) also show induced alterations in *M. vanbaalenii* are significant compared to *P. fluorescens*. Furthermore, after long-term exposure (12 days), Gram-negative *P. fluorescens* exhibit a broad range of spectral alterations assigned to lipids and/or fatty acid (*e.g.*, 1458 cm^{-1}, 1740 cm^{-1}), which are absent in Gram-positive *M. vanbaalenii*, mainly attributed to their different cell wall structures. The rigidity and extended cross-linking may reduce the target sites in cell membranes for environmental exposures and afford further protection to cells from antimicrobial penetration[12, 49]. It implies that cell membranes of Gram-negative bacteria are more likely to be influenced compared to Gram-positive bacteria under certain antibacterial treatments (*e,g,*, AgNP)[12, 46, 56]. Past studies report the oxidation of smaller AgNPs (1-10 nm) by intercellular reactive oxygen species (ROS) in Gram-negative bacteria, resulting in the release of silver ions during AgNP penetration through the cell membrane and entrance into the cytoplasm[56]. These silver ions could be further transferred to other Gram-negative bacterial cells, the

membrane and cytoplasm which contain many sulfur-containing proteins for the released Ag^+ to bind to and inactivate[46, 56]. A recent study also reported some novel findings related to the Ag exposure; such treatment could increase cellular lipid content while decreasing membrane fluidity resulted from a possible mechanism that upregulated lipid biosynthesis and therefore decreasing membrane fluidity, which is known to be associated with reduced membrane permeability[57].

Besides bacterial type, exposure time and exposure category, nutrient depletion is also found to be an influential factor in the bacterial antimicrobial response. Here, bacterial cells tend to adapt to new environmental stimuli after entering into a long-term nutrient-deprived situation. From the cluster vectors analysis (Figure 1), spectral alterations in both strains from Day 6 show slight peak shifts, which can be regarded as a potential signal showing that bacterial cells are undergoing adaption. Additionally, *M. vanbaalenii* becomes a persistent suspension in the media on entering a dormant state from Day 6. This is because bacteria in a non-growing state can survive for much longer time under conditions of reduced oxygen or nutrient deprivation[42, 43]. Upon starvation, bacterial cells fragment into small spheroids exhibiting rapid and drastic decreases in endogenous metabolism. This reorganization gives bacteria maximum survival during long-term starvation. Specifically, bacteria on starvation initially induce dwarfing generating cell number increases *via* fragmentation over the first 1 to 2 h and continuous size reductions in

the fragmented cells, but no further increase in numbers. After dwarfing phases, cell size continues to get smaller, with little or no metabolic activity, and slow loss of viability[58]. It has been reported that non-growing phase bacteria adapt to and increase their tolerance to environmental stresses and such developed persistent bacilli are capable of surviving several months of combinatorial antibiotic treatment[43], which implies that stressed living conditions, to some extent and paradoxically, could help microbial resistance to antimicrobial effects.

4. Conclusions

In the present study, we employed spectrochemical analysis coupled with multivariate analysis as a robust tool towards investigating bacterial responses to long-term and low-level exposure of antimicrobials under nutrient depletion conditions. ATR-FTIR spectroscopy shows feasibility in revealing sufficient biochemical information continuously even at extremely low-level exposures in a starvation situation, which fits better with real-world circumstances and the natural state of microcosms. From the multivariate analysis of spectra coupled with MRT, we evaluate the significance of different factors on long-term bacterial responses to antimicrobials and find pivotal roles for exposure time and nutrient depletion. Nutrient depletion can drive bacterial cells to either enter into a dormant state or exhibit extra-cellular components against environmental antimicrobials, consequently causing a broader range of spectral alteration compared to short-term

exposures. Differences in bacterial behaviours towards antimicrobials are also found between bacterial types (Gram-positive *versus* Gram-negative) attributed to variations in cell wall structure. Our work is the first revealing of the more important roles of exposure duration and nutrient depletion, rather than of antimicrobial reagents, on microbial responses to low-level and prolonged environmental exposures. We believe this approach has an important future with potential feasibility in *in situ* screening of environmental exposures in real-time.

Conflicts of interest There are no conflicts of interest to declare.

ACKNOWLEDGEMENTS N.J. was funded by Chinese Academy of Sciences and China Scholarship Council.

References

1. J. Conly, *Can. Med. Assoc. J.*, 2002, **167**, 885-891.
2. J. W. Harrison and T. A. Svec, *Quintessence Int.*, 1998, **29**, 223-229.
3. J. C. Chee-Sanford, R. I. Aminov, I. J. Krapac, N. Garrigues-Jeanjean and R. I. Mackie, *Appl. Environ. Microbiol.*, 2001, **67**, 1494-1502.
4. G. Hamscher, S. Sczesny, H. Hoper and H. Nau, *Anal. Chem.*, 2002, **74**, 1509-1518.
5. X. L. Ji, Q. H. Shen, F. Liu, J. Ma, G. Xu, Y. L. Wang and M. H. Wu, *J. Hazard. Mater.*, 2012, **235**, 178-185.
6. L. Cantas, S. Q. A. Shah, L. M. Cavaco, C. M. Manaia, F. Walsh, M. Popowska, H. Garelick, H. Burgmann and H. Sorum, *Front. Microbiol.*, 2013, **4**, 14.
7. A. Koluman and A. Dikici, *Crit. Rev. Microbiol.*, 2013, **39**, 57-69.
8. M. Tandukar, S. Oh, U. Tezel, K. T. Konstantinidis and S. G. Pavlostathis, *Environ. Sci. Technol.*, 2013, **47**, 9730-9738.
9. J. L. Martinez and F. Baquero, *Ups. J. Med. Sci.*, 2014, **119**, 68-77.
10. J. S. Kim, E. Kuk, K. N. Yu, J. H. Kim, S. J. Park, H. J. Lee, S. H. Kim, Y. K. Park, Y. H. Park, C. Y. Hwang, Y. K. Kim, Y. S. Lee, D. H. Jeong and M. H. Cho, *Nanomed.-Nanotechnol. Biol. Med.*, 2014, **10**, 1119-1119.
11. C. N. Lok, C. M. Ho, R. Chen, Q. Y. He, W. Y. Yu, H. Sun, P. K. H. Tam, J. F. Chiu and C. M. Che, *J. Biol. Inorg. Chem.*, 2007, **12**, 527-534.
12. H. H. Lara, N. V. Ayala-Nunez, L. D. I. Turrent and C. R. Padilla, *World J. Microbiol. Biotechnol.*, 2010, **26**, 615-621.
13. C. Marambio-Jones and E. M. V. Hoek, *J. Nanopart. Res.*, 2010, **12**, 1531-1551.
14. R. J. Griffitt, N. J. Brown-Peterson, D. A. Savin, C. S. Manning, I. Boube, R. A. Ryan and M. Brouwer, *Environ. Toxicol. Chem.*, 2012, **31**, 160-167.

15. A. Gupta and S. Silver, *Nat. Biotechnol.*, 1998, **16**, 888-888.
16. N. F. Jin, D. Y. Zhang and F. L. Martin, *Integr. Biol.*, 2017, **9**, 406-417.
17. P. Marschner, C. H. Yang, R. Lieberei and D. E. Crowley, *Soil Biol. Biochem.*, 2001, **33**, 1437-1445.
18. E. K. Costello, C. L. Lauber, M. Hamady, N. Fierer, J. I. Gordon and R. Knight, *Science*, 2009, **326**, 1694-1697.
19. C. L. Lauber, M. Hamady, R. Knight and N. Fierer, *Appl. Environ. Microbiol.*, 2009, **75**, 5111-5120.
20. M. Wietz, B. Wemheuer, H. Simon, H. A. Giebel, M. A. Seibt, R. Daniel, T. Brinkhoff and M. Simon, *Environ. Microbiol.*, 2015, **17**, 3822-3831.
21. H. B. Li, F. L. Martin and D. Y. Zhang, *Anal. Chem.*, 2017, **89**, 3909-3918.
22. P. S. Stewart and J. W. Costerton, *Lancet*, 2001, **358**, 135-138.
23. N. Hoiby, T. Bjarnsholt, M. Givskov, S. Molin and O. Ciofu, *Int. J. Antimicrob. Agents*, 2010, **35**, 322-332.
24. C. G. Mayhall and E. Apollo, *Antimicrob. Agents Chemother.*, 1980, **18**, 784-788.
25. M. R. W. Brown, D. G. Allison and P. Gilbert, *J. Antimicrob. Chemother.*, 1988, **22**, 777-780.
26. S. M. Ede, L. M. Hafner and P. M. Fredericks, *Appl. Spectrosc.*, 2004, **58**, 317-322.
27. O. I. Kalantzi, R. Hewitt, K. J. Ford, L. Cooper, R. E. Alcock, G. O. Thomas, J. A. Morris, T. J. McMillan, K. C. Jones and F. L. Martin, *Carcinogenesis*, 2004, **25**, 613-622.
28. J. L. Barber, M. J. Walsh, R. Hewitt, K. C. Jones and F. L. Martin, *Mutagenesis*, 2006, **21**, 351-360.
29. O. Fridman, A. Goldberg, I. Ronin, N. Shoresh and N. Q. Balaban, *Nature*, 2014, **513**, 418-421.

30. F. L. Martin, J. G. Kelly, V. Llabjani, P. L. Martin-Hirsch, Patel, II, J. Trevisan, N. J. Fullwood and M. J. Walsh, *Nat. Protoc.*, 2010, **5**, 1748-1760.

31. M. J. Riding, F. L. Martin, J. Trevisan, V. Llabjani, Patel, II, K. C. Jones and K. T. Semple, *Environ. Pollut.*, 2012, **163**, 226-234.

32. J. Y. Li, R. Strong, J. Trevisan, S. W. Fogarty, N. J. Fullwood, K. C. Jones and F. L. Martin, *Environ. Sci. Technol.*, 2013, **47**, 10005-10011.

33. M. J. Baker, J. Trevisan, P. Bassan, R. Bhargava, H. J. Butler, K. M. Dorling, P. R. Fielden, S. W. Fogarty, N. J. Fullwood, K. A. Heys, C. Hughes, P. Lasch, P. L. Martin-Hirsch, B. Obinaju, G. D. Sockalingum, J. Sule-Suso, R. J. Strong, M. J. Walsh, B. R. Wood, P. Gardner and F. L. Martin, *Nat. Protoc.*, 2014, **9**, 1771-1791.

34. K. A. Heys, M. J. Riding, R. J. Strong, R. F. Shore, M. G. Pereira, K. C. Jones, K. T. Semple and F. L. Martin, *Analyst*, 2014, **139**, 896-905.

35. J. G. Kelly, J. Trevisan, A. D. Scott, P. L. Carmichael, H. M. Pollock, P. L. Martin-Hirsch and F. L. Martin, *J. Proteome Res.*, 2011, **10**, 1437-1448.

36. J. Trevisan, P. P. Angelov, P. L. Carmichael, A. D. Scott and F. L. Martin, *Analyst*, 2012, **137**, 3202-3215.

37. N. Jin, M. Paraskevaidi, K. T. Semple, F. L. Martin and D. Y. Zhang, *Anal. Chem.*, 2017, **89**, 9814-9821.

38. N. Jin, K. T. Semple, L. Jiang, C. Luo, D. Zhang and F. L. Martin, *Analyst*, 2018, **143**, 768-776.

39. J. Trevisan, P. P. Angelov, A. D. Scott, P. L. Carmichael and F. L. Martin, *Bioinformatics*, 2013, **29**, 1095-1097.

40. F. L. Martin, M. J. German, E. Wit, T. Fearn, N. Ragavan and H. M. Pollock, *J. Comput. Biol.*, 2007, **14**, 1176-1184.

41. J. Y. Li, G. G. Ying, K. C. Jones and F. L. Martin, *Analyst*, 2015, **140**, 2687-2695.

42. J. C. Betts, P. T. Lukey, L. C. Robb, R. A. McAdam and K. Duncan, *Mol. Microbiol.*, 2002, **43**, 717-731.

43. T. Hampshire, S. Soneji, J. Bacon, B. W. James, J. Hinds, K. Laing, R. A. Stabler, P. D. Marsh and P. D. Butcher, *Tuberculosis*, 2004, **84**, 228-238.

44. Z. Movasaghi, S. Rehman and I. U. Rehman, *Appl. Spectrosc. Rev.*, 2008, **43**, 134-179.

45. M. Drapal, P. R. Wheeler and P. D. Fraser, *Microbiology-(UK)*, 2016, **162**, 1456-1467.

46. J. R. Morones, J. L. Elechiguerra, A. Camacho, K. Holt, J. B. Kouri, J. T. Ramirez and M. J. Yacaman, *Nanotechnology*, 2005, **16**, 2346-2353.

47. D. Schnappinger and W. Hillen, *Arch. Microbiol.*, 1996, **165**, 359-369.

48. S. R. Connell, C. A. Trieber, G. P. Dinos, E. Einfeldt, D. E. Taylor and K. H. Nierhaus, *Embo J.*, 2003, **22**, 945-953.

49. A. M. Fayaz, K. Balaji, M. Girilal, R. Yadav, P. T. Kalaichelvan and R. Venketesan, *Nanomed.-Nanotechnol. Biol. Med.*, 2010, **6**, 103-109.

50. C. Jernberg, S. Lofmark, C. Edlund and J. K. Jansson, *Microbiology-(UK)*, 2010, **156**, 3216-3223.

51. M. Argast and C. F. Beck, *Antimicrob. Agents Chemother.*, 1984, **26**, 263-265.

52. R. W. Bundtzen, A. U. Gerber, D. L. Cohn and W. A. Craig, *Rev. Infect. Dis.*, 1981, **3**, 28-37.

53. K. Fuursted, A. Hjort and L. Knudsen, *J. Antimicrob. Chemother.*, 1997, **40**, 221-226.

54. F. Pomati, A. G. Netting, D. Calamari and B. A. Neilan, *Aquat. Toxicol.*, 2004, **67**, 387-396.

55. S. B. Levy, *J. Antimicrob. Chemother.*, 2002, **49**, 25-30.

56. Z. M. Xiu, J. Ma and P. J. J. Alvarez, *Environ. Sci. Technol.*, 2011, **45**, 9003-9008.

57. R. Gurbanov, S. O. N, S. Tuncer, F. Severcan and A. G. Gozen, *Journal of biophotonics*, 2017, DOI: 10.1002/jbio.201700252.

58. S. Kjelleberg, B. A. Humphrey and K. C. Marshall, *Appl. Environ. Microbiol.*, 1983, **46**, 978-984.

Chapter 4 Infrared spectroscopy coupled with a dispersion model for quantifying the real-time dynamics of kanamycin resistance in artificial microbiota

Naifu Jin, Maria Paraskevaidi, Kirk T. Semple, Francis L. Martin, Dayi Zhang

Analytical Chemistry 2017, 89, 9814 – 9821.

Biospectrochemical tool for quantifying the real-time dynamics of kanamycin resistance in artificial microbiota

Naifu Jin[1], Maria Paraskevaidi[2], Kirk T. Semple[1], Francis L. Martin[2,*], Dayi Zhang[1,*]

[1]Lancaster Environment Centre, Lancaster University, Lancaster, LA1 4YQ, UK;

[2]School of Pharmacy and Biomedical Sciences, University of Central Lancashire, Preston PR1 2HE, UK

Corresponding authors:

Dayi Zhang, Lancaster Environment Centre, Lancaster University, Lancaster LA1 4YQ, UK; Tel.: +44(0)1524 510288; Fax: +44(0)1524 510082, Email: d.zhang@lancaster.ac.uk

Francis L. Martin, School of Pharmacy and Biomedical Sciences, University of Central Lancashire, Preston PR1 2HE, UK; Tel.: +44(0)1772 896482; Email: flmartin@uclan.ac.uk

Abstract

Over-usage of antibiotics leads to the widespread induction of antibiotic resistance genes (ARGs). Developing an approach to allow real-time monitoring and fast prediction of ARGs dynamics in clinical or environmental samples has become an urgent matter. Vibrational spectroscopy is potentially an ideal technique towards the characterization of the microbial composition of microbiota as it is non-destructive, high-throughput and label-free. Herein, we employed attenuated total reflection Fourier-transform infrared (ATR-FTIR) spectroscopy and developed a spectrochemical tool to quantify the static and dynamic composition of kanamycin resistance in artificial microbiota to evaluate microbial antibiotic resistance. Second order differetiation was introduced in identifying the spectral biomarkers, and principal component analysis followed by linear discriminant analysis (PCA-LDA) was used for the multivariate analysis of the spectral data. The calculated results of the mathematical model based on spectral features showed high similarity to the designed microbiota structure, with no significant difference (p>0.05) in the static treatments. Moreover, our model successfully predicted the dynamics of kanamycin resistance within artificial microbiota under kanamycin pressures. This work lends new insights into the potential role of spectrochemical analyses in investigating the existence and trends of antibiotic resistance in microbiota.

Keywords Antibiotic resistance, Artificial microbiota, ATR-FTIR spectroscopy, Kanamycin, Multivariate analysis, spectrochemical

Introduction

Antibiotics have played a vital role in modern medicine contributing to a considerable reduction in childhood mortality and increasing life expectancy[1]. However, the increasing number of fatal infections caused by antibiotic-resistant bacteria is gradually developing into a global threat. The environment has become the primary "sink" for most applied antibiotics and their residues arising from human or animal excretion[1-3]. Since bacteria with antibiotic resistance genes (ARGs) can tolerate antibiotics, selection pressures from contaminated water or soil will boost the abundance of ARGs in the environment and increase the possibility of their spread through microbial species[4,5]. Therefore, real-time monitoring and quantification of ARGs or antibiotic-resistant bacteria is urgently required.

Besides measuring the concentration of antibiotics via chemical analysis, various biological analytical methods have been used to determine the presence, abundance and diversity of ARGs in the microbiota to capture a "static map" of their existence, e.g. meta-sequence and quantitative polymerase chain reaction (qPCR)[6,7]. However, genetically identical cells from the same population have stochasticity in gene expression, meaning that there is significant variation in their molecular content and phenotype, even under similar environmental influences. Moreover, bacterial resistance to the antibiotics can also be affected and regulated epigenetically[8]. In combination, these factors provide an opportunity for phenotypic and cell-type

diversity regardless of genotype[9]. This questions the reliability of determining ARGs abundance by molecular biological approaches in real-world situations, leading to the necessity of developing a phenotypic assay that depicts in situ dynamics of ARGs or microbial antibiotic resistance.

It is well accepted that genetic and epigenetic factors cannot be studied independently as a complete phenotype emerges from both together[10]. The spectrochemical analysis is an alternative approach to characterize the phenotypic features of organisms and has already demonstrated its ability to investigate clinical samples, as well as to describe and identify bacterial specie[11,12]. Previous literatures indicate biospectroscopy is capable of studying phenotypic features, at either population[13] or single-cell[14] level, such as diagnosing the distinct spectral signatures and metabolomes from isogenic cell lines[15]. However, the current techniques have limited application in characterizing ARGs under antibiotic pressures, mainly due to the lack of appropriate analytical models and well-trained databases. Recently, some biospectroscopic studies have been attempted to investigate biological response to environmental stress, like nanomaterials[16,17] and antimicrobial reagents[18,19]. The introduction of biospectroscopy coupled with a suitable prediction model to characterize microbial composition may bring new insights in detecting the presence or even the dynamics of microbial antibiotic resistance in environmental microbiota in real-time, owing to its non-destructive, high-throughput and label-free

character[20,21]. It also allows for *in situ* spectral measurements, helping in understanding the interactions between microbes and their physical environment. Kanamycin is a subclass of aminoglycoside antibiotics, one of the most widely applied antibiotics in health and molecular biology[22]. Because of the well-established mechanisms of kanamycin resistance and characterized sequence[23], it was selected as the model antibiotic in the present study. Herein, we used a biospectroscopic method *via* attenuated total reflection Fourier-transform infrared (ATR-FTIR) spectroscopy, coupled with the multivariate analysis and the dispersion indicator model, to quantify the abundance of kanamycin resistance gene within artificial microbiota and evaluate their phenotypic change associated with kanamycin resistance, from both static and dynamic perspectives. This work raises the potential feasibility of applying biospectroscopy to diagnose ARGs phenotypic dynamics in the microbial community *in situ*.

Experimental section

Sample preparation

The present study included two strains without kanamycin-resistant-gene, *Mycobacterium vanbaalenii* PYR-1 and *Escherichia coli* DH5α, and one kanamycin-resistant strain *Acinetobacter baylyi* ADPWH_recA, which has a continuously expressed kanamycin resistance gene kan^R (from Mini-Tn5/Km[24], Genbank accession number: U32991.1) inserted into the *recA* gene in the chromosome of *A. baylyi* ADP1[25]. Before the experiment, they were all cultured in Luria-Bertani (LB) broth medium for 24 h at 30±2ºC.

The three control groups contained pure *M. vanbaalenii* PYR-1, *E. coli* DH5α and *A. baylyi* ADPWH_recA, respectively. The artificial microbiotas were prepared for both static (M1 to M5) and dynamic (AM1 and AM2) experiments by gently mixing the cells in the compositions listed in Table 1. The optical density at 600 nm (OD_{600}) in each treatment was monitored continuously for 24 hrs by a multimode plate reader (FLUOstar Omega, Germany) to evaluate bacterial growth. For static tests, the cells were directly collected by centrifugation (4000 rpm for 5 min), washed three times with sterile deionized water to remove the residues of growth media and then suspended in 70% ethanol to fix the bacterial cells. For dynamic tests, all the artificial microbiotas were treated with kanamycin (final concentration 10 mg/L). After exposure for 4, 8, 12 or 24 hrs, the cells from microbiotas were harvested following the same procedure as above.

Table 1. The compositions of artificial microbiota (volume ratio, v:v:v).

Treatments	Control			Static test					Dynamic test	
	M. vanbaalenii	***E. coli***	***A. baylyi***	**M_1**	**M_2**	**M_3**	**M_4**	**M_5**	**AM_1**	**AM_2**
M. vanbaalenii	100%	-	-	40%	30%	30%	15%	5%	40%	25%
E. coli	-	100%	-	50%	45%	20%	10%	5%	40%	25%
A. baylyi	-	-	100%	10%	25%	50%	75%	90%	20%	50%

ATR-FTIR spectroscopy

The washed cell pellets (minimal amount >5 μL) were applied onto Low-E slides for interrogation by ATR-FTIR spectroscopy. A TENSOR 27 FTIR spectrometer (Bruker Optics Ltd., UK) equipped with a Helios ATR attachment (containing a diamond

internal IRE; incidence angle of the IR beam: 45°) was used for the interrogation. Instrument parameters were set at 32 scans and spatial resolution of 8 cm^{-1}. Before the measurement of a new sample, the crystal was cleaned with deionized water and background readings were retaken. A total of 30 spectra were acquired for each treatment (3 replicates).

Computational analysis

The principal analysis methods in this study involved multivariate analysis and dispersion indicator model. The initial data generated from ATR-FTIR spectroscopy were analyzed within MATLAB R2011a (*TheMathsWorks, Natick, MA, USA*) software, coupled with IrootLab toolbox (http://irootlab.googlecode.com)[26]. Unless otherwise stated, the acquired spectra were cut to the biochemical-cell fingerprint region (1800-900 cm^{-1}), rubberband baseline corrected and normalized to Amide I (1650 cm^{-1}). Second order differentiation baseline correction and vector normalization was also performed as an alternative mean to process the data. Principal component analysis followed by linear discriminant analysis (PCA-LDA) was subsequently applied to the pre-processed data to reduce the number of spectra to 10 uncorrelated principal components (PCs), which account for >99% of the total variance; LDA is a supervised technique coupled with PCA in order to maximize inter-class and minimize intra-class variance[21]. In addition, cluster vector approach was conducted to visualise the discriminating difference[21,27]. This method takes input from PCA-LDA to create a loadings vector for each category contributing to respective data points. The pseudo-spectra allow identifying which variables (or wavenumber) are responsible for variance in the data set related to the original

spectra[21,27]. The detailed information of the dispersion indicator model was described in the Electronic Supplementary Information (ESI).

Biological analysis

The copy numbers of total bacterial 16S rRNA and targeted kanamycin resistance gene (kan^R) were determined by quantitative polymerase chain reaction (qPCR). For 16S rRNA, the primer pair set was 341F (5'-CCTACGGGNGGCWGCAG-3') and 805R (5'-GACTACHVGGGTATCTAATCC-3'), and the primer pair for kan^R was KanF (5'-TGTCATACCACTTGTCCGCC-3') and KanR (5'-ATCGAGCTGTATGCGGAGTG-3'). The 20 μL qPCR system consisted of 2 μL of each primer, 1 μL DNA template, 5 μL molecular water and 10 μL iTaq™ Universal SYBR® Green Supermix (BioRad, USA). The microbial kanamycin resistance within the artificial microbiota was calculated as the ratio of *A. baylyi* population to the total bacterial population.

Statistical analysis

One-way analysis of variance (ANOVA) with Tukey's post hoc test/or T-test was employed to examine the discriminating differences. All statistical analysis was carried out in GraphPad Prism 6.

Results and Discussion

Growth and kanamycin resistance gene of individual strains

All the three bacterial strains (*A. baylyi* ADPWH_recA, *M. vanbaalenii* PYR-1 and *E. coli* DH5α) had similar growth curves without kanamycin pressure (see ESI

Figure S1A). Cultivated in 10 mg/L kanamycin, only *A. baylyi* ADPWH_recA maintained positive growth because of the expression of kan^R gene and resistance to kanamycin (see ESI, Figure S1B). Neither *M. vanbaalenii* PYR-1 nor *E. coli* DH5α grew post-exposure to 10 mg/L kanamycin. The results of qPCR further confirmed that the high copy numbers of kan^R gene were only found in *A. baylyi* ADPWH_recA (1.47×10^8 in medium without kanamycin and 1.95×10^8/mL in medium with 10 mg/L kanamycin respectively, no significant difference), whereas it was less than 2.5×10^6/mL or below the limit of detection for *M. vanbaalenii* PYR-1 or *E. coli* DH5α (see ESI, Figure S2). It was further proved that kanamycin resistance gene is only detectable in *A. baylyi* ADPWH_recA, but neither *M. vanbaalenii* PYR-1 nor *E. coli* DH5α, and the latter two cannot tolerate kanamycin pressure. The active group of kanamycin, 2-deoxystreptamine, impairs bacterial protein synthesis through binding to prokaryotic ribosomes 30S subunit [22]. The kan^R encoding neomycin phosphotransferase is an aminoglycoside-modifying enzyme, using ATP as donor to modify the hydroxyl functions of 2-deoxystreptamine and inhibit its binding to ribosomes[28]. The kan^R gene is therefore a reliable molecular indicator in detecting the kanamycin resistance.

IR spectral fingerprints of individual strains and microbiota

The IR spectral fingerprint region (1800 - 900 cm^{-1}) of the three strains and artificial microbiotas are shown in Figure 1. The representative peaks of the biochemical fingerprint include lipids (~1750 cm^{-1}), Amide I (~1650 cm^{-1}), Amide II (~1550 cm^{-1}), Amide III (~1260 cm^{-1}), carbohydrate (~1155 cm^{-1}), asymmetric phosphate stretching vibrations ($\nu_{as}PO_2^-$; ~1225 cm^{-1}), symmetric phosphate stretching

vibrations ($\nu_s PO_2^-$; ~1080 cm^{-1}), glycogen (~1030 cm^{-1}) and protein phosphorylation (~970 cm^{-1})[20 21]. Past literatures[12,20,29,30] suggest the characteristic peaks given by the region can be used as biomarkers to characterize microbial cell types (even at subspecies level) and diagnose microbe-induced diseases.

However, the visual spectral differences with the mean spectra are almost identical regardless of the bacterial species or community composition. For this reason, we applied the cluster vectors after multivariate analysis (PCA-LDA) and the second order differentiation baseline correction and to further reveal the underlying biochemical differences between each strain or microbiota. Based on the derived spectral biomarkers from PCA-LDA (Figure 1B), all the microbiota samples showed marked segregation (see ESI, Table S1). Characteristics associated with microbial composition were observed in particular wavenumber-absorbance intensities. For instance, the intensities at 980 cm^{-1} and 1740 cm^{-1} were increased with increasing ratio of ARGs but fluctuated in some artificial microbiotas, particularly for microbiota M3 (*M. vanbaalenii* PYR-1: *E. coli* DH5α: *A. baylyi* ADPWH_recA = 30%:20%:50%). Additionally, IR spectral analysis (Figure 2A) based on the second order differentiation baseline correction and vector normalization highlighted several key biomarkers. Two apparent shifts from ~1630 cm^{-1} to ~1640 cm^{-1} (Amide I) and from ~1222 cm^{-1} to ~1235 cm^{-1} ($\nu_{as} PO_2^-$) associated with *A. baylyi* were regarded as biomarkers for the presence of kanamycin resistance. These spectral alterations might be attributed to the upregulated activities of the kan^R encoding aminoglycoside *O*-phosphotransferase, which contributes to microbial resistance by inactivating kanamycin molecular via catalyzing ATP-dependent phosphorylation of specific

aminoglycoside hydroxyl groups[31]. Some other weaker discriminations included the polysaccharide fingerprint region (1000-1150 cm^{-1}) and the protein absorbance region (1500-1700 cm^{-1})[27]. These alterations were probably induced by the interference of extracellular polymeric substances (EPS) produced by different species[32-34] and resulted in the difficulties in distinguishing biomarkers from the PCA-LDA extracted peaks. Based on the previous studies[32,35,36], we speculate that these extracellular materials may interact with each other and generate new biochemical compositions within the communities, influencing the discriminating peaks obtained with spectrochemical interrogation.

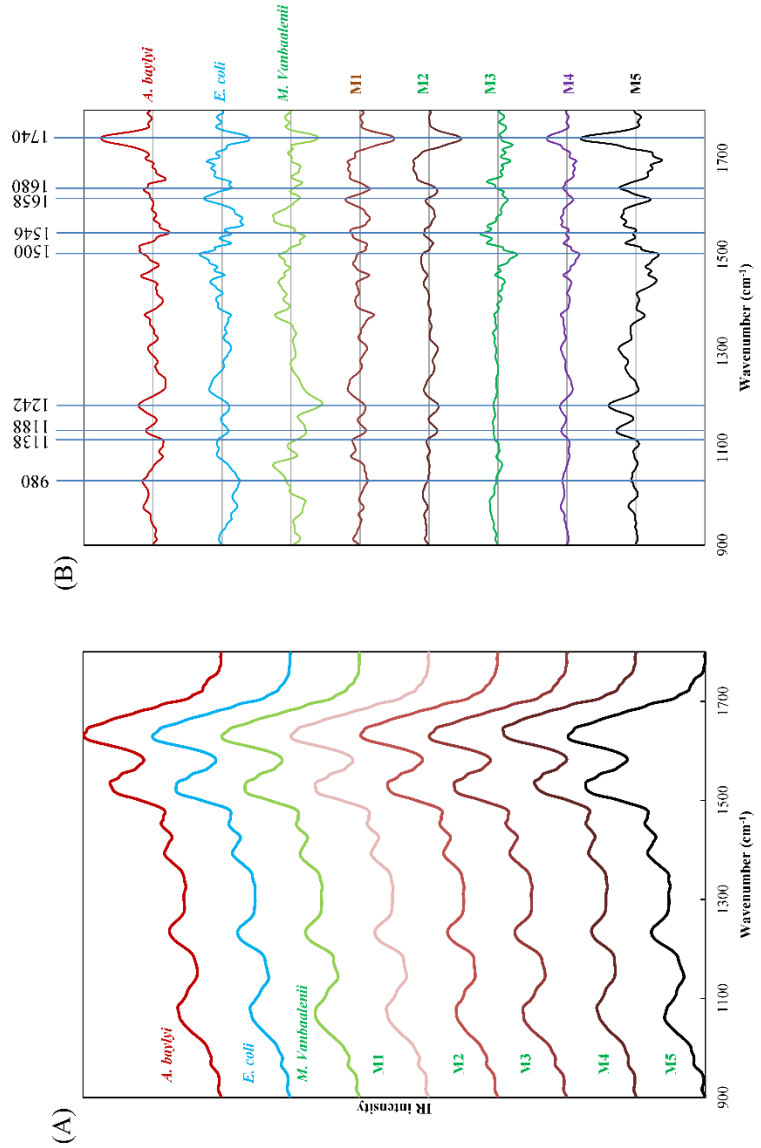

Figure 1. (A) Infrared spectra of *A. baylyi*, *M. vanbaalenii*, *E. coli* and five artificial microbiotas (M1-M5). (B) Cluster vector plots after PCA-LDA, indicating significant wavenumbers for the segregation between bacterial species and artificial microbiotas.

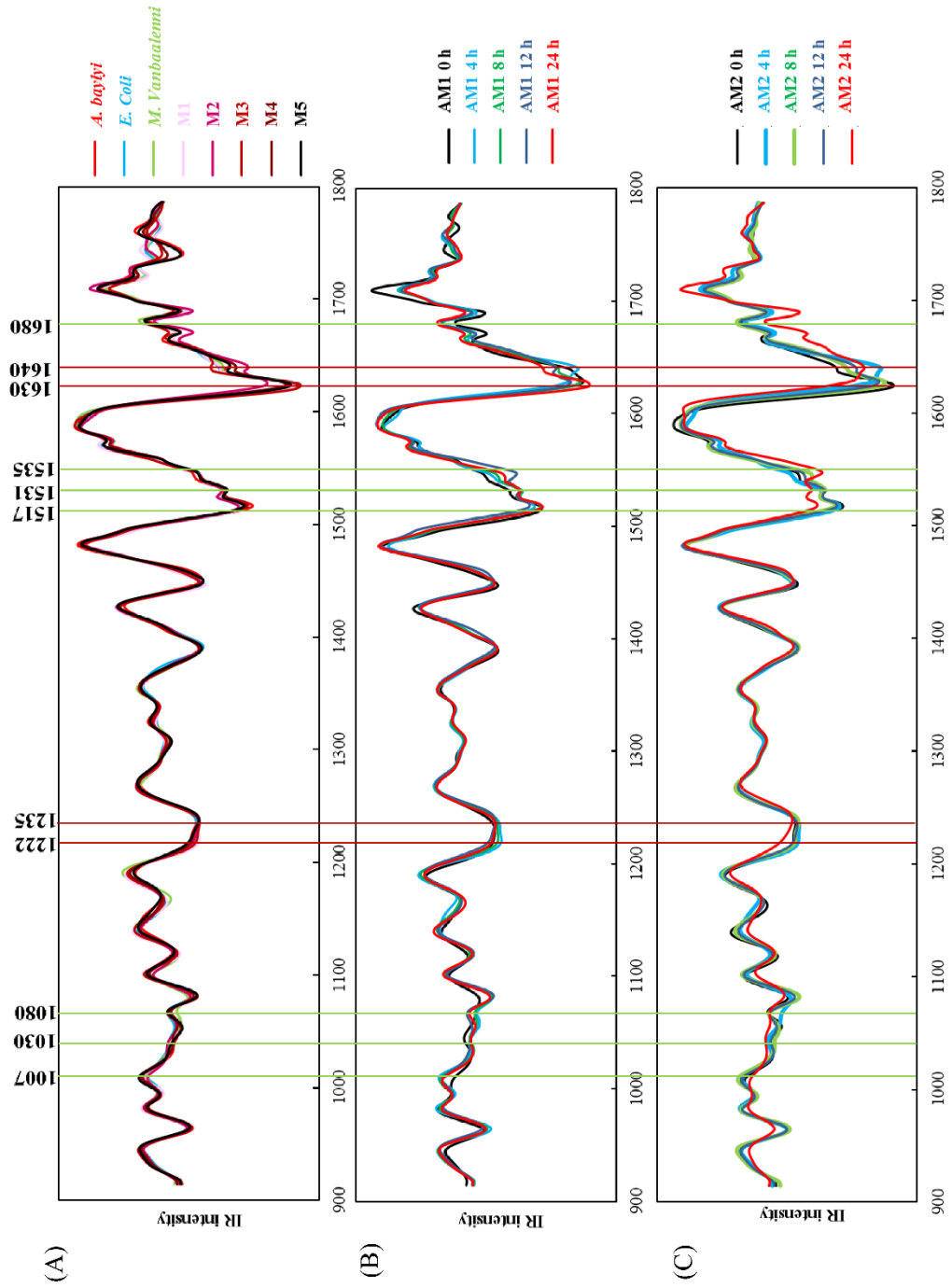

Figure 2. Class means spectra of pre-processed data based on second order differentiation baseline correction and vector normalization. (A) Processed spectra of *A. baylyi*, *M. vanbaalenii*, *E. coli* and five artificial microbiotas (M1-M5). (B)

Processed spectra of AM1 at different time point in dynamic experiment. (C) Processed spectra of AM1 at different time point in dynamic experiment.

Predicting community composition in artificial microbiota

Comparing to the IR spectra in the static tests, we observed identical spectral biomarkers in artificial community dynamics (Figure 2B and 2C) that the same shifts from ~1630 cm^{-1} to ~1640 cm^{-1} (Amide I) and from ~1222 cm^{-1} to ~1235 cm^{-1} ($\nu_{as}PO_2^-$) developed along with the time. The results indicated the consistent spectral biomarkers in both static and dynamic microbiotas in analyzing the phenotypic presence and abundance of kanamycin resistance gene in the targeted microbiota.

The PCA-LDA scores plot (Figure 3A) also illustrates a significant segregation of the different groups, associated with differing microbiota compositions. The control groups (*M. vanbaalenii*, *E. coli,* and *A. baylyi*) are clearly separated from each other. In contrast to *M. vanbaalenii* and *E. coli*, all the converted spectral values of *A. baylyi* are aligned as negative along linear discriminant one (LD1), likely attributed to its kanamycin resistance. Meanwhile, along with linear discriminant two (LD2), the group of *M. vanbaalenii* (Gram-positive bacteria) is located on the negative axis alone, separated from the other two groups (*E. coli* and *A. baylyi*), which are Gram-negative. The five artificial microbiota samples (M1 to M5) are located inbetween, and their distances to the control groups are correlated with their community compositions.

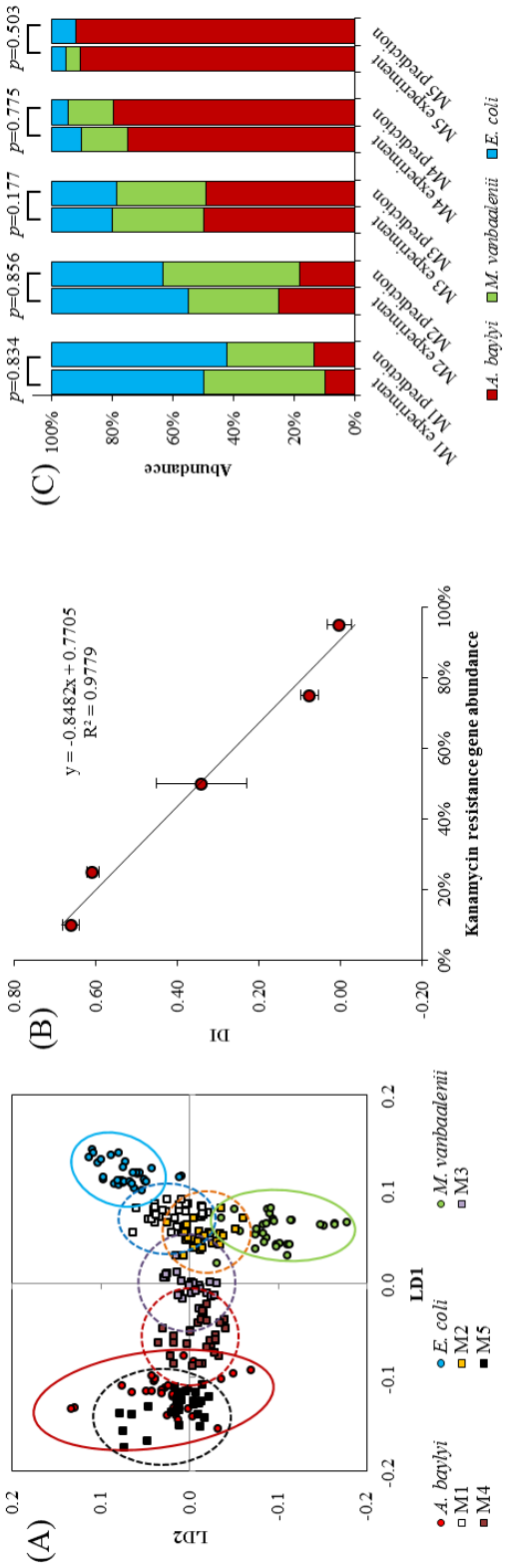

Figure 3. (A) Two-dimensional (LD1, LD2) scores plot after PCA-LDA of pure

microbial strains and artificial microbiotas with different composition. (B) Correlation between kanamycin resistance gene abundance and group distance dispersion. (C) Comparison of artificial microbiota composition between experimental data and model prediction.

In order to predict the composition of the artificial microbiota, the dispersion indicator model[37] was carried out by transferring the dispersion analysis from the IR spectral variables to the vectors (LD1 and LD2) and using D_I as the indicator, comparing to the ARGs gene copy numbers quantified by qPCR as reference. This method used the summarized spectral information from PCA-LDA which accounts for over 90% of spectral variations in the present study, and was more conclusive than the limited biomarkers from second order differentiation. Here, microbiotas with less abundance of *A. baylyi* were further separated from the *A. baylyi* group, but closer to those of *E. coli* and *M. vanbaalenii*, leading to an increasing D_I against the decreasing kanamycin resistance (kanamycin resistance genes in *A. baylyi*). Figure 3B illustrates the negative linear correlation between D_I and the abundance of *A. baylyi* (kanamycin resistance gene abundance) within the artificial microbiotas ($D_I = -0.8482 \times [kanamycin\ resistance\ gene] + 0.7705$). The high coefficient (R^2=0.9779) suggests a good linear regression of D_I against kanamycin resistance gene abundance. The composition of each microbiota was, therefore, calculated from the D_I linear regression based on PCA-LDA, as shown in Figure 3C. The results indicated that the predicted microbial compositions had high similarity to their theoretical structure with no significant differences found (p>0.05). The standard deviation of microbiota M3 (middle point in Figure 3B) was greater than the others,

possibly attributing to their higher Shannon-Wiener index (1.02) than other microbiotas (0.35 to 0.94 for M1, M2, M4 and M5). Shannon-Wiener index represents the diversity of microbial community, and higher microbial diversity has been reported to increase complicated intracommunity interaction[32]. It might cause huge variation of microbial chemical composition, consequently leading to the difficulties in interrogating spectral biomarkers and significant standard deviation in data prediction.

Quantification of kanamycin resistance dynamics within microbiota

Figure 4A illustrates the PCA-LDA plot of microbiotas post-exposure to kanamycin, derived from the spectral dynamics of the artificial microbiotas (see ESI Figure S3). All the interrogated communities exhibit a dramatic shift from the original location as the exposure time increases. The *M. vanbaalenii* category moves towards a different direction when compared to *A. baylyi* and *E. coli*, which might be attributed to distinct cell structures between Gram-positive (*M. vanbaalenii*) and Gram-negative bacteria (*A. baylyi* and *E. coli*). Specifically, there is only one lipid bilayer in the membrane of Gram-positive bacteria, with a thick ring of peptidoglycan and teichoic acid[38,39]. On the other hand, the cell membrane of Gram-negative bacteria contains two lipid associated bilayers, which appear to increase the chance that the applied treatments influence their structur[38,39]. The artificial microbiotas, AM1 and AM2, follow similar trends as the *A. baylyi* and they come even closer to *A. baylyi* after extended exposure to the kanamycin antibiotic. After PCA-LDA, the most discriminating peaks were observed in Gram-negative bacteria and were attributed to lipids (~1750 cm^{-1}), $\nu_{as}PO_2^-$ (~1225 cm^{-1}) and $\nu_sPO_2^-$ (~1080 cm^{-1}). Kanamycin's

antimicrobial mechanism is associated with aminoglycosides, interfering with aminoacyl-tRNA recognition at the ribosomal A site and disrupting protein expression[40]. Such a mechanism causes series of secondary effects, *e.g.*, membrane damage. Our results are consistent with previous findings showing that the damage is mainly linked to a broad range of alterations associated with the elements of membranes, *e.g.*, proteins, supported by derived peaks the protein absorbance region from 1500 to 1700 cm^{-1}, such as Amide II (~1517 cm^{-1}, ~1543 cm^{-1}) and Amide I (~1650 cm^{-1}, ~1680 cm^{-1})[16,21,41,42].

Applying the linear D_I regression model, we successfully predicted the dynamic abundance of *A. baylyi* and kanamycin resistance within the microbiotas under kanamycin antibiotic pressures. Both artificial microbiotas, AM1 (Figure 4B) and AM2 (Figure 4C), had defined community composition at 0 h, with *A. baylyi* (kanamycin resistance gene) accounting for 10% and 40% of the total population, respectively. Post-exposure to kanamycin, the ARGs abundance from qPCR results gradually increased to 85.0% in AM1 and 92.2% in AM2 after 12 hrs, which is explained by the competitive advantages of bacteria with kanamycin resistance gene in the community[43]. It therefore led to a faster growth of *A. baylyi* compared to other strains and subsequent dominancy of *A. baylyi* within the microbiota. From the dynamics of discriminant functions, the predicted ARGs abundance in both microbiotas fitted efficiently with experimental data (Figure 4B and 4C). The linear correlation at each time point did not show significant difference between predicted and experimental ARGs abundance (Figure 4D), with a Pearson correlation coefficient of 0.9487. The prediction via biospectroscopy coupled and multivariate

analysis fitted the experimental data better at higher ARGs abundance, but was slightly lower than the qPCR results at low ARGs abundance, *e.g.* 33% in Figure 4D, which might underestimate the ARGs abundance to some extent. These results not only prove that our model can be used for static community composition and abundance/dynamics of kanamycin resistance gene, but they also evaluate the impact of antibiotic pressure on kanamycin resistance gene transfer or dominancy.

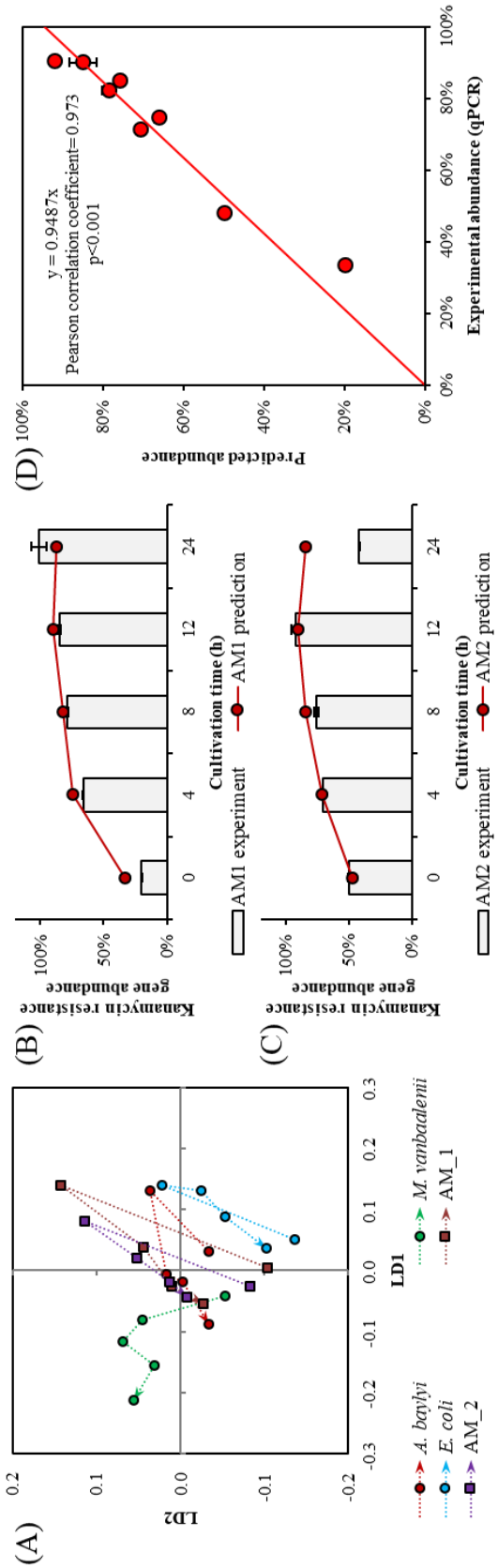
(A)
LD2
LD1
A. baylyi
E. coli
AM_2
M. vanbadenni
AM_1
(B)
Kanamycin resistance gene abundance
Cultivation time (h)
AM1 experiment
AM1 prediction
(C)
Kanamycin resistance gene abundance
Cultivation time (h)
AM2 experiment
AM2 prediction
(D)
Predicted abundance
Experimental abundance (qPCR)
y = 0.9487x
Pearson correlation coefficient= 0.973
p<0.001

Figure 4. (A) Two-dimensional (LD1, LD2) scores plot after PCA-LDA of IR dynamics of artificial microbiotas. Dots along with the arrow point in each colour refer to the measurement at 0, 4, 8, 12 and 24 hrs, respectively. The prediction of kanamycin resistance gene abundance is based on the dispersion among the classification groups in PCA-LDA for artificial microbiota AM1 (B) and AM2 (C). (D) Regression correlation of kanamycin resistance gene abundance between experimental data via qPCR and model prediction.

It is worth mentioning that less dispersion is observed for *A. baylyi* after exposure because *A. baylyi* ADPWH_recA contains the kan^R kanamycin resistance gene, which is capable of tolerating kanamycin pressure. In the present study, the kan^R kanamycin resistance gene belongs to *npt* encoding neomycin phosphotransferase and shows high similarity to *addA* encoding aminoglycoside phosphotransferase (aminoglycoside kinase), which modifies the aminoglycosides by phosphoryl transfer, catalysing the phosphate addition from ATP to 3'-hydroxyl group[40]. By expressing kan^R, *A. baylyi* ADPWH_recA inactivates the interference of protein expression by kanamycin, achieves fast recovery from suppression, and minimizes spectral alterations as compared to others. It is confirmed by the presence of consistent shifts and discriminating peaks in *A. baylyi* postexposure to kanamycin, including Amide I (~1630 cm^{-1}, ~1640 cm^{-1}) and $\nu_{as}PO_2^-$ (~1222 cm^{-1}, ~1235 cm^{-1})[42].

An unexpected decline of kanamycin resistance gene was observed for AM2 artificial microbiota after 24 hrs exposure to kanamycin (42%, Figure 4C), but the predicted kanamycin resistance by D_I regression model remained close to 100%. It might be explained by the dramatically decreasing kanamycin concentration via the

metabolism of aminoglycoside modifying enzyme and the change in microbial community structure. The functions of *kan*^{R} encoding aminoglycoside kinase are stabilizing a metaphosphate transition state and inactivating kanamycin[31], and the spectral alterations represent the alignment disruption of ß-phosphate and γ-phosphate by amide backbone. The declining kanamycin results in less inhibition on bacteria without kanamycin resistance gene (*M. vanbaalenii* and *E. coli*), and their growth and regeneration consequently reduce the abundance of A. *baylyi* and *kan*^{R} gene. Alternatively, the FTIR spectral alteration reflects such phenotypic changes of the whole microbiota under the low kanamycin exposure, illustrating the fact that the majority of microbial cells within the microbiota have the pseudo-resistance to kanamycin. The spectrochemical interrogation therefore actually quantifies the microbial phenotypic antibiotic resistance rather than the ARGs abundance only.

Biospectroscopy has demonstrated the ability to diagnose the phenotypic alteration of the cellular components induced by kanamycin, hinting its potential possibility for the application to other members of the aminoglycoside family. Our findings indicate that this PCA-LDA-based model is a potential approach for monitoring the population dynamics within a microbiota in real-time. Additionally, the model applied in the present study summarizes the whole spectral information derived from the multivariate analysis, rather than only several biomarkers, showing its potential as a universal predicting tool for a broad spectrum of antibiotics based on well-trained databases. Though only successfully applied in the case of kanamycin through phosphotransferase resistance pathway, this technique is also feasible for detecting *N*-acetyltransferases and *O*-nucleotidyltransferases, which also belong to

aminoglycoside-modifying enzymes assisted by acetyl-coenzyme A and ATP respectively[22], attributing to their similar anti-kanamycin mechanisms as *kan*^{R} encoding neomycin phosphotransferase. Future work should refer to more comprehensive range of antibiotics and their mechanisms including penicillin-class (*e.g.*, ampicillin and amoxicillin), which disrupts the synthesis of peptidoglycan layer and inhibits bacterial cell wall synthesis [44], and tetracycline, which inhibits the binding of aminoacyl-tRNA and suppresses protein expression[45]. For the urgent need to characterize antibiotic resistance in complex environmental microbiota with biospectroscopy, the primary challenges are raised as the lack of routine protocols, reproducible computational analysis, and reliable database[10]. Validated in the artificial microbiota, our work provides the solutions for the first two barriers by distinguishing biomarkers representing antibiotic resistance from the numerous biological fingerprints. A well-built dataset along with robust analytical models coupled with biospectroscopy methods are suggested to address the antibiotic resistance dynamics in real environmental samples.

The present study indicates that biospectroscopy, in conjunction with multivariate analysis, is a potential tool for diagnosing the phenotypic existence and dynamics of ARGs within microbial communities. Our work employed ATR-FTIR spectroscopy coupled with a dispersion model to quantify microbial kanamycin resistance gene, based on secondary derivative and PCA-LDA. This method not only quantified the static community composition of the artificial microbiota but also successfully predicted the population dynamics of microbial communities and kanamycin resistance under antibiotic pressure. We also suggest that biospectroscopy has great

potential in real-time monitoring of microbiota of interest in medical or environmental fields; this would provide an excellent opportunity to visualize the vivid phenotypic transformation during a biological and biochemical process rather than only intermittent pictures.

Acknowledgements N.J. was funded by Chinese Academy of Sciences and China Scholarship Council. Research is supported by the Engineering and Physical Sciences Research Council in F.L.M.'s laboratory (EPSRC; grant no: EP/K023349/1) and National Natural Science Foundation of China in D.Z.'s laboratory (NFSC; grant no: 41301331).

References

(1) Blair, J. M.; Webber, M. A.; Baylay, A. J.; Ogbolu, D. O.; Piddock, L. J. *Nat. Rev. Microbiol.* **2015**, *13*, 42-51.

(2) Chee-Sanford, J. C.; Aminov, R. I.; Krapac, I. J.; Garrigues-Jeanjean, N.; Mackie, R. I. *Appl. Environ. Microbiol.* **2001**, *67*, 1494-1502.

(3) Cantas, L.; Shah, S. Q. A.; Cavaco, L. M.; Manaia, C. M.; Walsh, F.; Popowska, M.; Garelick, H.; Burgmann, H.; Sorum, H. *Front. Microbiol.* **2013**, *4*.

(4) Potera, C. *Environ. Health Perspect.* **2013**, *121*, A255-A255.

(5) Smillie, C. S.; Smith, M. B.; Friedman, J.; Cordero, O. X.; David, L. A.; Alm, E. J. *Nature* **2011**, *480*, 241-244.

(6) Colomer-Lluch, M.; Imamovic, L.; Jofre, J.; Muniesa, M. *Antimicrob. Agents Chemother.* **2011**, *55*, 4908-4911.

(7) Riesenfeld, C. S.; Goodman, R. M.; Handelsman, J. *Environ. Microbiol.* **2004**, *6*, 981-989.

(8) Paraskevaidi, M.; Martin-Hirsch, P. L.; Kyrgiou, M.; Martin, F. L. *Mutagenesis* **2017**, *32*, 335-342.

(9) Kaern, M.; Elston, T. C.; Blake, W. J.; Collins, J. J. *Nat. Rev. Genet.* **2005**, *6*, 451-464.

(10) Jin, N. F.; Zhang, D. Y.; Martin, F. L. *Integr. Biol.* **2017**, *9*, 406-417.

(11) Naumann, D.; Helm, D.; Labischinski, H. *Nature* **1991**, *351*, 81-82.

(12) Dunn, W. B.; Ellis, D. I. *Trends Anal. Chem.* **2005**, *24*, 285-294.

(13) Freedman, B. G.; Zu, T. N. K.; Wallace, R. S.; Senger, R. S. *Biotechnol. J.* **2016**, *11*, 877-889.

(14) Sun, S. W.; Wang, X. T.; Gao, X.; Ren, L. H.; Su, X. Q.; Bu, D. B.; Ning, K. *BMC Bioinformatics* **2015**, *16*.

(15) Winnard, P. T.; Zhang, C.; Vesuna, F.; Kang, J. W.; Garry, J.; Dasari, R. R.; Barman, I.; Raman, V. *Oncotarget* **2017**, *8*, 20266-20287.

(16) Li, J. Y.; Strong, R.; Trevisan, J.; Fogarty, S. W.; Fullwood, N. J.; Jones, K. C.; Martin, F. L. *Environ. Sci. Technol.* **2013**, *47*, 10005-10011.

(17) Bankapur, A.; Krishnamurthy, R. S.; Zachariah, E.; Santhosh, C.; Chougule, B.; Praveen, B.; Valiathan, M.; Mathur, D. *PLoS One* **2012**, *7*.

(18) Tao, Y. F.; Wang, Y.; Huang, S.; Zhu, P. F.; Huang, W. E.; Ling, J. Q.; Xu, J. *Anal. Chem.* **2017**, *89*, 4108-4115.

(19) Siddhanta, S.; Paidi, S. K.; Bushley, K.; Prasad, R.; Barman, I. *Chemphyschem* **2017**, *18*, 72-78.

(20) Baker, M. J.; Trevisan, J.; Bassan, P.; Bhargava, R.; Butler, H. J.; Dorling, K. M.; Fielden, P. R.; Fogarty, S. W.; Fullwood, N. J.; Heys, K. A.; Hughes, C.; Lasch, P.; Martin-Hirsch, P. L.; Obinaju, B.; Sockalingum, G. D.; Sule-Suso, J.; Strong, R. J.; Walsh, M. J.; Wood, B. R.; Gardner, P., et al. *Nat. Protoc.* **2014**, *9*, 1771-1791.

(21) Martin, F. L.; Kelly, J. G.; Llabjani, V.; Martin-Hirsch, P. L.; Patel, II; Trevisan, J.; Fullwood, N. J.; Walsh, M. J. *Nat. Protoc.* **2010**, *5*, 1748-1760.

(22) Mingeot-Leclercq, M. P.; Glupczynski, Y.; Tulkens, P. M. *Antimicrob. Agents Chemother.* **1999**, *43*, 727-737.

(23) Sadovskaya, I.; Vinogradov, E.; Li, J. J.; Hachani, A.; Kowalska, K.; Filloux, A. *Glycobiology* **2010**, *20*, 895-904.

(24) Delorenzo, V.; Herrero, M.; Jakubzik, U.; Timmis, K. N. *J. Bacteriol.* **1990**, *172*, 6568-6572.

(25) Song, Y.; Li, G.; Thornton, S. F.; Thompson, I. P.; Banwart, S. A.; Lerner, D. N.; Huang, W. E. *Environ. Sci. Technol.* **2009**, *43*, 7931-7938.

(26) Trevisan, J.; Angelov, P. P.; Scott, A. D.; Carmichael, P. L.; Martin, F. L. *Bioinformatics* **2013**, *29*, 1095-1097.

(27) Butler, H. J.; McAinsh, M. R.; Adams, S.; Martin, F. L. *Anal. Methods* **2015**, *7*, 4059-4070.

(28) Yenofsky, R. L.; Fine, M.; Pellow, J. W. *Proc. Natl. Acad. Sci. U. S. A.* **1990**, *87*,

3435-3439.

(29) Bosch, A.; Serra, D.; Prieto, C.; Schmitt, J.; Naumann, D.; Yantorno, O. *Appl. Microbiol. Biotechnol.* **2006**, *71*, 736-747.

(30) Mariey, L.; Signolle, J. P.; Amiel, C.; Travert, J. *Vib. Spectrosc.* **2001**, *26*, 151-159.

(31) Wright, G. D. *Curr. Opin. Microbiol.* **1999**, *2*, 499-503.

(32) Flemming, H. C.; Wingender, J. *Nat. Rev. Microbiol.* **2010**, *8*, 623-633.

(33) Holman, H. Y. N.; Miles, R.; Hao, Z.; Wozei, E.; Anderson, L. M.; Yang, H. *Anal. Chem.* **2009**, *81*, 8564-8570.

(34) Stewart, P. S. *Int. J. Med. Microbiol.* **2002**, *292*, 107-113.

(35) Hoiby, N.; Bjarnsholt, T.; Givskov, M.; Molin, S.; Ciofu, O. *Int. J. Antimicrob. Agents* **2010**, *35*, 322-332.

(36) Karunakaran, E.; Mukherjee, J.; Ramalingam, B.; Biggs, C. A. *Appl. Microbiol. Biotechnol.* **2011**, *90*, 1869-1881.

(37) Li, H. B.; Martin, F. L.; Zhang, D. Y. *Anal. Chem.* **2017**, *89*, 3909-3918.

(38) Ede, S. M.; Hafner, L. M.; Fredericks, P. M. *Appl. Spectrosc.* **2004**, *58*, 317-322.

(39) Morones, J. R.; Elechiguerra, J. L.; Camacho, A.; Holt, K.; Kouri, J. B.; Ramirez, J. T.; Yacaman, M. J. *Nanotechnology* **2005**, *16*, 2346-2353.

(40) Boehr, D. D.; Thompson, P. R.; Wright, G. D. *J. Biol. Chem.* **2001**, *276*, 23929-23936.

(41) Heys, K. A.; Riding, M. J.; Strong, R. J.; Shore, R. F.; Pereira, M. G.; Jones, K. C.; Semple, K. T.; Martin, F. L. *Analyst* **2014**, *139*, 896-905.

(42) Movasaghi, Z.; Rehman, S.; Rehman, I. U. *Appl. Spectrosc. Rev.* **2008**, *43*, 134-179.

(43) Hibbing, M. E.; Fuqua, C.; Parsek, M. R.; Peterson, S. B. *Nat. Rev. Microbiol.* **2010**, *8*, 15-25.

(44) Strominger, J. L.; Park, J. T.; Thompson, R. E. *J. Biol. Chem.* **1959**, *234*, 3263-

3268.

(45) Connell, S. R.; Trieber, C. A.; Dinos, G. P.; Einfeldt, E.; Taylor, D. E.; Nierhaus, K. H. *EMBO J.* **2003**, *22*, 945-953.

Table of Content Graphic

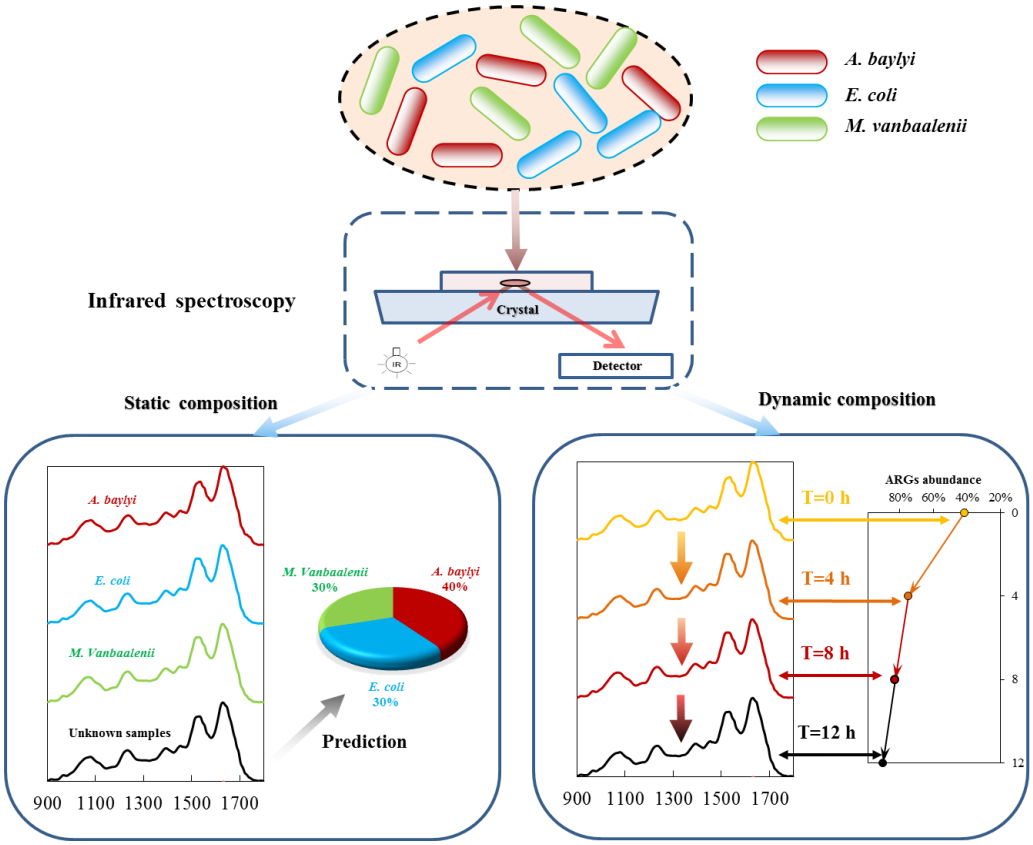

For TOC only.

Supplementary Information

Biospectrochemical tool for quantifying the real-time dynamics of kanamycin resistance in artificial microbiota

Naifu Jin[1], Maria Paraskevaidi[2], Kirk T Semple[1], Francis L. Martin[2,*], Dayi Zhang[1,*]

[1] Lancaster Environment Centre, Lancaster University, Lancaster, LA1 4YQ, UK

[2] School of Pharmacy and Biomedical Sciences, University of Central Lancashire, Preston PR1 2HE, UK

No. of Pages = 7

No. of Figures = 3

No. of Tables = 1

1. Materials and Methods

1.1 Dispersion indicator model

The initial spectral dataset is an ensemble of multivariate observations partitioned into M distinct groups (different microbiota composition in this study). For the n_m observation in each group (m runs from 1 to M and refers to the m^{th} group). The multivariate observation vectors can be written as n_{mi} where i is the i^{th} observation. To search for the linear combination in LDA that optimally separates our multivariate observation into M groups [1], the linear transformation of y_{mi} is written as z_{mi}:

$$z_{mi} = w^T y_{mi} \tag{1}$$

Here, w^T represents the linear transformation matrix, and the mean of the m^{th} group of the transformed data ($\langle z_m \rangle$) is:

$$\langle z_m \rangle = w^T \langle y_m \rangle \tag{2}$$

where y_m is the mean of the observations within a group and defined as:

$$\langle y_m \rangle = \sum_{j=1}^{n_m} y_{mj} / n_m \tag{3}$$

The dispersion among groups (B) and within groups (E) are defined in the following equations:

$$B_y = \sum_{m=1}^{G} n_m (\langle y_{mi} \rangle - \langle y \rangle)(\langle y_{mi} \rangle - \langle y \rangle)^T \tag{4}$$

$$E_y = \sum_{m=1}^{G} n_g \sum_{j=1}^{n_m} (\langle y_{mi} \rangle - \langle y_m \rangle)\,(\langle y_{mi} \rangle - \langle y_m \rangle)^T \tag{5}$$

where $\langle y \rangle = \frac{1}{M} \sum_{m=1}^{G} \frac{1}{n_m} \sum_{j=1}^{n_m} y_{mj}$ is the total average of the dataset. Using Fisher's linear discriminant, the optimal linear regression in PCA-LDA is to find the vector w maximizing λ (the rate of between-groups sum of squares to within-groups sum of squares):

$$\lambda = \frac{w^T B_y w}{w^T E_y w} \tag{6}$$

The solutions of Equation (6) are the eigenvalues $|\lambda|$, which are associated to the

eigenvectors $|w|$. In the most cases, the first two ranked λ_1 and λ_2 account for the most of $|\lambda|$, and the discriminant functions are obtained as LD1 ($z_1 = w_1^T Y$) and LD2 ($z_2 = w_2^T Y$) to represent the spectra variables of each community.

To predict the composition of the artificial microbiota, the three control groups (*A. baylyi* [a], *E. coli* [b] and *M. vanbaalenii* [c]) are set as the reference classes. The dispersions of the among groups (B) and within groups (E) (Fig. 2B) are defined in the following equations:

$$O_{y,q}|(q = a, b, c) = w^T B'_{y,q} w = w^T \left\{ \sum_{i=1}^{M} \sum_{j=1}^{M} n_m \left(\langle y_{mi} \rangle - \langle y_{qj} \rangle\right)\left(\langle y_{mi} \rangle - \langle y_{qj} \rangle\right)^T \right\} w = \sum_{i=1}^{M} \sum_{j=1}^{M} n_g \left(\langle w^T y_{mi} \rangle - \langle w^T y_{qj} \rangle\right)\left(\langle w^T y_{mi} \rangle - \langle w^T y_{qj} \rangle\right)^T = \sum_{i=1}^{M} \sum_{j=1}^{M} n_g \left(\langle z_{mi} \rangle - \langle z_{qi} \rangle\right)\left(\langle z_{mi} \rangle - \langle z_{qi} \rangle\right)^T \quad (7)$$

$$T_y = w^T E'_y w = \sum_{q=a,b,c} \sum_{i=1}^{M} \sum_{j=1}^{M} n_g \left(\langle z_{mi} \rangle - \langle z_{qj} \rangle\right)\left(\langle z_{gi} \rangle - \langle z_{qj} \rangle\right)^T \quad (8)$$

Here, we introduced the dispersion indicator (D_I) to calculate the composition of antibiotic resistance bacteria (*A. baylyi*) within the community, defined as:

$$D_I = \frac{O_{y,a}}{T_y} \quad (9)$$

$$\sum_{q=a,b,c} D_{I,q} = \frac{O_{y,q}}{T_y} = 100\% \quad (10)$$

Reference

(1) Ami, D.; Mereghetti, P.; Doglia, S. M. *Multivariate analysis for Fourier transform infrared spectra of complex biological systems and processes*; INTECH Open Access Publisher, 2013.

Table S1. Significant peaks derived from cluster vectors of artificial microbiota.

Microbiota	Significant peaks (cm^{-1})
A. baylyi	1188, 1242, 1508, 1547, 1659, 1744
E. coli	980, 1034, 1501, 1562, 1616, 1740
M. vanbaalenii	1065, 1134, 1192, 1377, 1582, 1744
M1	1223, 1377, 1578, 1612, 1694, 1740
M2	1138, 1188, 1304, 1632, 1678, 1740
M3	1501, 1543, 1612, 1651, 1694, 1728
M4	980, 1188, 1501, 1616, 1694, 1740
M5	1138, 1188, 1447, 1501, 1697, 1740

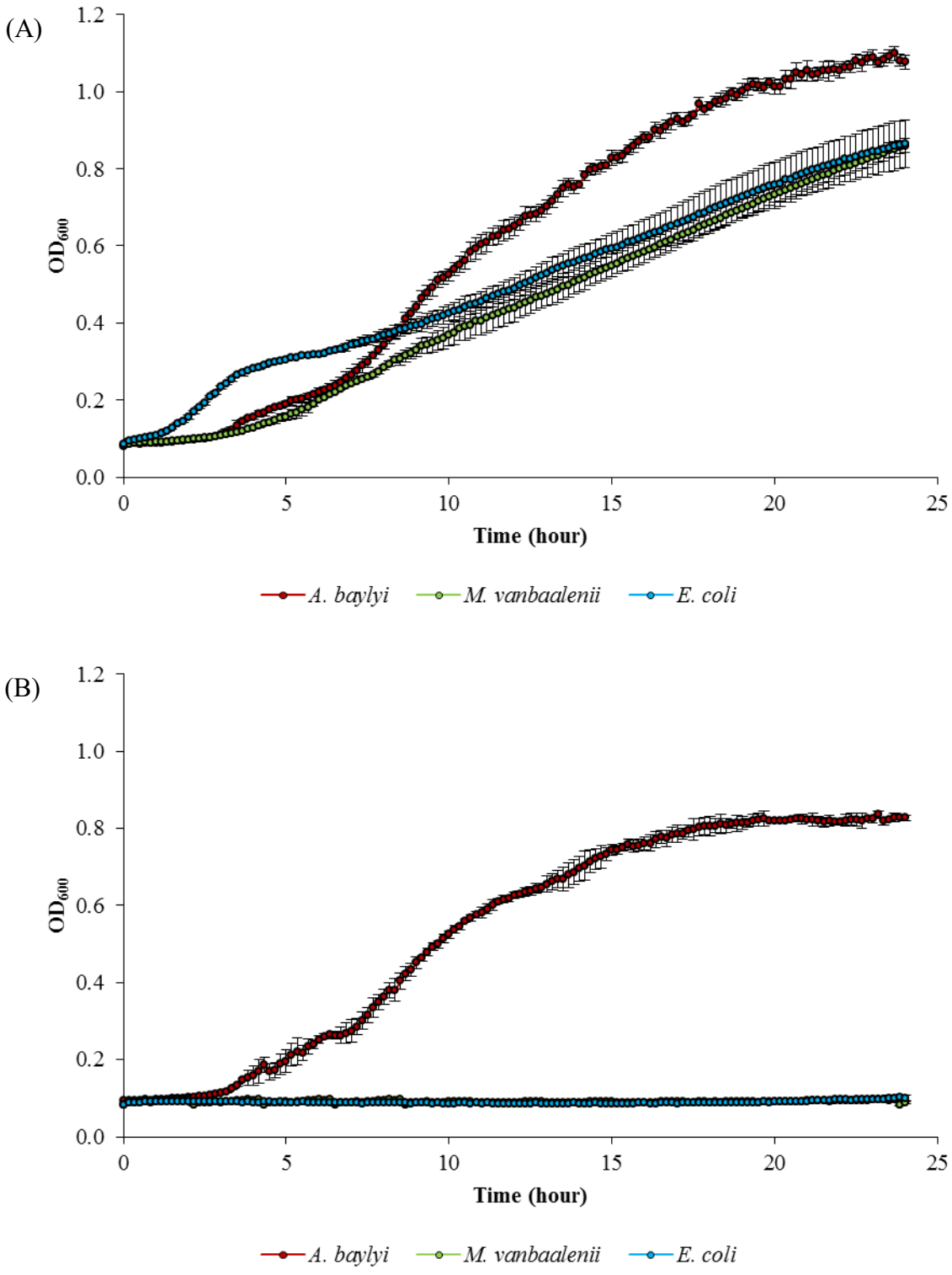

Figure S1. Growth curve of *Mycobacterium vanbaalenii* PYR-1, *Escherichia coli* DH5α and *Acinetobacter baylyi* ADPWH_recA in mineral medium without kanamycin pressure (A) or with 10 mg/L kanamycin (B).

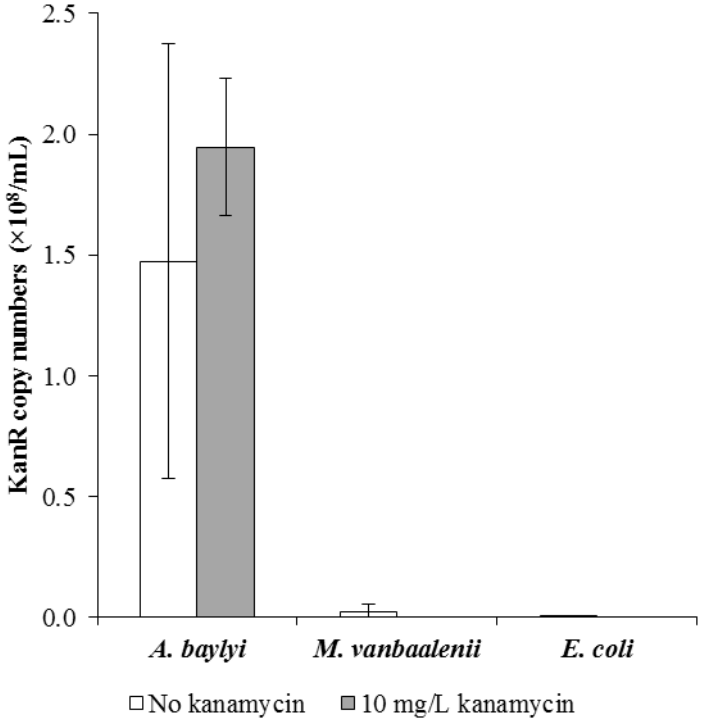

Figure S2. Copy numbers of kanamycin resistance gene in *Mycobacterium vanbaalenii* PYR-1, *Escherichia coli* DH5α and *Acinetobacter baylyi* ADPWH_recA after 16-h cultivation without kanamycin pressure (A) or with 10 mg/L kanamycin (B). Data are presented in mean ± standard error.

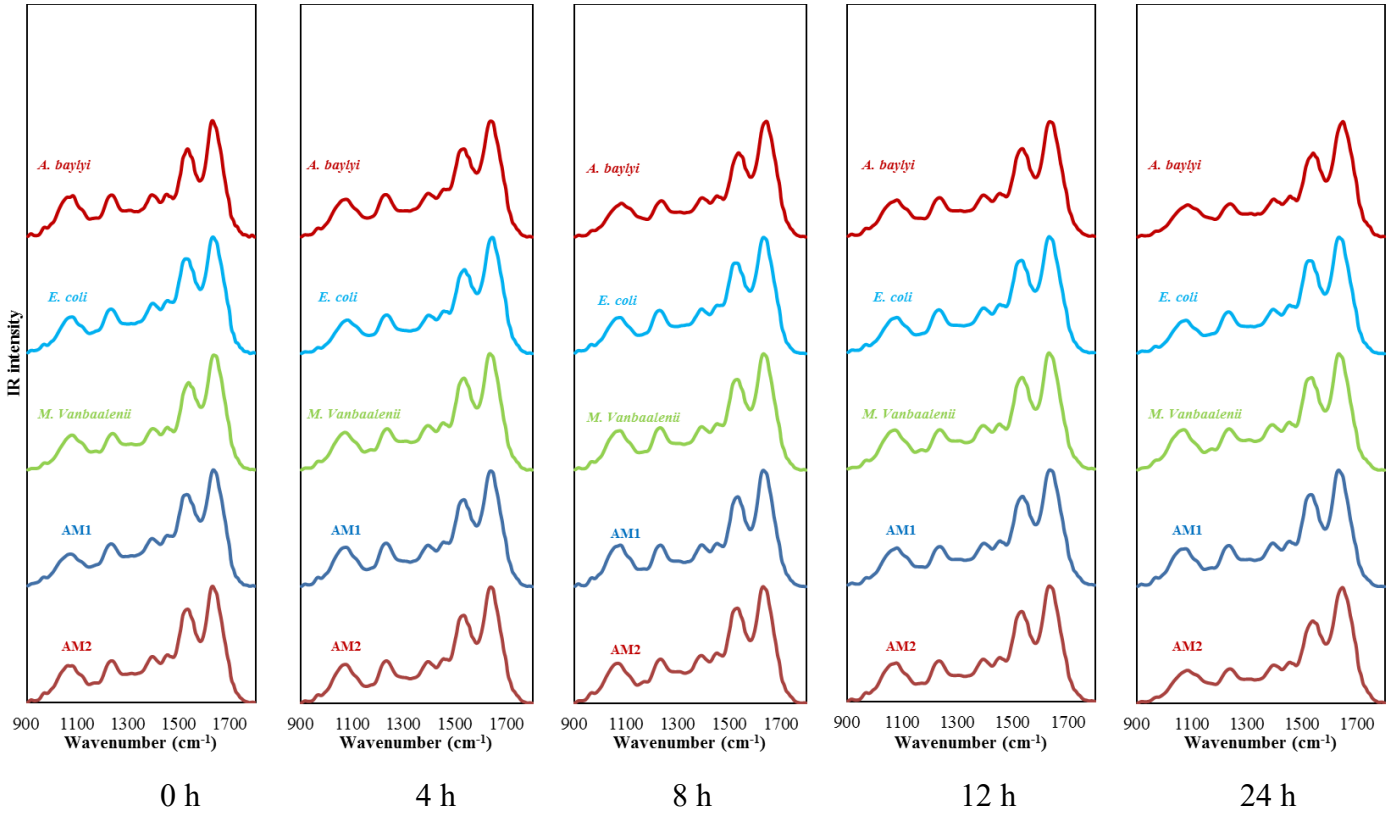

Figure S3. ATR-FTIR spectral dynamics of artificial microbiota.

Chapter 5 Interrogating mechanisms of fungal adsorption of cadmium and lead via infrared spectroscopy

Naifu Jin, Zhongmin Jin, Tuo Zhang, Lijie Liu, Yanfu Zhang, Yuchen Wen, Tom Black, Jones C Kevin, Hao Zhang, Francis L. Martin, Dayi Zhang

Manuscript for submission.

Interrogating mechanisms of fungal adsorption of cadmium and lead via infrared spectroscopy

Naifu Jin[1], Zhongmin Jin[1,2], Tuo Zhang[1], Lijie Liu[2], Yanfu Zhang[2], Yuchen Wen[2], Tom Black[1], Jones C Kevin[1], Hao Zhang[1], Francis L. Martin[4], Dayi Zhang[3,*]

1. Lancaster Environment Centre, Lancaster University, Lancaster LA1 4YQ, UK
2. College of Agriculture, Forestry and Life Science, Qiqihar University, Qiqihar 161006, PR China
3. School of Environment, Tsinghua University, Beijing 100084, PR China
4. School of Pharmacy and Biomedical Sciences, University of Central Lancashire, Preston PR1 2HE, UK

***Corresponding author**

Dr Dayi Zhang

School of Environment, Tsinghua University, Beijing, 100084, PR China

Tel.: +86(0)1062773232

Fax: +86(0)1062785687

Email: zhangdayi@tsinghua.org.cn

Abstract

Fungi-associated phytoremediation is an environmentally friendly and cost-efficient approach to remove heavy metals from contaminated soils. Most of the fungal strains are studied for their physiological features and metal-biosorption behaviour in rich or defined medium, which is far away from the real-world scenario where limited nutrients are available. Understanding their metal-biosorption capability and influential factors in soil environment can expand their application potential and is urgently needed. This study applied attenuated total reflection Fourier-transform infrared (ATR-FTIR) coupled with Phenotype Microarrays (PM) to study the biospectral alterations of fungus *Simplicillium chinense* when cultivated by 48 different carbon sources and explain their different behaviour in biosorption of Cd and Pb. As the first study using spectroscopic tools to analysis the metal adsorption by fungal cells in a high throughput manner, our results indicated spectral biomarkers associated with phosphor-lipids and proteins (1745 cm^{-1}, 1456 cm^{-1} and 1396 cm^{-1}) were significantly correlated with Cd biosorption, suggesting the cell wall components of *S. chinense* as the primary interactive targets. In contrast, there was no any biomarker associated with Pb biosorption. Additionally, the metal biosorption isotherms also demonstrated different mechanisms, Langmuir model for Cd biosorption and Freundlich model for Pb biosorption. Accordingly, our results implied Pb and Cd biosorptions of *S. chinense* followed two discriminating mechanisms. Cd biosorption was more likely driven by the cell surface sorption that both proteins and carbohydrate factions are involved in the binding of Cd ions. The Pb biosorption, which describes both monolayer and multilayer adsorptions by considering the

heterogeneous surfaces and suggests that extracellular precipitation contributes the majority of Pb adsorption and EPS possess a substantial quantity of anion functional groups adsorbing Pb ions. This work lends new insights into the characterization of metal biosorption via the IR spectrochemical mean, which provides more in-depth data support for biosorption related mechanisms with a nondestructive manner at real-time solving the traditional barrier regarding the rapid biosorption mechanism determination in real-world scenario.

1. Introduction

With the increasing development of many metal-related industries, *e.g.*, metal mining, matal surface treating, energy production, and fertilizer manufacturing, heavy metal contamination has become one of the most critical environmental challenges[1]. The released industrial residues containing metals are continuously discharged into the environment, causing vital contaminations and posing threats to human life[1-3]. It has been recognized that the presence of heavy metals even in traces is harmful to both flora and fauna, cadmium exposure for instance, which may cause irreversible tubular damage in kidney[2, 4]. The heavy metal-induced toxicity can last for an extended time in nature and be accumulated via food chain[5].

To remediate the heavy metal contamination and reduce the possible contract to exposure, several means have been applied, including chemical precipitation, ion-exchange, membrane filtration, and biosorption.[6-9]. However, chemical precipitation is not applicable in the solid media, e.g., soil; even in the aqueous phase, it is ineffective to deal with low metal ion concentration (i.e., 1~100 mg/L) producing a large amount of waste which becomes even more challenging to handle[5]. Ion exchange and membrane filtration are costly and not suitable for large-scale treatment[2, 5]. Biosorption as an alternative approach, which uses biomaterials such as bacteria, fungi, yeast and algae, has also been highlighted in the past studies[5], Phytoremediation, in particular, uses plant to remove pollutants from the envivronment driven by solar energy and it is therefore consided as an environemtally sustainable mean for heavey metal removal[10] Biosorption is relatively efficient compared with the chemical precipitation and electrochemical treatments, particularly in the low level of metal ion

concentrations, and also less expensive than the ion exchange, membrane technologies, and activated carbon adsorption[2, 11].

Fungi, as one critical group of microorganisms, have been applied as metal biosorbents in prior researches[2, 12]. The mechanisms of metal biosorption by fungi are complicated and mainly consist of two principal stages: direct adsorption of fungal membrane and penetration through the cell wall. The first step is passive biosorption independent on fungal metabolism, and the critical influential factor is the functional groups of the cell wall which affect the interactions between fungal membrane and metals and. Secondly, metal ions penetrate the cell membrane and enter the cell via active biosorption, which is metabolism-dependent and related to metal transportation and deposition[2]. Accordingly, from where metals eventually allocate, biosorption can be classified as extracellular accumulation/precipitation, cell surface sorption/precipitation, and intracellular accumulation[13]. Heavy metal uptake by *Aureobasidium pullanans* and *Cladosprim resinae* for instance, consists of metabolism independent cell wall uptake followed by an energy-dependent cellular uptake[13, 14]. Another study carried out by Huang *el al* found the removal of Cd by nine species of fungi was controlled by adsorption instead of surface precipitation[13, 15]. However, most of the previous works address the metal fungal biosorption in rich or defined media with limited carbon sources, not representing the real-world scenario in which the process of biosorption is be altered by many environmental factors, such as metal availability, growth condition and available carbon sources[16-18]. Thus, understanding fungi's natural capability and mechanism of heavy metals adsorption, and exploring the possible phenotypic variations existing in the real world are urgently needed.

To investigate the phenotypic features of microbes and the relevant metabolism, it is critical to find a reliable analytical method. Biospectroscopy as a group of interdisciplinary tools has many advantages in microbiological study owing to their measurement attribute with a high-throughput, nonintrusive and nondestructive manner[19-22]. Infrared spectroscopy, for instance, relies on the principle that the bending, stretching and twisting of bonds (such as C-H, O-H, N-H, C=O, C-C, etc.) are produced when the energy from the infrared radiation is absorbed by the sample, resulting in characteristic transmittance and reflectance patterns[21, 23]. Nevertheless, previous spectroscopic studies on fungi mainly attempt to detect the presence of fungal cells, characterize fungal species, and diagnose fungi induced disease[23-25]. Recently, spectroscopic approaches are expanded to determine microbial interaction with environmental stimuli, *e.g.*, antibiotic resistance[22, 26]. Accordingly, biospectroscopy might have considerable potentials in studying fungal biosorption of heavy metals and bring new insights into the relevant mechanism; however, such attempt has not been reported.

The present study applied attenuated total reflection Fourier-transform infrared (ATR-FTIR) spectroscopy coupled with phenotype microarrays to characterize the biosorption of cadmium (Cd) and lead (Pb) by fungus *Simplicillium chinense* cultivated with 48 different carbon sources. This is the first study using spectrochemical tool to analyse the impacts of carbon source on fungal biosorption of heavy metals, providing valuable database to enhance fungi-associated phytoremediation and providing an opportunity to look deeper into the biosorption mechanism from a novel perspective. It also reveals biosorption related mechanisms

with a nondestructive manner in real-time showing the potential feasibility for the rapid determination of microbial metabolism activities in the real-world scenario.

2. Materials and Methods

2.1 Strains and cultivation condition

The fungal strain *Simplicillium chinense* was isolated in the soils collected in Zhalong Wetland (47°32'30"N, 124°37'50"E, Qiqihar City, China) in October 2015. The strain was cultivated in potato dextrose medium (200 g potato, 20 g glucose and 20 g agarose dissolved in 1,000 mL deionized water and autoclaved) at shaking speed of 160 rpm and 28ºC for five days. Cd and Pb stock solutions were prepared by dissolving $Pb(NO_3)_2$ and $CdSO_4$ salts in deionized water, respectively. The final concentration of Cd and Pb was 20 mg/L.

PM1 plate (Biolog, USA) was used to examine the carbon metabolic features of *S. chinense*. Fifteen microliters of the washed cells were resuspended in 135 µL minimal medium and then added to each well of PM1 plate. To monitor fungal growth, additional 1.5 µL Redox Dye Mix A (100×, Biolog, USA) was added to each well. The plate was then incubated at 30ºC for five days, and the colour development was measured every 4 hours for absorbance at 590 nm wavelength (respiratory unit, RU) by a multimode microplate reader (FLUOstar Omega, BMG Labtech, UK). To avoid the impacts of Redox Dye on fungal biospectra, another treatment was prepared without the addition of Redox Dye Mix A and directly cultivated at 30ºC for five days. All the treatments were carried out in triplicates.

2.2 Cd/Pb adsorption and chemical analysis

After 5-day cultivation, the cells were directly collected by centrifugation (3000 rpm for 5 min) and washed three times with fresh carbon-free medium. Subsequently, each well was subjected with 20 μL of Pb or Cd stock solution and kept shaking for 2 hours (final Pb or Cd concentration 2 mg/L). Subsequently, the supernatant was collected after 3,000 rpm centrifugation for 20 min. The cell pellets were further washed with 5 mL deionized water and centrifuged again (3,000 rpm) for another 20 min. The supernatants were combined, spiked with 20 μL internal standards (103Rh, 45Sc, 209Bi), and diluted with deionized water to the final volume of 50 mL for metal analysis. Cd and Pb were analyzed by inductively coupled plasma mass spectrometry (ICP-MS, X-series 2, Thermo Scientific, USA), and the detection wavelength was 228.8 nm and 283.3 nm, respectively. The standard calibration solution contained the mixture of Cd and Pb in HNO_3 (0.1M), and their concentrations ranged from 0 to 100 μg/L.

2.3 Infrared spectra measurement

The cell pellets after adsorption were further washed three times with sterile deionized water to remove the residues of growth media and then suspended in 70% ethanol for fixation. The washed cell pellets (minimal amount >5 μL) were applied onto Low-E slides for interrogation by ATR-FTIR spectroscopy. A TENSOR 27 FTIR spectrometer (Bruker Optics Ltd., UK) equipped with a Helios ATR attachment (containing a diamond internal IRE; incidence angle of the IR beam: 45°) was used and the instrument parameters were set at 32 scans and spatial resolution of 8 cm^{-1}.

Before the measurement of a new sample, the crystal was cleaned with deionized water, and the background readings were retaken. A total of 20 spectra were acquired for each treatment.

2.4 Data analysis

The RU data were collected and further analysed by MARS software (BMG Labtech, UK). The relative RU for fungal growth with each carbon source was calculated as the average of RUs on day 5. The growth index for fungal growth with each carbon source was calculated as the ratio of the relative RU cultivated with this carbon source to that without any carbon source (well A1, negative control).

The linear regression between the relative RU and biomass (dry cell weight, DCW) was obtained by serially diluted fungal suspension with the known relative RU and biomass, following Equation (1).

$$\text{Biomass} = 0.196 \times \text{RU} + 0.168 \quad (1)$$

The initial spectral data generated from ATR-FTIR spectroscopy were analyzed within MATLAB R2011a software (TheMathsWorks, Natick, MA, USA), coupled with IrootLab toolbox (http://irootlab.googlecode.com)[27]. Unless otherwise stated, the acquired spectra were cut to the biochemical-cell fingerprint region (1800-900 cm^{-1}), rubberband baseline corrected and normalized to Amide I (1650 cm^{-1}). Second order differentiation baseline correction and vector normalization were also performed as an alternative mean to process the data. Principal component analysis followed by linear discriminant analysis (PCA-LDA) was subsequently applied to the preprocessed data to reduce the number of spectra to 10 uncorrelated principal components (PCs), which

account for >99% of the total variance; LDA is a supervised technique coupled with PCA in order to maximize inter-class and minimize intra-class variance[28]. Also, cluster vector approach was conducted to visualize the discriminating difference[28, 29]. Additionally, all the statistical analysis was carried out in GraphPad Prism 6 unless specific statement.

3. Results

3.1 S. chinense growth profiles with 48 carbon sources

The growth curves of *S. chinense* were obtained from the measurement of RU data, illustrating significant differences across cultivation in minimal medium with 48 carbon sources (Figure 1A). All the treatments showed an obvious lag phase for about 8 hours and then a dramatical increasing RU was observed in some wells. Following a log growth phase with various growth rate until 72 hours, the cells entered the stationary phase. The results demonstrated that *S. chinense* could effectively utilize some carbon sources and behave positive growth for three days. Based on the chemical structure and functional groups, the 48 carbon sources are categorized into five groups, including nucleic acid, carbohydrate, carboxylic acid, amino acid and others. However, no significant difference in fungal growth was observed between groups. Thus, in order to have a more crystal image of the carbon sources impact on growth, the utilization efficiency of carbon was further divided into three categories based on growth index in Figure 1B. Four carbon sources with significantly higher growth index (>1.0) were L-glutamine, Tween 80, glycolic acid and methylpyruvate. Fourteen carbon sources moderately supporting fungal growth (growth indices between 0.5 and

1.0) included a-hydroxyglutaric acid-g-lactone, a-hydroxybutyric acid, adenosine, Gly-Asp, fumaric acid, bromosuccinic acid, glyoxylic acid, D-cellobiose, inosine, Gly-Glu, tricarballylic acid, p-hydroxyphenyl acetic acid, m-hydroxyphenyl acetic acid, and 2-aminoethanol. The other carbons sources were barely useable by *S. chinense* owing to the low growth indices (<0.5).

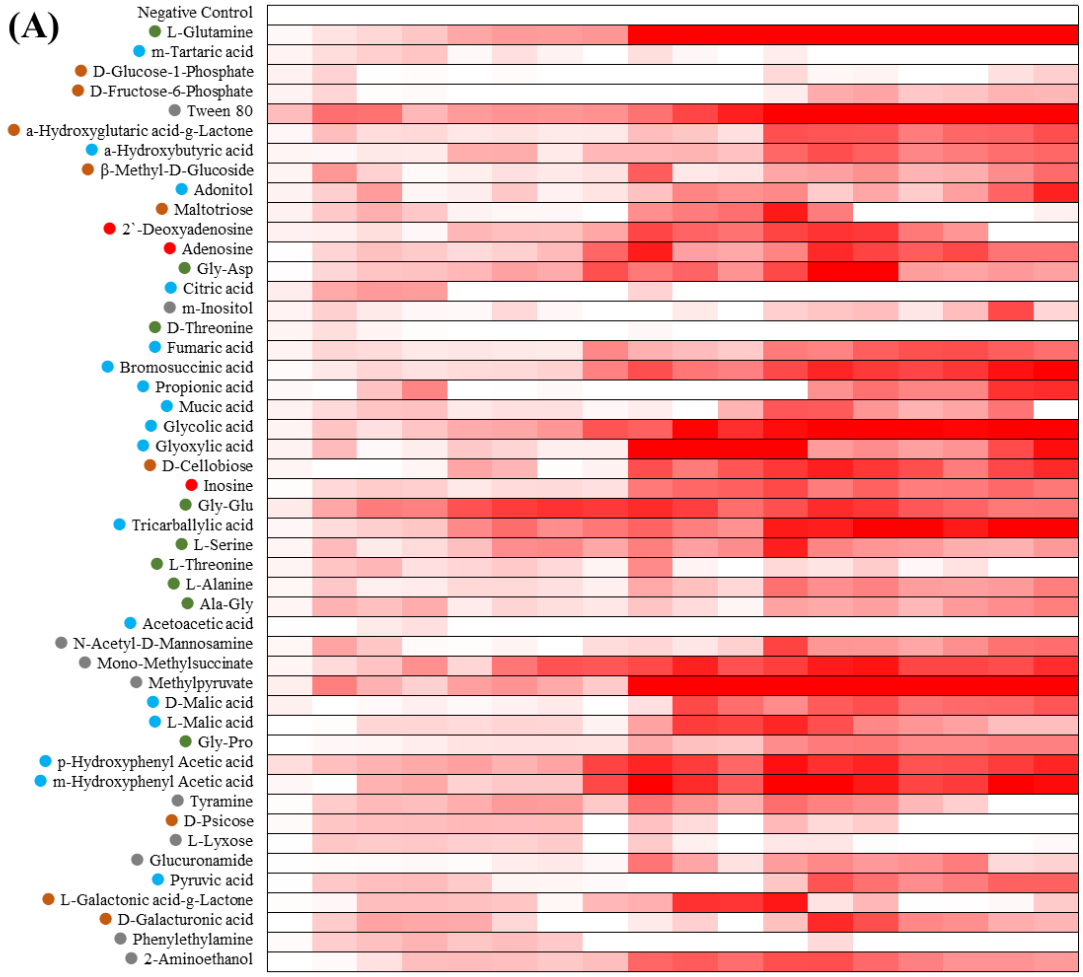

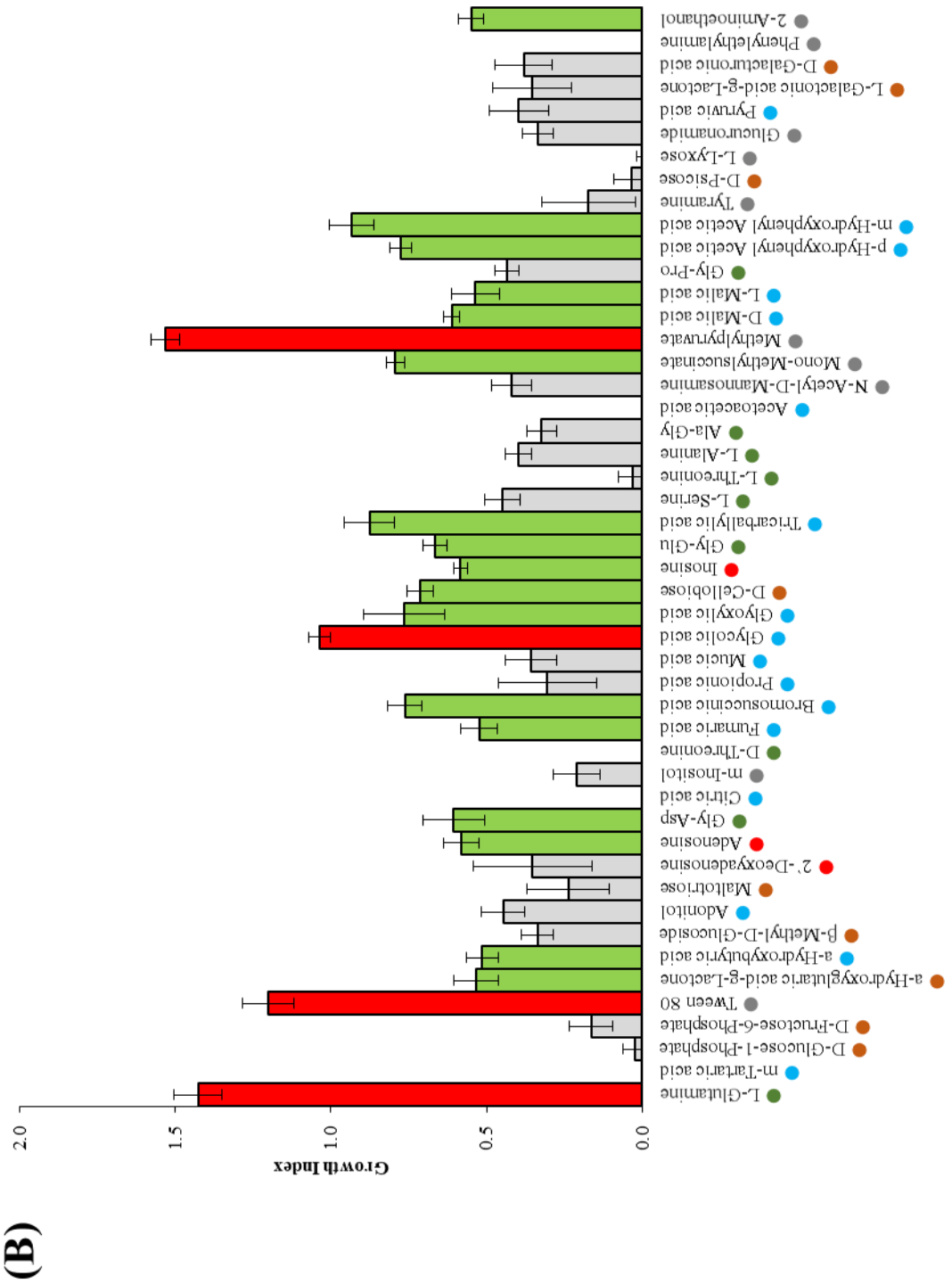

Figure 1. Growth profiles of *S. chinense* in minimal medium with 48 different carbon sources. (A) Growth curves during 144-hour cultivation. (B) Growth indices of *S.*

chinense in comparison with the negative control (A1, no carbon source).

3.2 Cd and Pb adsorption with S. chinense cultivated with 48 carbon sources

Both Cd and Pb were efficiently adsorbed by *S. chinense* cultivated in minimal medium with 48 different carbon sources and the adsorption efficiency achieved >90% for all the treatments. Two biosorption equilibrium models (Langmuir and Freundlich) were applied to help in understanding the absorption mechanisms of Cd and Pb on *S. chinense*. The Langmuir isotherm model represents the monolayer adsorption mechanism with a restriction of no stacking of adsorbed molecules, as described in Equation (2). The Freundlich isotherm model represents both monolayer and multilayer adsorptions by considering the heterogeneous surfaces possessing different sorption energy sites, as described in Equation (3).

$$Q_e = Q_{max} \frac{K_L C_e}{1 + K_L C_e} \quad (2)$$

$$Q_e = K_F C_e^{1/n} \quad (3)$$

Here, Q_e (mg/g DCW) refers to the total metal ion absorption capacity, and C_e (g/L) represents the equilibrium metal concentration in the liquid phase concentration of total ions. Q_{max} (mg/g DCW) is the maximum adsorption capacity for monolayer adsorption in Langmuir isotherm model, and K_L (L/mg) is the Langmuir constant associated with adsorption energy. K_F (mg/g DCW) represents the adsorption capacity in both monolayer and multilayer mechanism in Freundlich isotherm model, and $1/n$ is the heterogeneous sorption sites. Either Langmuir or Freundlich isotherm model can be expressed in the linear form as shown in Equation (4) and (5),

respectively.

$$\frac{C_e}{Q_e} = \frac{1}{Q_{max} \cdot K_L} + \frac{C_e}{Q_{max}} \quad (5)$$

$$\log Q_e = \log K_F + \frac{1}{n} \log C_e \quad (6)$$

Figure 2A illustrates that Cd adsorption fitted better with Langmuir isotherm (R^2=0.7324) than Freundlich isotherm (R^2=0.0653). In Langmuir isotherm, the maximum adsorption capacity (Q_{max}) was 1.81 (mg/g DCW) and the Langmuir constant associated with adsorption energy (K_L) is -1.75 L/mg. On the contrast, Pb biosorption fitted better with Freundlich isotherm (R^2=0.9458) than Langmuir isotherm (R^2=0.1121, Figure 2). The heterogeneous sorption sites ($1/n$) was 0.84 and the adsorption capacity (K_F) was 0.77 (mg/g DCW) in Freundlich isotherm.

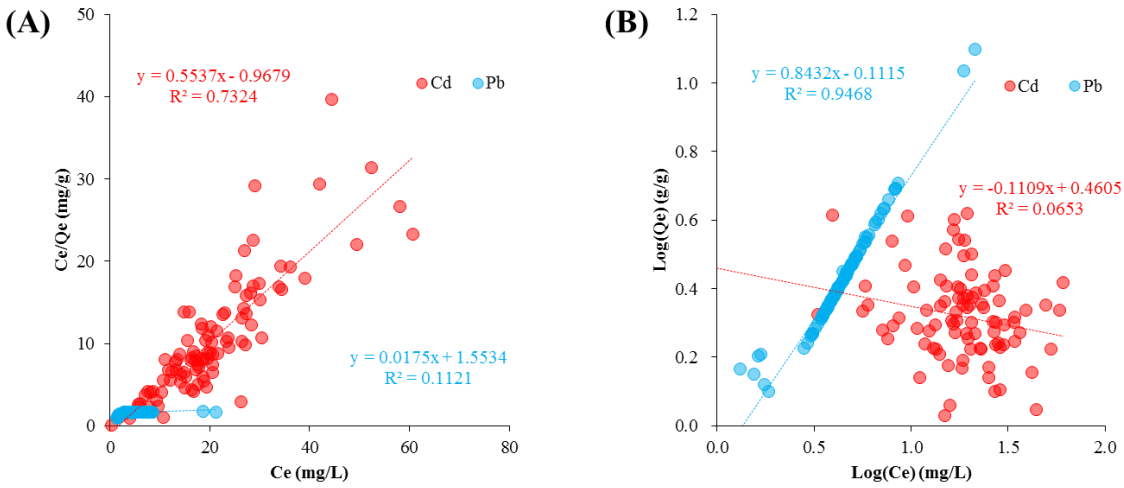

Figure 2. Adsorption isotherms of Cd and Pb on *S. chinense* cultivated in minimal medium with 48 different carbon sources. (A) Langmuir isotherm model representing the monolayer adsorption mechanism. (B) Freundlich isotherm model representing both monolayer and multilayer adsorptions by considering the heterogeneous surfaces

possessing different sorption energy sites. Initial Cd and Pb concentration was 100 mg/L and the adsorption time was 2 hours.

3.3 Infrared spectra of S. chinense cultivated in 48 carbon sources

In general, *S. chinense* shares similar spectral patterns across 48 carbon sources regarding the cellular structures, including lipid (~ 1750 cm^{-1}), Amide I (~ 1650 cm^{-1}), Amide II (~ 1550 cm^{-1}), Amide III (~ 1260 cm^{-1}), carbohydrate (~ 1155 cm^{-1}) and symmetric phosphate stretching vibrations (~ 1080 cm^{-1}) [21, 30] (Figure 3A). The 1D score plot of PCA-LDA (Figure 3B) indicates the variations between each category of carbon source. The results of one-way ANOVA test coupled with Turkey's multiple comparisons demonstrate all classes are significantly differentiated (p<0.05), except for the variation between the groups of amino acid and others (p>0.05).

The cluster vector analysis reveals more information regarding the biomolecular difference (Figure 4), which includes five primary peaks derived from original spectra as relevant biomarkers for each group of carbon sources. Specifically, the biomarkers of *S. chinense* cultivated with amino acids are (~1134 cm^{-2}), PO_2^- asymmetric (~ 1265 cm^{-2}), Amide III (~ 1185 cm^{-2}), Amide II (~ 1517 cm^{-2}) and C=O (~ 1728 cm^{-2}). Besides the peak of PO_2^- asymmetric (~ 1265 cm^{-2}), the other most significant peaks of carbohydrate-cultivated fungal cells are RNA (~ 1117 cm^{-2}), CH in-plane bend (~ 1510 cm^{-2}), Amide I (~ 1659 cm^{-2}) and C=O, lipids (~ 1740 cm^{-2}). In nucleic acid group, the characteristic peaks are v(CO), v(CC) (~ 1018 cm^{-2}), deoxyribose (~ 1188 cm^{-2}), (~ 1269 cm^{-2}), Amide II (~ 1540 cm^{-2}) and lipids (~ 1740 cm^{-2}), and the same peak presented in carbohydrate group and associated with lipid is also found at ~ 1740

cm^{-2}. In the group of carboxylic acid, the characteristic peaks include stretching vibrations of hydrogen-bonding, C-OH groups (~ 1153 cm^{-2}), N-H thymine (~ 1276 cm^{-2}), C=C, deformation C-H (~ 1496 cm^{-2}), Ring base (~ 1555 cm^{-2}), base carbonyl stretching and ring breathing mode (~ 1620 cm^{-2}). Characteristic peaks for other carbon sources have no clear pattern, and the significant peaks include stretching C-O deoxyribose (~ 1056 cm^{-2}), C-O stretching vibration (~ 1150 cm^{-2}), PO_2^- asymmetric (~ 1256 cm^{-2}), ring base (~ 1555 cm^{-2}) and lipids (~ 1740 cm^{-2}).

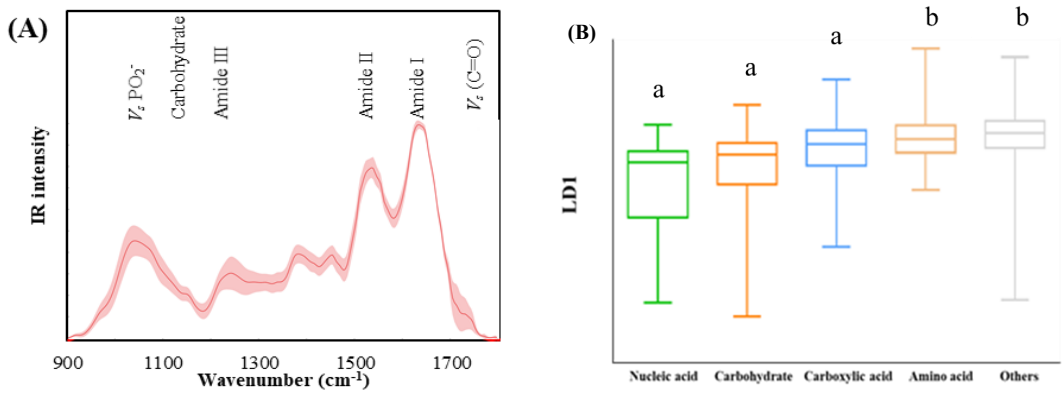

Figure 3. (A) Mean spectra of all pre-processed data with different carbon sources based on rubberband baseline correction and Amide I (1650 cm^{-1}) normalization. (B) PCA-LDA categorizations of *S. chinense* cultivated in minimal medium with five groups of carbon sources, including nucleic acid, carbohydrate, carboxylic acid, amino acid and others. Twenty infrared spectra were randomly obtained per treatment. Different small letters indicate significant difference (Duncan's test, $p<0.05$) among treatments at the same sampling time.

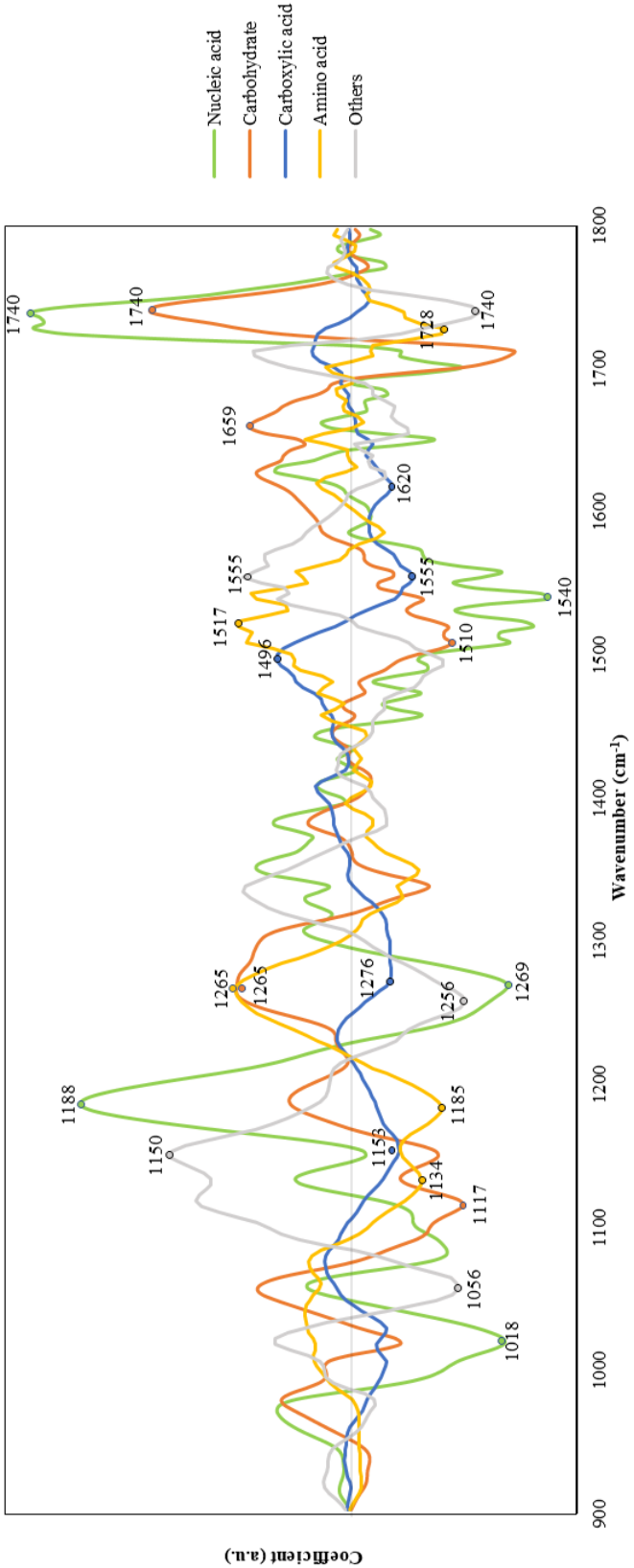
Nucleic acid
Carbohydrate
Carboxylic acid
Amino acid
Others
Coefficient (a.u.)
Wavenumber (cm-1)
900
1000
1100
1200
1300
1400
1500
1600
1700
1800
1740
1740
1728
1740
1659
1620
1555
1555
1517
1496
1510
1540
1265
1265
1276
1256
1269
1188
1185
1150
1158
1134
1117
1056
1018

Figure 4. Cluster vector analysis of *S. chinense* cultivated in minimal medium with five groups of carbon sources shows their unique spectral biomarkers. Twenty infrared spectra were randomly obtained per treatment.

3.4 Mechanisms of Cd and Pb biosorption via spectral analysis

As metal biosorption by fungi consists of two principal stages of direct adsorption on fungal membrane and penetration through cell wall, it can be characterized via analyzing the functional groups of cellular components or extracellular polymeric substance (EPS). Although PCA-LDA is applied to assess the 'fingerprint region' to distinguish the relationship between the whole spectra and fungal growth or biosorption efficiency, it is very challengeable owing to the enormous spectral alterations across 48 carbon sources (Figure 5A). We, therefore, attempted to identify discriminating alterations by introducing Pearson correlations to determine the relationship between spectral variations based on cluster vector analysis and microbial activities (e.g., biomass and the adsorption of Pb or Cd). The results indicate that several discriminating alterations positively correlated with fungal biomass (Figure 5A), include 1340 cm^{-1} (collagen, $p<0.05$), 1136 cm^{-1} (collagen, $p<0.05$) and 966 cm^{-1} ($p<0.05$, C-C DNA), suggesting these peaks can be viewed as biomarkers for fungal growth (Figure 5B-D). For the significant peaks associated with adsorption of heavy metals, the biomarkers related to Cd adsorption are 1745 cm^{-1} (phospholipids, $p<0.05$), 1620 cm^{-1} (nucleic acid, $p<0.05$), 1456 cm^{-1} (lipids and proteins, $p<0.05$), 1396 cm^{-1} (proteins, $p<0.05$) and 1057 cm^{-1} (stretching C-O deoxyribose, $p<0.05$), as illustrated in Figure 5E-I. However, there is no biomarker significantly correlated with Pb adsorption, further confirming the different adsorption mechanisms between Cd and

Pb as suggested by the results of adsorption isotherms.

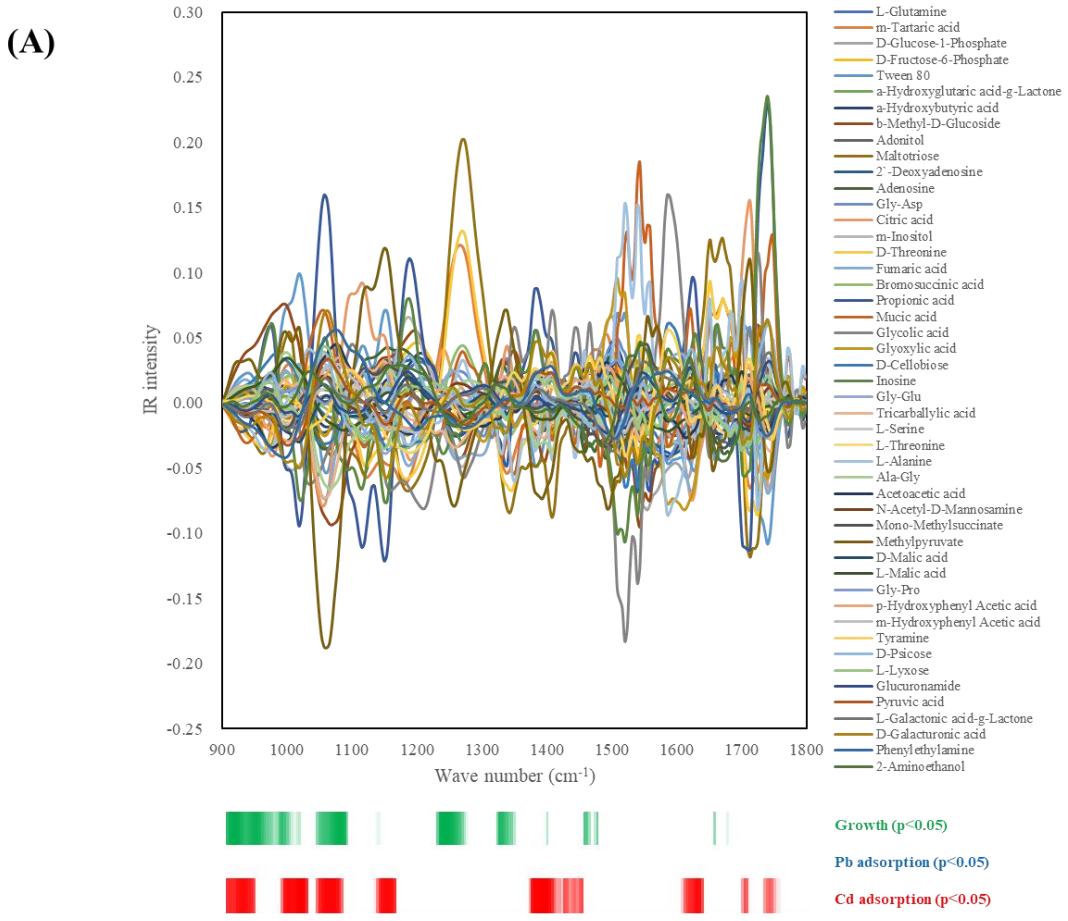

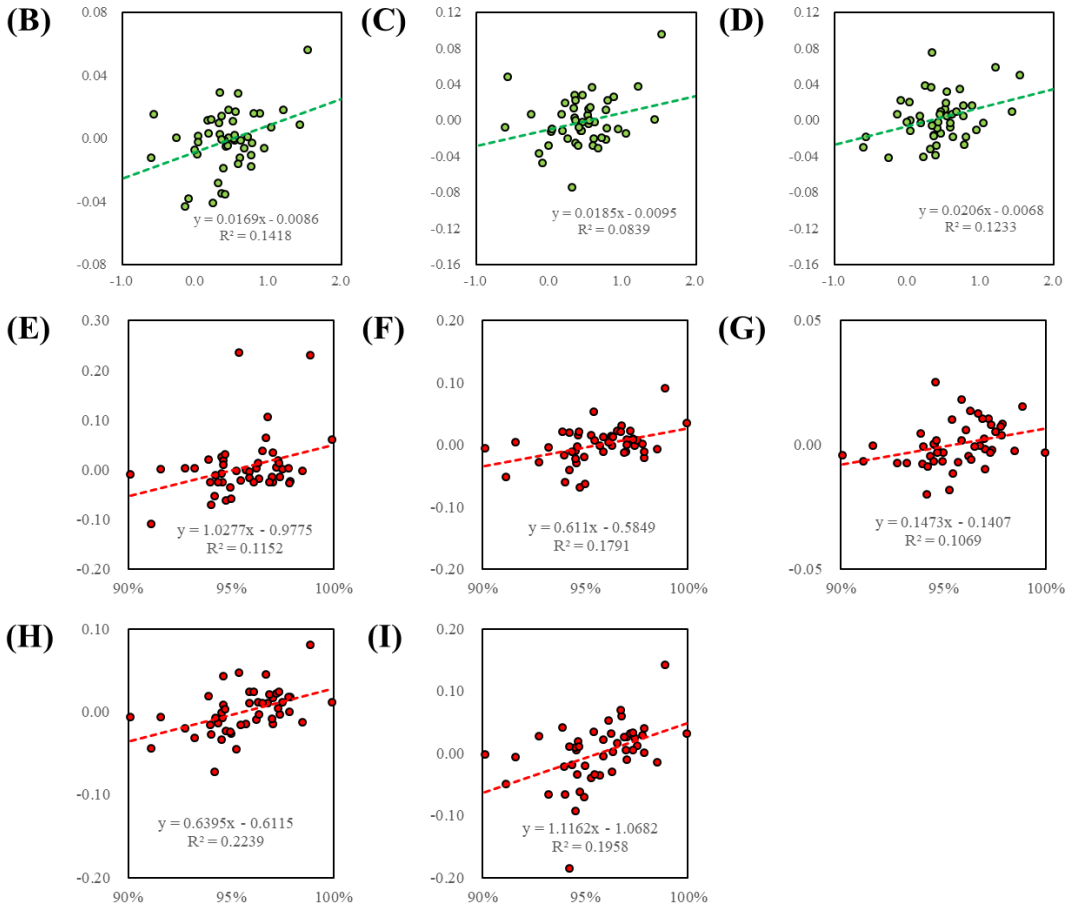

Figure 5. (A) Cluster vector of *S. chinense* cultivated with 48 carbon sources. The color bar illustrates the significant levels ($p<0.05$) of correlation of IR bands intensity with growth index (green), Pb adsorption (blue) and Cd adsorption (red). IR bands significantly correlated with growth index include: (B) 1340 cm^{-1} (collagen), (C) 1136 cm^{-1} (collagen) and (D) 966 cm^{-1} (C-C DNA). IR bands significantly correlated with Cd adsorption efficiency include: (E) 1745 cm^{-1} (phospholipids), (F) 1620 cm^{-1} (nucleic acid), (G) 1456 cm^{-1} (lipids and proteins), (H) 1396 cm^{-1} (proteins) and (I) 1057 cm^{-1} (stretching C-O deoxyribose).

4. Discussion

4.1 Biosorption capability of S. chinense on Cd and Pb

Previous studies investigating microbes as biosorbent have demonstrated that microbial cells have robust ability to remove heavy metals. *Saccharomyces Cerevisiae*, belonging to the yeast for instance, is a species exclusively reported [5, 31, 32]. Based on the equilibrium sorption process, the metal biosorption capability of *S. Cerevisiae* ranged from 10 to 300 mg/g DCW for Pb and 10 to 100 mg/g DCW for Cd[5]. Metal biosorption by fungal species has also been investigated, such as *Penicillium* sp. MRF-1 which has a substantial adsorption capacity of Cd (0.13-9.39 mg/g DCW)[33] and *Exiguobacterium sp.* with a maximum adsorption capacity of 15.6 mg/g DCW for Cd in Langmuir isotherm[34]. In the present study, the adsorption capacity of Pb (0.77 mg/g DCW) was similar with previous studies, whereas the adsorption capacity of Cd (1.81 mg/g DCW) was much lower. The usage of defined medium might be the primary contribution to the difference between the present study and previous literature. The limited nutrients within the defined medium with specific carbon sources is insufficient for the saturated fungal growth, and their activities are therefore surpressed[35-37]. Accordingly, finite active binding sites on fungal cell membranes consequently resulted in less adsorption capacity of Cd by *S. chinense*. This circumstance, however, fits better with the real situation in natural habitats, where microbes survive under nutrient depletion conditions demonstrating less biosorption ability than most of the previous studies. Thus, our result provides a relatively realistic database regarding the evaluation of fungal adsorption in the real world.

4.2 Biospectral fingerprints of S. chinense

Biospectroscopy has a long history of studying the biological materials. IR spectroscopy can be traced back to 1950s[22] and is extensively applied when FTIR spectroscopy was innovatively introduced as a sensitive and rapid screening tool for characterization of microbes[22, 38]. Over past 20 years, IR spectroscopy has been applied in the examination of biological materials, particularly at the cell or tissue level, including bacteria, yeast and mammalian cells[21, 30, 39]. However, only limited works have focused on fungi, and there is lack of a well-established database for fungal spectral biomarkers. In the present study, our results illustrated similar spectra with several vital biological biomarkers of fungi comparing to those of bacterial cells based on past literatures, including lipid (~ 1750 cm^{-1}), Amide I (~ 1650 cm^{-1}), Amide II (~ 1550 cm^{-1}), carbohydrate (~ 1155 cm^{-1}) and symmetric phosphate stretching vibrations (~ 1080 cm^{-1}) [21, 30, 40]. There was only slight difference in intensities that the peaks of ~ 1400 cm^{-1} (proteins) and ~ 1260 cm^{-1} (PO_2^- asymmetric, phosphate I), consistent with previous report that the peak at approximately 1100 cm^{-1} (ν(CO), ν(CC) ring of polysaccharides) and 1400 cm^{-1} (proteins)[40]. It might be attributed to the difference in cell wall structure, in which the fungal cells are protected by a true cell wall which is rigid as in bacterial cells[41].

4.3 Spectral biomarkers for S. chinense growth across carbon source groups

Although the growth indices of *S. chinense* cultivated with each carbon source group showed no significant difference, the cluster vector analysis raised more discriminating biomarkers regarding the carbon source categories induced spectral

characters. These biomarkers revealed the metabolic features of *S. chinense* responsive to carbon sources. Carbohydrate, for instance, had the isolated biomarkers including PO_2^- asymmetric (~ 1265 cm^{-2}), RNA (~ 1117 cm^{-2}), CH in-plane bend (~ 1510 cm^{-2}), Amide I (~ 1659 cm^{-2}) and C=O, lipids (~ 1740 cm^{-2}), which indicated the complex carbohydrate metabolic processes. Carbohydrates are reported to associate with fungal metabolism, not only providing energy for the synthesis of trehalose, polyols, glycogen, fatty acids and other compounds but also supplying carbon skeleton for other metabolic processes, such as hyphal growth and amino acid biosynthesis[42-44]. As the metabolisms vary across intra- and inter-groups of different carbon sources, there is no clear relationship between growth and carbon source categories.

We further applied Pearson correlation analysis based on cluster vector analysis to link the spectral variations with fungal biomass and identify the critical biomarkers for fungal growth. The IR bands significantly correlated with growth indices include 1340 cm^{-1} (collagen), 1136 cm^{-1} (collagen) and 966 cm^{-1} (C-C DNA) (Figure 5B-5D), implying these components change dramatically regarding biological processes. Among them, the DNA involvement indicates a high potential that fungi are undergoing cell reproduction. Additionally, the collagen-associated spectral alterations are very likely linked to the formation of fungal fimbriae, which are composed of collagen and produced on extracochlear surfaces[45]. Our results suggested that the isolated spectral biomarkers could be applied as general indicators for the evaluation of fungal growth.

4.4 Derived biospectral biomarkers explaining different mechanisms of Cd and Pb biosorption

Cultivated with different carbon sources, our results illustrated that Cd and Pb adsorption followed different models, Langmuir and Freundlich isotherm respectively, implying the distinct mechanisms behind the biosorption of Pb and Cd by *S. chinense*. As the Langmuir isotherm represents the monolayer adsorption mechanism and the Freundlich isotherm describes both monolayer and multilayer adsorptions by considering the heterogeneous surfaces possessing different sorption energy sites, the spectrochemical analysis might provide deeper insight *via* diagnosing spectral alterations associated with metal adsorption process[13, 41, 46]. The results of spectral analysis indicated that phosphor-lipids and proteins (1745 $cm^{-}1$, 1456 $cm^{-}1$, 1396 cm^{-1}) are strongly correlated with biosorption of Cd (Figure 5E-5I). It suggested that the cell wall components of *S. chinense* are the primary interactive targets for Cd biosorption, such as polysaccharides, proteins and lipids which offer abundant metal-binding functional groups, *e.g.*, carboxylate hydroxyl, sulphate, phosphate and amino groups[13, 47]. It was consistent with our metal adsorption data that Cd biosorption isotherm followed Langmuir isotherm and was more likely driven by the cell surface sorption that both proteins and carbohydrate factions are involved in the binding of Cd ions. In contrast, no spectral biomarker was observed to significantly associate with Pb biosorption. This result was also explained by the Freundlich isotherm of Pb biosorption, which describes both monolayer and multilayer adsorptions by considering the heterogeneous surfaces and suggests that extracellular precipitation contributes the majority of Pb adsorption and EPS possess a substantial quantity of

anion functional groups adsorbing Pb ions[5]. As EPS are a mixed group of biomaterials, such as polysaccharides, glycoproteins, lipopolysaccharide and soluble peptide, it is very challengable to distinguish and extract specific spectral biomarkers associated with consistent extracellular components that are responsible for such adsorption mechanism.

The different biosorption mechanisms are principally contributed by either independent cell wall absorption or cellular uptake which requires energy and a combination of these two steps[2], which may induce specific biosorbent and heavy metals follow its own pattern. Past literature also reported as compared to other metals, exopolysaccharide presented an interesting affinity for Pb, which is a metabolism-independent process driven by the interaction between cations and negative charges of acidic functional groups of EPS[48]. In order to determine the mechanism types of fungal biosorption, several investigating means (such as adsorption kinetic, transmission electron microscopy, scanning electron microscopy and atomic force microscopy etc.) have been developed[49-52]. The current study applied IR spectroscopy coupled with multivariate analysis also achieved recognition of fungal biosorption indicating discriminating peaks derived from IR spectra could reveal the biochemical information regarding the distinct functional group or cellular components[21, 30], which shows a new direction in such field. By far, many studies have successfully built the relationship between the spectral changes and the functions of biomaterials, e.g., antimicrobial response, toxicity diagnosis and microbial chemotaxis demonstrating biospectroscopy is a reliable and effective tool regarding the investigation of molecular interaction between microbes and physical environment[19, 22, 26, 30].

4.5 Conclusion and remarks

Biosorption is important in phytoremediation to remove heavy metals from contaminated soils. The present study introduced ATR-FTIR spectroscopy coupled with Biolog PM plate as a high throughput approach to investigate the different performance and mechanisms of Cd and Pb biosorption by a fungal strain *S. chinense*. For the first time, we found several spectral biomarkers associated with fungal growth and Cd biosorption of *S. chinense* cultivated with 48 different carbon sources. Cd biosorption primarily followed monolayer Langmuir isotherm and was mainly driven by the cell surface sorption, which was unraveled by the spectral alterations affiliated with protein and the carbohydrates. For Pb biosorption, EPS possibly possessed a substantial quantity of anion functional groups adsorbing metal ions as extracellular precipitation, thus following multilayer Freundlich adsorption and representing no significant spectral biomarkers associated with Pb biosorption. Our results suggested biospectroscopy as a powerful tool in investigating the interaction between fungal cells and metals, distinguishing both functional groups and mechanisms related to metal biosorption process. This study lends new sights into fungal biosorption of heavy metals and offers database about fungal across various carbon sources, revealing the tip of the iceberg regarding the interaction between microbes and heavy metals in the real-world scenario from spectroscopic perspective.

5. REFERENCE

1. Dong, X. Q.; Li, C. L.; Li, J.; Wang, J. X.; Liu, S. T.; Ye, B., A novel approach for soil contamination assessment from heavy metal pollution: A linkage between discharge and adsorption. *J. Hazard. Mater.* **2010,** *175*, (1-3), 1022-1030.

2. Leonard, S. S.; Harris, G. K.; Shi, X. L., Metal-induced oxidative stress and signal transduction. *Free Radic. Biol. Med.* **2004,** *37*, (12), 1921-1942.

3. Liu, X. M.; Song, Q. J.; Tang, Y.; Li, W. L.; Xu, J. M.; Wu, J. J.; Wang, F.; Brookes, P. C., Human health risk assessment of heavy metals in soil-vegetable system: A multi-medium analysis. *Sci. Total Environ.* **2013,** *463*, 530-540.

4. Järup, L., Hazards of heavy metal contamination. *Br. Med. Bull.* **2003,** *68*, (1), 167-182.

5. Wang, J.; Chen, C., Biosorption of heavy metals by Saccharomyces cerevisiae: a review. *Biotechnol. Adv.* **2006,** *24*, (5), 427-451.

6. Matlock, M. M.; Howerton, B. S.; Atwood, D. A., Chemical precipitation of heavy metals from acid mine drainage. *Water Res.* **2002,** *36*, (19), 4757-4764.

7. Dąbrowski, A.; Hubicki, Z.; Podkościelny, P.; Robens, E., Selective removal of the heavy metal ions from waters and industrial wastewaters by ion-exchange method. *Chemosphere* **2004,** *56*, (2), 91-106.

8. Chen, G., Electrochemical technologies in wastewater treatment. *Sep. and Purif. Technol.* **2004,** *38*, (1), 11-41.

9. Ahluwalia, S. S.; Goyal, D., Microbial and plant derived biomass for removal of heavy metals from wastewater. *Bioresour. Technol.* **2007,** *98*, (12), 2243-2257.

10. Salt, D. E.; Blaylock, M.; Kumar, N. P.; Dushenkov, V.; Ensley, B. D.; Chet, I.; Raskin, I., Phytoremediation: a novel strategy for the removal of toxic metals from the environment using plants. *Nat. Biotechnol.* **1995,** *13*, (5), 468.

11. Yan, G.; Viraraghavan, T., Heavy-metal removal from aqueous solution by fungus Mucor rouxii. *Water Res.* **2003,** *37*, (18), 4486-4496.

12. Say, R.; Denizli, A.; Arıca, M. Y., Biosorption of cadmium (II), lead (II) and copper (II) with the filamentous fungus Phanerochaete chrysosporium. *Bioresour. Technol.* **2001,** *76*, (1), 67-70.

13. Veglio, F.; Beolchini, F., Removal of metals by biosorption: a review. *Hydrometallurgy* **1997,** *44*, (3), 301-316.

14. Gadd, G. M.; de Rome, L., Biosorption of copper by fungal melanin. *Appl. Microbiol. Biotechnol.* **1988,** *29*, (6), 610-617.

15. Huang, C.; Westman, D.; Quirk, K.; Huang, J., The removal of cadmium (II) from dilute aqueous solutions by fungal adsorbent. *Water Sci. Technol.* **1988,** *20*, (11-12), 369-376.

16. Hamdy, A., Biosorption of heavy metals by marine algae. *Curr. Microbiol.* **2000,** *41*, (4), 232-238.

17. He, J.; Chen, J. P., A comprehensive review on biosorption of heavy metals by algal biomass: materials, performances, chemistry, and modeling simulation tools. *Bioresour. Technol.* **2014,** *160*, 67-78.

18. Wang, J.; Chen, C., Chitosan-based biosorbents: modification and application for biosorption of heavy metals and radionuclides. *Bioresour. Technol.* **2014,** *160*, 129-141.

19. Li, H.; Martin, F. L.; Zhang, D., Quantification of chemotaxis-related alkane accumulation in Acinetobacter baylyi using Raman microspectroscopy. *Anal. Chem.* **2017,** *89*, (7), 3909-3918.

20. Heys, K. A.; Riding, M. J.; Strong, R. J.; Shore, R. F.; Pereira, M. G.; Jones, K. C.; Semple, K. T.; Martin, F. L., Mid-infrared spectroscopic assessment of nanotoxicity in gram-negative vs. gram-positive bacteria. *Analyst* **2014,** *139*, (5), 896-905.

21. Martin, F. L.; Kelly, J. G.; Llabjani, V.; Martin-Hirsch, P. L.; Patel, II; Trevisan, J.; Fullwood, N. J.; Walsh, M. J., Distinguishing cell types or populations based on the computational analysis of their infrared spectra. *Nat. Protoc.* **2010,** *5*, (11), 1748-60.

22. Jin, N.; Zhang, D.; Martin, F. L., Fingerprinting microbiomes towards screening for microbial antibiotic resistance. *Integr. Biol. (Camb.)* **2017,** *9*, (5), 406-417.

23. Naumann, A.; Navarro-González, M.; Peddireddi, S.; Kües, U.; Polle, A., Fourier transform infrared microscopy and imaging: Detection of fungi in wood. *Fungal Genet. Biol.* **2005,** *42*, (10), 829-835.

24. Gordon, S.; Jones, R.; McClelland, J.; Wicklow, D.; Greene, R., Transient infrared spectroscopy for detection of toxigenic fungi in corn: potential for on-line evaluation. *J. Agric. Food Chem.* **1999,** *47*, (12), 5267-5272.

25. Kos, G.; Lohninger, H.; Krska, R., Fourier transform mid-infrared spectroscopy with attenuated total reflection (FT-IR/ATR) as a tool for the detection of Fusarium fungi on maize. *Vib. Spectrosc.* **2002,** *29*, (1), 115-119.

26. Jin, N.; Paraskevaidi, M.; Semple, K. T.; Martin, F. L.; Zhang, D. Y., Infrared Spectroscopy Coupled with a Dispersion Model for Quantifying the Real-Time Dynamics of Kanamycin Resistance in Artificial Microbiota. *Anal. Chem.* **2017,** *89*, (18), 9814-9821.

27. Trevisan, J.; Angelov, P. P.; Scott, A. D.; Carmichael, P. L.; Martin, F. L., IRootLab: a free and open-source MATLAB toolbox for vibrational biospectroscopy data analysis. *Bioinformatics* **2013,** *29*, (8), 1095-7.

28. Martin, F. L.; Kelly, J. G.; Llabjani, V.; Martin-Hirsch, P. L.; Patel, II; Trevisan, J.; Fullwood, N. J.; Walsh, M. J., Distinguishing cell types or populations based on the computational analysis of their infrared spectra. *Nat. Protoc.* **2010,** *5*, (11), 1748-60.

29. Butler, H. J.; McAinsh, M. R.; Adams, S.; Martin, F. L., Application of vibrational spectroscopy techniques to non-destructively monitor plant health and development. *Anal. Methods* **2015,** *7*, (10), 4059-4070.

30. Baker, M. J.; Trevisan, J.; Bassan, P.; Bhargava, R.; Butler, H. J.; Dorling, K. M.; Fielden, P. R.; Fogarty, S. W.; Fullwood, N. J.; Heys, K. A.; Hughes, C.; Lasch, P.; Martin-Hirsch, P. L.; Obinaju, B.; Sockalingum, G. D.; Sule-Suso, J.; Strong, R. J.;

Walsh, M. J.; Wood, B. R.; Gardner, P.; Martin, F. L., Using Fourier transform IR spectroscopy to analyze biological materials. *Nat. Protoc.* **2014,** *9*, (8), 1771-91.

31. Özer, A.; Özer, D., Comparative study of the biosorption of Pb (II), Ni (II) and Cr (VI) ions onto S. cerevisiae: determination of biosorption heats. *J. Hazard. Mater.* **2003,** *100*, (1), 219-229.

32. Goyal, N.; Jain, S.; Banerjee, U., Comparative studies on the microbial adsorption of heavy metals. *Adv. in Environ. Res.* **2003,** *7*, (2), 311-319.

33. Velmurugan, N.; Hwang, G.; Sathishkumar, M.; Choi, T. K.; Lee, K.-J.; Oh, B.-T.; Lee, Y.-S., Isolation, identification, Pb (II) biosorption isotherms and kinetics of a lead adsorbing Penicillium sp. MRF-1 from South Korean mine soil. *J. Environ. Sci.* **2010,** *22*, (7), 1049-1056.

34. Park, J. H.; Chon, H.-T., Characterization of cadmium biosorption by Exiguobacterium sp. isolated from farmland soil near Cu-Pb-Zn mine. *Environ. Sci. and Pollut. Res.* **2016,** *23*, (12), 11814-11822.

35. Sipiczki, M., Metschnikowia strains isolated from botrytized grapes antagonize fungal and bacterial growth by iron depletion. *Appl. Environ. Microbiol.* **2006,** *72*, (10), 6716-6724.

36. Smith, S. E.; Smith, F. A.; Jakobsen, I., Mycorrhizal fungi can dominate phosphate supply to plants irrespective of growth responses. *Plant Physiol.* **2003,** *133*, (1), 16-20.

37. Manzoni, S.; Taylor, P.; Richter, A.; Porporato, A.; Ågren, G. I., Environmental and stoichiometric controls on microbial carbon-use efficiency in soils. *New Phytologist* **2012,** *196*, (1), 79-91.

38. Picorel, R.; Holt, R. E.; Heald, R.; Cotton, T. M.; Seibert, M., Stability of Isolated Bacterial and Photosystem-Ii Reaction Center Complexes on Ag Electrode Surfaces - a Surface-Enhanced Resonance Raman-Study. *J. Am. Chem. Soc.* **1991,** *113*, (8), 2839-2843.

39. Movasaghi, Z.; Rehman, S.; ur Rehman, D. I., Fourier Transform Infrared (FTIR)

Spectroscopy of Biological Tissues. *Appl. Spectrosc. Rev.* **2008,** *43*, (2), 134-179.

40. Maquelin, K.; Kirschner, C.; Choo-Smith, L.-P.; Ngo-Thi, N.; Van Vreeswijk, T.; Stämmler, M.; Endtz, H.; Bruining, H.; Naumann, D.; Puppels, G., Prospective study of the performance of vibrational spectroscopies for rapid identification of bacterial and fungal pathogens recovered from blood cultures. *J. Clin. Microbiol.* **2003,** *41*, (1), 324-329.

41. Sağ, Y., Biosorption of heavy metals by fungal biomass and modeling of fungal biosorption: a review. *Sep. Purif. Methods* **2001,** *30*, (1), 1-48.

42. Deveau, A.; Kohler, A.; Frey-Klett, P.; Martin, F., The major pathways of carbohydrate metabolism in the ectomycorrhizal basidiomycete Laccaria bicolor S238N. *New Phytologist* **2008,** *180*, (2), 379-390.

43. Rasmussen, S.; Parsons, A. J.; Fraser, K.; Xue, H.; Newman, J. A., Metabolic profiles of Lolium perenne are differentially affected by nitrogen supply, carbohydrate content, and fungal endophyte infection. *Plant Physiol.* **2008,** *146*, (3), 1440-1453.

44. Bago, B.; Pfeffer, P. E.; Abubaker, J.; Jun, J.; Allen, J. W.; Brouillette, J.; Douds, D. D.; Lammers, P. J.; Shachar-Hill, Y., Carbon export from arbuscular mycorrhizal roots involves the translocation of carbohydrate as well as lipid. *Plant Physiol.* **2003,** *131*, (3), 1496-1507.

45. Celerin, M.; Ray, J. M.; Schisler, N. J.; Day, A. W.; Stetler-Stevenson, W. G.; Laudenbach, D., Fungal fimbriae are composed of collagen. *The EMBO journal* **1996,** *15*, (17), 4445.

46. Michalak, I.; Chojnacka, K.; Witek-Krowiak, A., State of the art for the biosorption process—a review. *Appl. Biochem. Biotechnol.* **2013,** *170*, (6), 1389-1416.

47. Kapoor, A.; Viraraghavan, T., Fungal biosorption—an alternative treatment option for heavy metal bearing wastewaters: a review. *Bioresour. Technol.* **1995,** *53*, (3), 195-206.

48. Pérez, J. A. M.; García-Ribera, R.; Quesada, T.; Aguilera, M.; Ramos-Cormenzana,

A.; Monteoliva-Sánchez, M., Biosorption of heavy metals by the exopolysaccharide produced by Paenibacillus jamilae. *World J. Microbiol. and Biotechnol.* **2008,** *24*, (11), 2699.

49. Reddad, Z.; Gerente, C.; Andres, Y.; Le Cloirec, P., Adsorption of several metal ions onto a low-cost biosorbent: kinetic and equilibrium studies. *Environ. Sci. Technol.* **2002,** *36*, (9), 2067-2073.

50. Tsezos, M.; Remoudaki, E.; Angelatou, V., Biosorption sites of selected metals using electron microscopy. *Comp. Biochem. and Physiol. Part A: Physiology* **1997,** *118*, (3), 481-487.

51. Volesky, B.; May, H.; Holan, Z., Cadmium biosorption by Saccharomyces cerevisiae. *Biotechnol. Bioeng.* **1993,** *41*, (8), 826-829.

52. Pan, J.; Ge, X.; Liu, R.; Tang, H., Characteristic features of Bacillus cereus cell surfaces with biosorption of Pb (II) ions by AFM and FT-IR. *Colloids Surf. B: Biointerfaces* **2006,** *52*, (1), 89-95.

General Discussion and Conclusion

Develop a new tool by combining bio-spectroscopy and multivariate analysis to investigate the bacterial response to antimicrobial reagents

The ultimate goal of this project is to develop a non-invasive sensor-based tool that could be applied to monitor the emergence of antibiotic-resistant microorganisms at real-time, as (a) more conventional approaches are too exposure and/or time-consuming and often predicated on prior knowledge of the microorganisms one wishes to study; (b) there is an increasing need to monitor the emergency of antibiotic resistance in a variety of contexts ranging from environment to human health scenarios.

Fingerprinting microbiomes towards screening for microbial antibiotic resistance

To meet the need of this final objective, a prospect was proposed and the technical details were also discussed regarding the fingerprinting microbiomes towards screening for microbial antibiotic resistance. It has been proven that Infrared (IR) and Raman spectroscopy have the capability of providing biochemical information regarding the structure, functional groups and even the environment of the molecules in the biological samples. However, to perform a biospectroscopic investigation on a biological sample of interest, a well-trained dataset is the critical component. Also, microbiome as a universal form of microbes living style, which causes many challenges to the study of microbial functions due to its complicated structure, growth

conditions, internal and external environmental variants. It, therefore, induced another primary concern for the overall study is the confounding factors, i.e., composition, species, dynamics of population, growth phase and nutrient depletion impacts associated with growth phase and environmental variants of interest.

Bio-spectroscopically investigate intrinsic (bacterial type) and external factors (exposure time and type) on bacterial responsive uniqueness to antimicrobials

To answer the questions regarding the growth phase and environment variants, the investigation of short- and long-term exposure was performed. In short-term exposure, significant lipid changes filling in 1705-1750 cm^{-1} were only present in *P. fluorescens* cells comparing to *M. vanbaalenii*, owing to the differences of cell wall structure between Gram-positive and negative bacteria. Also, the study found distinct spectral alterations in non-log phase comparing to log phase, confirming the bacterial growth-dependent response to environmental exposure. It implies that past studies on log phase only may underestimate the impacts from exposures of interest *in situ*, where bacteria stay in different growth stages. In long-term exposure, multivariate analysis coupled with multivariate regression tree (MRT) indicates nutrient depletion and exposure time are the primary influencing factors in bacterial behavior, followed by exposure category and bacterial type.

After the determination of confounding factors, the treatment effects were assessed in both short- and long-term exposure. We found the tendency of tetracycline-induced

biospectral alterations widely exists in many outer-cellular components, e.g., phosphor-lipids or proteins, while the AgNPs-induced change is mainly affiliated with proteins (~ 964 cm^{-1}, ~ 1485 cm^{-1}, ~ 1550 cm^{-1}, ~ 1650 cm^{-1}) in short-term. The primarily interacted targets are correlated with bacterial membrane or outer-cellular components. In long-term exposure, post-exposure to nanoparticulate silver (AgNP), tetracycline and their mixtures for 12 days, Gram-positive (*Mycobacterium vanbaalenii* PYR-1) and Gram-negative (*Pseudomonas fluorescens*) bacteria showed distinct IR spectral alterations. Nutrient depletion and starvation during long-term exposure drives the bacterial cells into a dormant state or to exhibit additional cellular components (e.g., fatty acids) against the antimicrobials, consequently causing a broader range of spectral alteration comparing to short-term exposure.

Quantify the occurrence and real-time dynamics of antibiotic resistance genes (ARGs) in complex microbiota via bio-spectroscopy

However, characterization work of bacterial response to antimicrobials alone is insufficient to monitor the emergency of antibiotic resistance in the real-world scenario. Quantification of antibiotic resistance gene or ability is the crucial criteria to ultimately achieve this final goal. Through the work of “Infrared Spectroscopy Coupled with a Dispersion Model for Quantifying the Real-Time Dynamics of Kanamycin Resistance in Artificial Microbiota”, we successfully predicted the dynamics of kanamycin resistance within artificial microbiota under kanamycin pressure. This work lends new

insights into the potential role of spectrochemical analyses in investigating the existence and trends of antibiotic resistance in microbiota.

Evaluate the performance of fungal response to heavy metal exposure and discuss the mechanisms of metal adsorption via bio-spectroscopy

Furthermore, the extended usage of the developed was also tested on other microbial activity, i.e., biosorption of heavy metal. We found spectral biomarkers associated with phosphor-lipids and proteins (1745 $cm^{-}1$, 1456 $cm^{-}1$, 1396 cm^{-1}) were significantly correlated with Cd adsorption indicating the cell wall components of *S. chinense* are the primary interactive targets. However, there was no biomarker associated with Pb adsorption. The analysis of biosorption equilibrium models showed a clue that Cd adsorption was relatively suited in Langmuir, but the Pb was well fitted with Freundlich isotherm model, which implies the absorptions of Pb and Cd by *S. chinense* follow two discriminating mechanisms that Cd adsorption is mainly driven by the cell surface sorption, but for Pb, the extracellular precipitation is possibly the main contribution. This work showed the potential biospectroscopic application was not only on the investigation of antimicrobial effects of microbes but also other microbial functions.

Conclusions

In conclusion, this thesis demonstrated the feasibility of application of biospectrsocpy,

including both IR and Raman spectroscopy, coupled with various of computation analysis to characterize and quantify the bacterial response to antimicrobials. In this study, the feasibility of applying biospectroscopy to investigate the microbial response to antimicrobials was validated. Through the project, we (a) proposed a Propose a prospect and discussed the technical details of fingerprinting microbiomes towards screening for microbial antibiotic resistance; (b) developed a new tool coupling bio-spectroscopy and multivariate analysis to investigate bacterial response to antimicrobial reagents; (c) bio-spectroscopically investigated intrinsic (bacterial type) and external factors (exposure time and type) on bacterial responsive uniqueness to antimicrobials; (d) quantified the occurrence and real-time dynamics of antibiotic resistance genes (ARGs) in complex microbiota via bio-spectroscopy; (E) evaluated the performance of fungal response to heavy metal exposure and discussed the mechanisms of metal adsorption via bio-spectroscopy. Overall, the outcomes showed the developed methods were excellent tools for monitoring the antibiotic resistance in microbiota. Furthermore, with the non-destructive character of bio-spectroscopic fast screening reducing the amount of interrogating targets, many other techniques can be attached to further investigation, e.g., single cell sorting and -omics. These combinations may significantly enhance the study of the relevant mechanisms providing an opportunity for direct determination of precisely functional genes and proteins. Ultimately, genotype and phenotype can be linked together from the

population, single cell, and molecular perspectives to determine the antibiotic resistance in the microbiota of interest and consequently help us better understand the actual interactions among humans, microbes, and the physical environment. Furthermore, although the present thesis solved issues of antibiotic resistance via spectroscopic tools to some extent, it is still a challenge to transfer the current developed approaches to real world scenario due to the current developed is heavily dependent on the well-trained database. However, sometimes, it is tough to obtain the reference microbes to set up such a database since most microbes in the environment are unculturable and therefore very challenging to isolate them. Consequently, the further work will be concentrated on finding a reliable approach which could distinguish the functional microbes; and/or build a spectral library which could be used as a cross-reference, which not only would identify the microbes existed in the dataset but also provide relevant information to recognize the non-existent ones but sharing similar characters.